Tribology Group

Department of Mechanical & Aerospace

University of Strathclyde

Glasgow, UK

Erosion Issues in Tidal Turbine Blades

BY

Emadelddin Hassan

A thesis submitted in fulfilment of the requirements

for the degree of Doctor of Philosophy

April 2023

Acknowledgements

Completing this PhD thesis would not have been possible without the support and assistance of many individuals and organizations, whom I would like to express my sincere gratitude towards.

Firstly, I would like to thank Almighty Allah for giving me the strength, guidance, and inspiration to embark on this journey and see it through to the end.

I would like to extend my heartfelt thanks to my supervisor, Prof. Margaret Stack, for her tireless support, encouragement, and guidance throughout this journey. Her expertise, invaluable insights, and patience have been a source of inspiration, and I am indebted to her for all that she has done for me.

I would also like to pay tribute to the late Dr. Ghulam Rasool, whose published work has been instrumental in providing direction and focus to my research. His contribution to the field will always be remembered.

I am also grateful to my family, especially my wife Tawasul, my daughter Yasmin, and my son Yassin, for their unwavering support, understanding, and love throughout my PhD journey. Their patience and encouragement during this challenging time have been invaluable, and I could not have done it without them.

I would also like to acknowledge my parents for their continuous support and encouragement, which have been a source of inspiration and motivation for me.

I would also like to express my gratitude to my siblings, father and mother-in-law, as well as my extended family, for their unwavering support, encouragement, and understanding throughout this journey. Their love, guidance, and motivation have been a source of strength and inspiration for me, and I could not have done it without them. I am truly grateful for their presence in my life and the support they have provided me during my PhD.

I would like to express my heartfelt gratitude to the Mechanical and Aerospace Engineering (MAE) department staff especially Diane McArthur, at the University of Strathclyde for their help and support throughout the project stages. Their guidance, feedback, and suggestions have been instrumental in shaping my research and ensuring its quality. I would also like to extend my sincere thanks to Iasonas Zekos, senior tribology researcher, for his invaluable support and guidance, and Drew Irvine for his continuous support during my experiments. Additionally, I

would like to thank Dr. Tiziana Marrocco and the AMRL team for their support in SEM analysis. Your contributions have been crucial to the success of my project, and I am honoured to have had the opportunity to work with such a talented and dedicated team.

Lastly, I would like to thank the Storage Platform for the Integration of Renewable Energy (SPIRE 2) for funding my PhD and my SPIRE 2 colleagues for their support and assistance throughout the project.

To all those who have supported me throughout my PhD journey, I extend my heartfelt thanks and appreciation.

Journal Publication

Hassan, Emadelddin, et al. "Erosion mapping of through-thickness toughened powder epoxy gradient glass-fibre-reinforced polymer (GFRP) plates for tidal turbine blades." *Lubricants* 9.3 (2021): 22.

Conference

- All Energy – Engineering A net Zero Future, Glasgow 2019.
- SPIRE 2 PhD Networking, Belfast, April 2019.

Dedication

To my beloved mother and father, for their unwavering love, encouragement, and support throughout my life, and for instilling in me a love of learning, this thesis is dedicated to you. Your sacrifices and dedication to my education have made it possible for me to achieve this milestone in my life, and I will always be grateful for your guidance and inspiration.

To my wife, Tawasul, for her unwavering support, love, and patience throughout my PhD journey, this thesis is dedicated to you. Your belief in me and your willingness to stand by my side during the ups and downs of this journey have been a constant source of inspiration and motivation, and I am deeply grateful for your presence in my life.

To my daughter Yasmin and my son Yassin, for their love, joy, and inspiration, this thesis is dedicated to you. Your laughter and smiles have brightened up my days, and your curiosity and enthusiasm for learning have reminded me of the joys of discovery and exploration. I hope that this thesis will inspire you to pursue your dreams and passions, and to never stop learning and growing.

Declaration of Authenticity and Author's Rights

This thesis is the result of the author's original research. It has been composed by the author and has not been previously submitted for examination which has led to the award of a degree.

The copyright of this thesis belongs to the author under the terms of the United Kingdom Copyright Acts as qualified by University of Strathclyde Regulation 3.50. Due acknowledgement must always be made of the use of any material contained in, or derived from, this thesis.

Signed: *Emadelddin Hassan*

Date: 18th April 2023

Thesis Structure

CHAPTER 1: Introduction: This chapter provides the background on erosion and tribological challenges in tidal energy, the design and material selection for tidal turbine blades.

CHAPTER 2: Literature Review: This chapter presents a critical review of the existing literature on erosion characteristics of composite materials, including GFRP composites, polymeric coatings, and their erosion behaviour under various environmental conditions. It summarises the theoretical framework, related studies, research gaps, methodological approaches, and key findings, and highlights the relevance of the literature to the current study.

CHAPTER 3: Research Methodologies This chapter describes the research design and approach, data collection methods and Jet rig tests techniques, sample selection, and data analysis procedures. It also discusses the research limitations and ethical considerations.

Chapter 4: Investigating Erosion Characteristics of UD GFRP Composites with Varied Fibre Orientations: This chapter presents the experimental investigation of the erosion characteristics of unidirectional GFRP composites with different fibre orientations. It describes the materials and experimental procedures, analyses the erosion behaviour and damage mechanisms, and discusses the implications for practice.

Chapter 5: Mapping the Erosion Performance of Toughened GFRP Plates for Tidal Turbine Blades Under Slurry Conditions: This chapter reports the erosion mapping of toughened GFRP plates used for tidal turbine blades under slurry conditions. It explains the research methodology, presents the experimental results and analysis, discusses the findings and implications, and identifies the limitations and suggestions for future research.

Chapter 6: Erosion mapping of coated composites in simulating conditions for tidal turbines blades: This chapter introduces a new paper that presents the erosion mapping of coated composites under simulating conditions for tidal turbine blades. It provides the background and motivation for the study, describes the research methodology, and outlines the expected contributions and impact of the new paper.

Chapter 7: Investigation of Depth Profiling and Erosion Behaviour in Composite Materials and Polymeric Coatings: This chapter investigates the depth profiling and erosion behaviour of composite materials and polymeric coatings. It explains the research design and approach, presents the experimental results and analysis, and discusses the findings and implications.

Chapter 8: Conclusion, Summary of Findings and Future research directions: This chapter summarises the key findings and contributions of the study, discusses the implications and recommendations for practice, identifies the limitations and suggestions for future research, and concludes the thesis with final remarks.

Abstract

The erosion of materials used in tidal turbine blades is a significant problem, as it can compromise the blade's structural integrity and efficiency over time. The present study aimed to investigate the erosion mechanism in composite and coating materials and the influence of seawater immersion on their mechanical properties. Scanning electron microscope and optical microscope were used to analyse the effect of various parameters such as impact velocity, impingement angle, erosion particle size, and fibre orientation on the character of erosion in the blade's material.

The investigation revealed that the erosion mechanism in GFRP was the result of the fibre matrix being eroded away, leading to a cracked surface composite, removal of the fibres, and exposure of the matrix. Moreover, seawater immersion significantly reduced the overall strength of the materials by de-bonding the glass fibres in the composite matrix. However, the GFRP material's tensile and flexural strengths could be regained by the desorption process.

To address the problem of erosion in tidal turbine blades, a gradient-toughened composite with varying proportions of standard and toughened powders was developed using an inventive powder-epoxy fabrication method. The study showed that the gradient-toughened plates outperformed the standard plates in general, with a more ductile response to erosion and a more constant erosion performance across the range of impingement angles examined.

The study also highlighted the importance of using erosion maps to visualise and analyse the level of material loss experienced by coatings under different impact conditions. The erosion map produced in the study provided valuable insights into the behaviour of the coating and can be used to optimise the design of the tidal turbine blades for increased durability and longevity.

Overall, the study's results and conclusions provide valuable insights into the erosion mechanism in UD-GFRP and coating materials and the impact of seawater environment on their mechanical properties. The findings could be useful for the development of more durable and reliable blades that can withstand the harsh marine environment.

Table of Contents

List of Figures

XV

List of Tables

Chapter One

Introduction

Chapter 1 Introduction

1.1 Research Aims and Objectives

The primary research aims and objectives of this study revolve around addressing the erosion and tribological challenges faced in the field of tidal energy, particularly in the context of tidal turbine blades. As the world seeks sustainable alternatives to fossil fuels, marine energy, specifically tidal energy, has emerged as a promising option due to its predictability and minimal environmental impact. However, despite its potential, the tidal power industry is hindered by several technical, design, material, reliability, cost, and operational challenges. This research seeks to contribute to the comprehensive commercialization and global adoption of tidal energy technologies by focusing on the design and material selection for tidal turbine blades.

The specific objectives include investigating the erosion and wear issues associated with tidal turbine blades exposed to harsh marine environments. These issues encompass rotor blade degradation, cavitation, erosion caused by solid particles, and interactions with seawater. The study aims to identify suitable materials that exhibit resistance to erosion, and wear while maintaining the necessary mechanical properties for efficient energy conversion. Additionally, the research seeks to explore novel coatings and surface treatment technologies that can enhance the durability and tribological performance of tidal turbine blades, thus extending their operational lifespan and reducing maintenance costs.

Furthermore, the investigation delves into the science of erosion induced by solid particle collisions. This involves analysing the impact angles, velocities, particle shapes, and material characteristics that influence erosion rates. By utilising experimental methods, the research aims to develop a deeper understanding of erosion mechanisms and to apply this knowledge to the design and development of erosion-resistant composite coatings for tidal turbine blades.

In summary, the research aims to contribute to the advancement of tidal energy technology by addressing the erosion and tribological challenges associated with tidal turbine blades. This involves exploring suitable materials, coatings, and surface treatments that can withstand the harsh marine environment, minimise erosion-induced performance degradation, and enhance the overall efficiency and longevity of tidal energy systems.

Introduction

1.2 Erosion and Tribological challenges in Tidal Energy

Researchers have been compelled to place a greater emphasis on alternative energy sources such as wind and solar power as a direct result of the diminishing availability of fossil fuels and the growing environmental consciousness of the general population [1]. When compared to other forms of renewable energy, marine energy possesses a number of specific characteristics that set it apart from the competition. The use of marine tidal energy does not necessitate the destruction of existing environmental infrastructure and is extremely predictable [2]. Additionally, saltwater has a larger density than freshwater (x 784). A wind turbine with the same diameter and impact velocity as a tidal turbine can create a significant amount more power when it is working in water as opposed to air. The authors [3] point out that the tidal power industry has a number of challenges before it can achieve comprehensive commercialization and widespread usage of these technologies on a global scale. This is despite the fact that tidal power has a significant number of benefits. It is feasible to divide each of these areas even further into the following subcategories: technical, design, materials, reliability, price, operation, and maintenance. Tidal turbines have the potential to supply vast amounts of clean, renewable energy; yet the installation and maintenance costs for these turbines are prohibitively expensive [4].

Tidal energy is converted into mechanical energy, which is then used to power an electric generator. An essential component of this system is the blade of the tidal turbine, which does the energy conversion. When constructing the rotor blade, it's important to make sure that the materials selected have antibi-fouling qualities, are resistant to weather and corrosion in salt water, and are robust enough to handle the harsh marine environment [5]. The manufacture of wind turbine blades frequently makes use of polymer composite materials. Traditional polymer composites are more prone to erosion, whereas fibre-reinforced polymer composites offer a greater strength-to-density ratio than those traditional polymer composites [6]. After undergoing the necessary surface treatment, fibre-reinforced polymer composites have the potential to be utilised as tidal turbine blades in a manner that is analogous to that of wind turbine blades [7].

There is currently no suitable material that has been produced, nor is there a design for tidal turbine blades that is considered to be ideal. Tribological difficulties such as rotor blade degradation and cavitation, as well as the influence of solid particles and seawater mixed, should be taken into consideration in order to maximise the performance of the material [8][9]. Tests evaluating rotor blade leading edge degradation in seawater containing particle

suspensions identical to those encountered in the real thing have previously been passed with flying colors by G10 epoxy glass laminates, which are available for purchase on the market. [9] [10] discovered a variety of tribological issues during the testing process. These problems included but were not limited to cutting of the matrix, debonding of the fibres and matrix, degradation of the reinforcement, gain in mass, interaction with salt solution, swelling, and erosion of the exposed surface. According to the findings of their research, the scientists found that metal-reinforced composites and reinforced composite materials both experience erosive wear in a manner that is comparable.

1.3 Design and Material Selection for Tidal Turbine Blades

To achieve this goal, it is necessary to make use of novel and renewable forms of energy as well as technologies that go hand in hand with these forms of energy. Solar power is one of the renewable energy sources that is gaining popularity while also holding the title of the world's most rapidly expanding energy source. They have not yet reached their full potential on the economic front and yet have a ways to go [7]. According to the International Energy Agency, offshore energy resources have the potential to generate 330,000 terawatt-hours of electricity each year around the globe [1].

Tidal turbines have had a tremendous impact on the development of technology for marine renewable energy despite the challenges that they have presented. This is due to the well-known behaviour of the tides as well as the steady supply of power that comes with each tide. When compared size for size and flow rate for flow, wind turbines produce a far smaller amount of energy than tidal turbines [3]. The abrasion of surfaces caused by the impact of hard particles, most often known as the process of solid particle erosion, which is often referred to as surface abrasion, can cause the surface to lose material or even shatter [11].

Tidal turbines provide a higher overall power output than wind turbines do. This is due to a number of variables, including the higher density of saltwater and the design of the blades, which rotate in the opposite direction. Because of the larger forces that are confined in a smaller space during the production of tidal turbine blades, it is vital to employ materials that have the maximum potential performance to make the blades. However, this is not always possible due to the nature of the construction process. It is necessary to first achieve victory on the technological and economic fronts with regard to tidal energy before it can be utilised as a dependable source of power.

Introduction

There has been some progress made in the field of the design of tidal turbine blades and the selection of materials, despite the fact that there are still conflicts. As a consequence of this, it is possible that the cost of generating electricity from this source can be reduced by employing more reliable, less expensive, and cutting-edge materials and surface treatment technologies. Fibre-reinforced composite materials, such as those used in the production of wind turbine blades, have the potential to be used in the production of tidal turbine blades due to their superior mechanical properties, resistance to corrosion, and overall cost efficiency [12].

There is no denying that the search for a workable composite material involves additional tribological challenges, particularly in light of the growing turbine rotor diameter. A few examples of elements that should be taken into account are erosion of sediments and solid particles, cavitation, and synergistic effects on tidal turbine blades [8] G10 epoxy glass laminate was subjected to a series of tribological tests in a range of solvent-sand solutions in the past, and the findings revealed that the materials possessed a few particular tribological issues that were not seen in other materials [9]. Matrix cutting (pit creation), cracked laminates (lamination searing), matrix swelling (fibre fracture), and so on were among the problems that needed to be addressed. A polymeric coating was applied to the surface of the composite to reduce the tribological friction caused by the seawater. By doing so, we increased the composite's efficiency and durability. The rapid drying times of polymeric compositions and similar surface coatings make them ideal for treating the common cold. They can be applied with a brush or a spray gun [13].

Using the slurry pot test setup, researchers studied the effects of varying impact angles and particle sizes while holding tip speed constant. According to the results of the tests conducted, the overall performance quality was greatly improved by using an erosion-resistant polymeric coating, particularly in terms of the tribological features and the resistance to the mass loss. Composites were tested for erosional wear in saltwater environments both as-is and with erosion-resistant polymeric coatings [11].

In addition to information about mass gain and volume loss, tribological studies made use of SEM micrographs of worn surfaces, E.D.X. analyses, and research that had been previously published. In recent years, there has been significant development in the use of composite materials for the blades of tidal turbines. In next research endeavors, the functionality and make-up of a variety of coatings, such as polymeric, gel, silicone, and rubber, will be investigated further [14].

1.4 The Science of Erosion Induced by Solid Particle Collision

The fundamental principles behind erosion caused by solid particle collisions have been investigated in both ductile and brittle components [15], [16]. Brittle materials were shown to be more susceptible to erosion than ductile materials [17]. An investigation of the published research on theoretical models of erosion indicated that there are a number of different models to choose from [18]. The most important of them was utilised to duplicate laboratory experiments on erosion brought on by solid particle impingement using gas jets. These experiments were carried out in a lab. When adequately supported by suitable adjusting of specific parameters, they perform in a remarkably effective manner. It would appear that theoretical models that are based on experiments cannot be used effectively in the creation of new materials for use in high-temperature applications. One possible reason for this is that such models require constant modification of the parameters in concern [2]. As a direct consequence of these discoveries, a brand-new methodology that is based on the finite element method has been devised as a solution. Given that it only requires knowledge of the major mechanical characteristics as a function of temperature, it appears to be useful for estimating erosion rates in a wide variety of applications. This is due to the fact that it only requires knowledge of the major mechanical properties.

It is a common occurrence for problems to arise when components such as compressor blades on a jet engine or pipeline walls in the oil and gas industry are hit by pollutants introduced into the system through airflow or sand transported through oil and gas [19], [20]. This can be a significant issue [21]. Plain carbon steel is frequently used in the production of pipelines for the oil and gas sector. They are also utilised in a wide variety of different business sectors. It's possible that particles or pollutants in the oil or gas that's being supplied could cause the pipe components to deteriorate over time. The angle and velocity at which an eroding particle strikes a material, as well as the qualities of the material itself, are both factors that can have an effect on the severity of erosion and the method by which it occurs [22]–[24]. Both the eroding mechanism and the amount of material that is removed from the surface are significantly influenced by the shape of the particles that are being removed. In instance, it has been found in the research that ductile materials, when subjected to the impact of spherical shaped impactors, tend to deform into a more circular shape [22].

When the same spherical particles that were used in this study collide with particles of the same size, they remove material from the particles at a rate that is lower than the rate at which they remove material from brittle materials [22]. Throughout history, removal rates for ductile

materials have historically increased until they reached a maximum between 30° and 45°, at which point they have begun to decrease. On the other hand, brittle materials can be removed at their greatest rate when they are removed at an angle that is normal to the surface [14], [23], [25]. Because they are so resistant to wear and corrosion, Ni-P coatings are a good option for use on pipelines that need to be protected [26]–[28]. Monolithic Ni-P coatings have a low hardness when they are first deposited because of the nature of the substance that they are made of. It has been found that several properties can be improved by incorporating nanoparticles into electroless Ni-P coatings. This discovery was made [27], [28]. A brittle component has the tendency to fracture when it is indented, just like the fracture that can be seen when the material is indented. If the protective coatings are tough and wear-resistant, yet brittle, the most common failure mechanism that might occur when they are subjected to erosive circumstances is the start and propagation of fractures. A brittle Ni-P matrix is formed during the deposition process, and the superelastic NiTi contributes to the material's overall strength. Recent research has shown that including NiTi particles into the Ni-P matrix results in a composite coating that is more resistant to being scratched and indented. This was demonstrated by the findings of the study [29].

The NiTi material goes through a reversible martensitic phase transition during the entirety of the procedure. the manufacturing process, which may lead to a change in the material's toughening. As a fracture extends, the high stress leads the superelastic particles to transform into martensitic and the high energy near the crack tip forces this transformation to take place. The deformation of the crystal lattice creates a compressive strain around the particles, in addition to the change that occurs in the particles themselves. This compression has the potential to halt the crack's progression and even close it completely, if it hasn't already done so. Zirconia-reinforced ceramics, such as heat barrier coatings [29]–[31] have also demonstrated the same behaviour.

When ductile reinforcements are combined with brittle matrixes, multiple mechanisms, including fracture deflection and bridging, as well as microcracking, have been discovered to result in a toughening of the reinforcements' overall properties. When a second-phase particle interacts with a crack that is traveling through space, crack deflection occurs as a result of the interaction. This causes the fracture toughness of the substance under investigation to increase, and crack propagation requires an increasing amount of energy as each mechanism is considered. When a particle or fibre comes into contact with the fracture path, it has the potential to change the direction in which a crack is propagating and, as a result, reduce the

amount of energy that is released after a break occurs. In reinforced composites, when crack bridging takes place, the energy of propagation is greatly amplified by interacting with a second phase, just as it was with the first phase in the initial instance. This is because the energy of propagation is being transferred from one phase to another. The process of cracking must be continued by moving through the second phase, which basically absorbs some of the fracture energy in order to bridge the crack. This must be done in order for the crack to be bridged [32]. In conclusion, it was discovered that micro-cracking increases fracture toughness and fracture toughness by reducing large cracks to a sequence of microscopic cracks. This is done by lowering the fracture energy. Identifying the erosive mechanisms can be accomplished by the use of single particle erosion. The phenomenon of erosion caused by a single particle has been the subject of a great deal of research [33]–[35]. Nevertheless, there is a lack of information regarding the effect that composite materials have on nanoparticles [33]–[36].

The greater the use of composite materials in industrial settings, the greater the necessity there will be to categorise these materials as having erosion behaviour. In light of the increasing need for ductile-reinforced brittle materials, a recent body of research has focused its attention on the solid particle erosion (multiple impacts) of composites, in particular coatings for materials that are used in environments that are prone to wear and erosion [37]. Researchers are employing an experimental method known as single particle impact in order to answer the question of how electroless Ni-P-nano-NiTi composite coatings deteriorate over time. The impact that a single particle has on electroless Ni-P-based composite coatings that contain superelastic NiTi additives is the primary focus of the current research. The behaviour of coating erosion in response to the impact angle, velocity, and particle form is currently being investigated. The inclusion of NiTi particles imparts a higher level of toughness to the material, and the processes that underlie this effect are now being researched.

Chapter Two

Literature Review

Chapter 2 Literature Review

A glass fibre-reinforced polymer will gain weight as a result of moisture absorption if submerged in seawater for an extended period of time [11]. G. Huang [38]discovered that materials' mechanical qualities, such as bending and tensile strength, degrade over time when exposed to salt water. There is also a mass gain due to sodium chloride solution penetration into the G10 epoxy glass composite layer. When the mass of the rotor blades increases, it can lead to unbalanced turbines [39], which can be problematic for the turbine's operation. Diffusion may also result in an increase in rotor blade mass, which could have a significant impact on the polymer composite's tribological behaviour.

Fibre-matrix interfaces are created when moisture condenses in the matrix's pores and gaps after being permitted to flow through. The process begins with condensation. G. Rasool and Shayan Sharifi [9] claim that this causes the matrix to swell, the reinforcement and resin to lose adhesion, and the reinforcement fibre and matrix to debond at the interface, all of which are harmful to the structure's integrity. These elements have the effect of speeding up the rate at which material is eroded away. It's possible that the infiltration of water into a composite material will result in soluble components from the composite material being extracted and dissolved in an acidic solution. It was calculated by Hailin Cao and colleagues [39]–[42]that the difference between the mass gained through diffusion and the mass lost through extraction processes is known as the net mass variation. In other words, the difference is equal to the net mass variation between what is obtained by diffusion and what is lost through extraction processes. The leading edge of a tidal turbine blade erodingcreates rough surfaces, much like the erosion of a wind turbine blade's leading edge.

In addition to quick moisture absorption and hastened mass gain, damaged exposed rotor blade surfaces can also cause the Reynolds number to rise, which increases drag while decreasing lift, causing the blade operation to be out of balance. Tidal turbine efficiency, availability, and reliability are all impacted by this collection of factors [43]–[46] as well as by an increase in operational costs, maintenance costs, failure rates, and turbine downtime. According to Davies and Rajapakse [47], for marine renewable energy (MRE) devices that qualify as renewable energy sources, the MRE business must ensure that MRE devices do not cause any environmental issues and do not require any maintenance throughout their life cycles.

Based on the results from this study, it can be concluded that a substrate's erosive-resistant polymeric coatings serve as a barrier to seawater while also increasing the substrate's erosion resistance.

Coatings to strengthen the erosive resistance of this fibre-reinforced composite constitute a significant development in the choice and employment of novel materials in the production the blades of tidal turbines [11], which is currently occurring. [Cause and effect] In subsequent investigations, which are anticipated to be finished in the not-too-distant future, the application of hybrid composite coatings and even more technologically advanced materials will be investigated and tested. In addition to more conventional approaches, the application of technologies that are both novel and renewable forms of energy, as well as those that supplement existing practices, are essential for achieving sustainable development. In spite of the fact that renewable energy is the source of energy that is expanding at a faster rate than any other in the globe, there are significant scientific and financial obstacles that need to be overcome before it can reach its full economic potential in the market [48]. In spite of the fact that they have been met with a number of challenges on both the technological and the economic fronts, offshore energy resources like tidal turbines, for example, have been cited by the International Energy Agency as having been instrumental in the development of technology for marine renewable energy [1].

Composite materials are rapidly being used in place of conventional materials in a number of engineering applications due to a multitude of features, including their durability, affordability, and strength [3]. Composite materials are also becoming more widely available. Applications include, but are not limited to, automobile and aerospace bodywork, sporting equipment, buildings, and maritime hardware.

Polymer composites are particularly susceptible to erosion damage because of the widespread usage of these materials in applications that involve potentially hazardous environments.

When it comes to a wide variety of applications, the mechanical properties of polymer composites and their resistance to erosion are the most crucial aspects to take into account [49]. As a direct consequence of this, the qualities of the polymer material should be improved. As a result of the potential use of polymer composites in a wide variety of engineering designs, the erosion behaviour of polymer composites is currently receiving an increased amount of attention [50].

2.1 Erosion Theory

Erosion of materials can be caused by high impact pressures that are concentrated at the surface of the material and are also localised. Examples of this type of erosion are cavitation erosion and drop impact erosion [51]. Many scientists are of the opinion that the erosional process can be kept under control by combining two processes that are in direct opposition to one another [52], [53]. To begin, the capacity of the substance changes to absorb impact energy after repeated indents, and then there is a modification in the substance's capacity to absorb energy over time following repeated indents. When the surface is damaged because of the increased travel distance, the impact forces are reduced, which results in attenuation. There appears to be a wide number of methods in which erosion might show itself, and this tends to be dependent on the type of equipment that was utilised.

Gas erosion is most likely the most well-known implementation of this method [54]. Cavitation erosion is a phenomenon that has been studied extensively for several decades and affects water turbines, pipelines, and pipes [55] [56]. When flying over areas of dense cloud cover, one encounters additional challenges such as corrosion of steam turbine rotor vanes and aircraft hulls caused by rain drops. At initially, a significant problem manifested itself, particularly after locally pulverised ash-rich fuels were introduced into the combustion process at thermal power plants' boilers [57]. When a force exerts itself on a surface because of a common driver such as sand, water, or wind, it either obliterates the material entirely or pulverises it before transporting the fragments to a new position. Corrosion, on the other hand, is typically the outcome of chemical processes as opposed to physical ones when it comes to its causes [58].

The process of erosion happens when a stream of solid particles collides with a surface that is softer, which results in the loss of material[59]. Cutting, deformation erosion, or some mix of the two can lead to wear. Wear can also be attributed to some combination of the two.

Cutting erosion happens when a particle strikes a surface at a lower impact angle [60]. This causes the particle to cut through the surface. The ductility of the material being worn away is a significant factor in determining the rate of wear that is generated by this form of erosion [61]. The rate of wear is minimal because particles would rather deflect away from the surface than distort fragile materials, hence this results in less material being deformed. Because of this, the rate of wear is greater for materials that have a higher brittleness [62].

After penetrating the surface, the particles create waste in the shape of ribbons, giving the impression that they were produced by a metal cutting operation. When an angle reaches a

particular point, known as the critical angle, cutting erosion transforms into deformation erosion. This critical angle might range anywhere from 45° to 50°, depending on the material that is being eroded [63]. Because of the complex relationship that exists between the impact angle, particle velocity, and the depth to which the particle enters the surface, cutting erosion is notoriously difficult to forecast.

As a direct consequence of this, deformation erosion will constitute the primary focus of the inquiry. This sort of material deterioration is caused when several particles strike the surface of a material at a normal incidence. The initial impacts leave behind impact craters and raise a minute ridge all the way around the perimeters of the depressions. The ridge is gradually worn down by subsequent particles, which leads to an increase in tension and ultimately brittle fractures. In addition, subsequent impacts cause the formation of lateral fissures at the base of the deformed region, which expanded to the surface and removed material in the form of small plates. This process occurred as the material was removed [64]. It is possible to construct a quantitative equation for this mechanism by employing a number of different simplifications. For instance, Hutchings [65] suggested an equation in which surface deformation is assumed to be entirely plastic and particle deformation is believed to be non-existent upon impact. This assumption was made in the context of an impact. Hutching's model was further improved upon by Sundararajan and Shewmon 1983, who introduced more adjustments. In this investigation, a formula that was developed in a later study is used to make predictions regarding the rate of erosion [66].

The equation for calculating the rate of erosion that was created by Sundararajan and Shewmon was dependent on a number of other assumptions that were obtained from Hutching's formulae. One way to simplify things is to say that the complete energy of the target receives the particle in the form of plastic work [67]. This makes a lot of things easier to understand. Early investigations on erosion using this method discovered that inversely related to the square of particle velocity was the rate of erosion [68]. Both heat and sound can be considered to be forms of energy loss. Since this is not true for very high particle velocities, we cannot use this equation to describe those conditions.

Assumption 2: According to the model, any particles that collide with metal surfaces will take on a spherical shape. As a direct consequence of this, the geometry that is calculated for impact craters will be simplified. If the environment that the erosion formula attempts to replicate

contains angular particles, then the amount of waste steel that is produced could be up to four times larger than what was projected [69]. As a consequence of this, this component of the erosion model is the one that has the greatest potential to be inaccurate.

In this study, the concentration of particles will be examined to determine the effect that they have. When the number of particles in the air is higher, it is logical to assume that erosion will occur at a faster rate. This is correct to a degree, but not completely. However, there is some evidence to imply that when the concentration of particles increases, the interactions between them lead to a loss of kinetic energy. This loss of energy can be attributed to the particles. The erosion rate will continue to decline until it reaches a critical concentration if the particle flux continues to increase. Because of this, the project will study relatively low particle concentrations.

2.2 Solid-State Erosion

Solid-state erosion is a structure of material degradation because of the impact of solid particles. The erosion occurs any time the surface of a solid material is repeatedly bombarded with solid particles, leading to the loss of material and the formation of pits and grooves on the surface [70]. This type of erosion is different from the erosion caused by wind or water, which involves the movement of earthen materials [71], [72]. Solid-state erosion can also occur in combination with other forms of degradation such as corrosion, known as erosion-corrosion [73]. The severity of solid-state erosion is influenced by the characteristics of the target material as well as the characteristics of the impacting particles, including their size, shape, and hardness, including its hardness, ductility, and microstructure [70]. It is a significant concern in various industries, including aerospace, where it can cause significant damage to engine components and other structures exposed to high-velocity particles.

Solid particle erosion is a common challenge in the sphere of industrial components for instance gas turbine blades and can also occur in tidal turbine blades [74]. the surface of the blade is impacted by solid particles, momentum is transferred to the material's surface, causing material removal from the surface. To learn more about turbine blade surface deterioration brought on by solid particle impacts, an integrated experimental and computational research programme was run [75]. In this study, different impact conditions were used to test the erosion of coated and uncoated blade materials. Materials with various mechanical characteristics exhibit various types of erosion [74].

Literature Review

Review of gas turbine compressor blade protective coatings and solid particle erosion behaviour was done, and it discusses various solid particle erosion-related variables behaviour, such as particle velocity and particle diameter [76]. The article mentions that solid particle erosion can cause damage to compressor blades, and the damage can lead to engine failure. However, there was no specific mention of tidal turbine blades in this review.

When the blades of the tidal turbine are taken into account, it seems as though there is erosion caused by solid particles. Solid particles have the ability to project themselves at any surface, regardless of whether they are in motion, in a slurry, or by themselves. When they impact a flow or a slurry with sufficient force, this causes a transfer of momentum into the surface of the material that they are striking [77]. The surface of a target takes damage from an impact force because the force transfers energy from one location to another. When the projected kinetic energy of the particles is transmitted to the material's surface, shockwaves are created. The force, angle, and surface elasticity of the material that is being hit all contribute to the creation of the shockwaves [78]. The shockwaves that are produced by the material are what cause the collapse and the beginning of the fractures in the first place.

The incubation period for solid particle erosion is quite lengthy. This is especially true when talking about tidal turbine blades due to the fact that the application of solid particle erosion occurs over a prolonged period of time, with the erosive process continuing across the entirety of the life of the equipment [79]. After an extended period of exposure to massive concentrations of solid particles and consequent plastic deformation in the actual material, Heat energy is created when kinetic energy from the erodent is transferred [78]. The material's melting point might get closer to being reached if this process is allowed to continue.

2.3 Erosion Concerning Brittleness and Ductility

There are many different ways that material can be lost due to solid particle erosion caused by brittle and ductile erosion, and these are the two fundamental forms of erosion that can be studied.
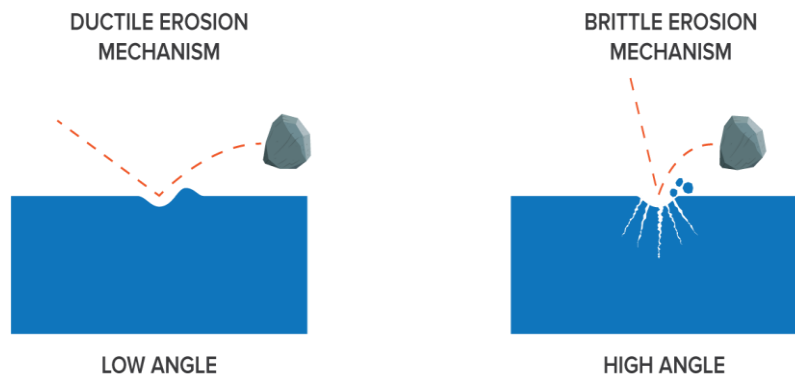
Figure 1. Brittle and Ductile Erosion

Figure. 1 provides a very clear illustration of how the target material reacts differently based on the kind of erosion process that is taking place. The brittle kind of erosion is characterised by a great lot more cracking and flaking of the material, while the ductile type of erosion is characterised by a significantly smoother hollow [80]. Plastic deformations and brittle fractures are responsible for the wear's obvious visible abnormalities, which have occurred over time [33]. In these settings, there are variations in the particle size, the impact's velocity, angle, and direction; nevertheless, the maximum angle of impact during mass loss is extremely varied depending on the kind of erosion [62].

When the material that is being eroded is moved by a solid erodent utilising procedures such as cutting and ploughing, a process that is known as ductile erosion takes place. This type of erosion is referred to as brittle erosion, and it occurs when there is a loss of mass as a result of the creation of cracks that expand and intersect at the locations of impact. There are several examples of brittle erosion all around the natural world. At this point, the degree of damage that has been done is in part influenced by the form of the erodent particle and the properties that are used to differentiate it from other types of particles [17].

Because of this, the erodent shape has an effect on the regions of a surface depression that have the highest plastic deformation, which results in a loss of mass for each indentation. When it comes to brittle materials, the sharpness quotient of the erodent has a direct bearing on the severity of cracks and fractures that are caused by it. When compared to round-shaped particles,

sharpness shows the intensity and location of fractures, indentations, and cracks. As a result, there is concentrated mass loss and higher wear as a result of these types of damage. Due to the fact that every form of erosion uses a distinct process to lose mass, the maximum amount of mass can be lost at a variety of different angles, depending on the circumstances [81].

2.4 Erosion Characteristics

The rate of eroding is largely governed not only by the velocity of the particles that are doing the eroding, but also by the angle that is generated between the primary surface regions and the trajectory of the particles [82]. This angle can be thought of as the angle of attack [83]. The rate of erosion an additional name for this particular angle of tilt is known as the impact inclination. The abrasive hardness ratio, particle size, shape, and concentration were also found to have an impact, All of these factors, along with the effects of liquid and solid additives, are very important in determining the type of erosion and the results it produces [84].
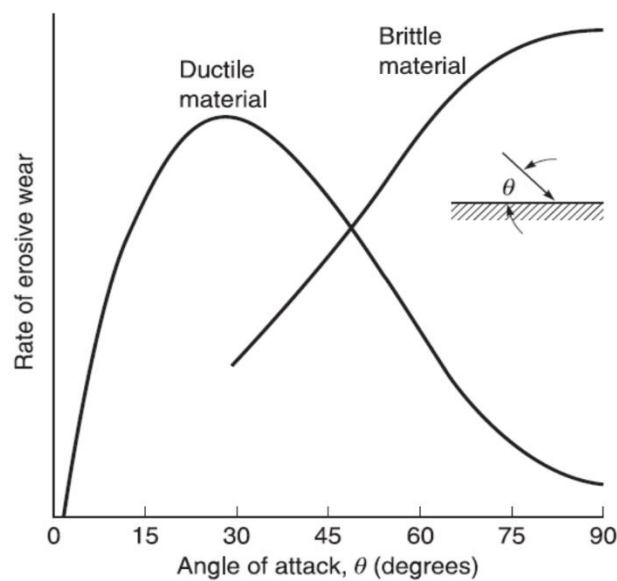
Figure 2. Rate of erosive wear versus angle of impingement [185]

Fig. 2 makes it very clear that the angles of attack that range from 15 to 45° are the most common ones for ductile erosion to take place. As a result, the leading edge of the turbine blade is less vulnerable to this phenomenon than the sides of the blades themselves. The highest value of attack angles for brittle erosion is greater than 90°, which indicates that, in the majority of instances, erosion-initiating particles and slurry are facing each other in a direction that is perpendicular. An illustration of what the typical images of a turbine blade's leading edge, with eroding particles coming in from the opposite direction of the blade's tip and cutting the leading

edge, which causes a fracture to form in the blade. This removes material from the blade because the solid particle caused a break in the surface of the blade.

When talking about unidirectional glass fibre reinforced polymers, ductile or brittle erosion can be the type of breakdown that occurs when solid particle impacts break down epoxy resin [85]. Once they are exposed to air, these delicate fibres will disintegrate a great deal more quickly than the resin that makes up the polymer. Under the conditions of the impact, the fibres quickly fracture and are subsequently further degraded, which exposes both the leftover resin and the fibres to the process of erosion [86]. When the core materials of the GFRP are placed in an environment that contains water, the material will absorb more water, which will have a substantial effect on the material's physical qualities.

2.5 Solid Particle Erosion

The complex process of solid particle erosion can cause material deterioration and failure. An analysis of published works on solid particle erosion of engineering materials [87] has revealed that a detailed modelling effort is underway to develop an analytical capability to predict erosion behaviour of structural materials. Studies have concentrated on the erosive properties of composite materials made of polymer, metal, and ceramic, as well as coatings for composite materials [88]. Research has shown that composite materials erode more easily than their corresponding matrix polymer, with the maximum erosion angle of composite material being more substantial than the matrix's [70]. The existing erosion information on materials of interest in fossil technology has also been collected, and existing erosion models have been evaluated for their capability to predict erosion behaviour [87]. These efforts will help in predicting and preventing material degradation due to solid state erosion.

Solid particle erosion is a dynamic process that occurs when fast-moving solid particles impinge on a target surface, causing material removal from that surface. Negative consequences of this procedure include component wear and surface roughening, surface deterioration, a scooping look at the macroscale, and a shorter structure's useful life [89].

Erosive wear in hydro turbines, also known as sand/silt erosion, is brought on by solid or liquid particles striking a solid surface. These particles, which are part of the flow medium and have extremely high kinetic energy, have the potential to harm particularly metallic target areas [90].

In addition, Solid Particle Erosion: A Systematic Review examines erosion brought on by solid particles: Incidence, Estimate and Mechanism, establishes erosion by plastic contact according

to a new energetic theory, grounded on concepts of brittle behaviour and plastic contact, composite structure models [91].

The particle sizes in solid particle erosion are typically between 5 and 500 µm. This type of erosion can occur in a variety of settings, including industrial environments and natural settings such as rivers and glaciers. To mitigate the negative effects of erosion, Understanding the variables that affect the process is crucial. These variables include the particle concentration, size, and shape, in addition the effects of additives, both liquid and solid [92].

Polymer composite materials have been found to be useful in various purposes due to their attractive properties such as high stiffness, strength, and low weight [93]. However, they are known to have low resistance to erosive wear compared to metallic materials [94]. As a result, it is critical to investigate how erosive wear occurs when using polymeric engineering materials, especially in applications such as oil refinery pipes, helicopter rotor blades [94].

To increase the polymer composites' erosive wear resistance, various techniques have been employed, such as fibre reinforcement, particle reinforcement, and coating [95]. These techniques can increase the toughness, strength, and ductility of polymer composites, resulting in improved resistance to erosive wear. Additionally, researchers have investigated the impact of operating conditions for instance particle size, impingement angle, temperature, and velocity on the erosive wear behaviour of polymer composites [94].

It is important to note that polymer composites have a higher rate of erosive wear than pure polymer matrices [96]. However, with proper reinforcement techniques and careful consideration of operating conditions, It is possible to increase the erosive wear rate of polymer composites, making them a viable option for many applications.

2.6 Erosion test on glass fibre-reinforced polymer

According to Fouad et al [97] the goal of their experiment was to investigate the eroding capabilities of a polymer matrix composite that was reinforced with unidirectional glass fibres in a single direction. It was necessary to experiment with the different input response factors to obtain the results a test for erosion to be as accurate as they possibly could be. The impingement angle with ranged from $30°$, $60°$, and $90°$, and the pressure with ranged from 1.75, 3, and 3.5 bar, the particle size was 150 µm, and the test length 30 minutes, were the factors that produced the greatest results was 3 min. When the angle of impingement is more than $60°$, it is vital to keep in mind that the impact pressure has a substantial influence on the pace of

erosion. This is something that must be taken into consideration at all times. This is something that ought not to be disregarded in any way. The eroded surface was subjected to a SEM investigation, which revealed, among other things, the presence of matrix elimination, exposed fibre, cracking, and the removing damaged fibres. The examination brought to light a number of traits, including those that have been described below.

Research on a glass fibre-reinforced thermoplastic polypropylene composite material was carried out by Barkoula and Karger [98]. They were interested in studying how the composite was affected by the amount of fibres present as well as the direction the fibres ran in. In the course of the experiment, measurements of length and weight, in addition to other criteria such as the impingement angle and the orientation of the fibres, were all taken into consideration. Although the results of the experiment indicated that the length of the fibre holds only a marginal impact on the frequency of erosive wear, the data also indicate that the amount of fibre that is present has a major effect on the rate. This is the case despite the fact that the experiment discovered that the rate of change is only slightly affected by the length of the fibre. impingement angles of more than $30°$ are required to see a considerable shift in the quantity of erosion when it comes to the matter of fibre orientation.

According to Chauhan [99], For a variety of applications, vinyl ester composites with glass fibre reinforcement were created. To determine the volumetric wear rate and evaluate it in relation to the sliding distance, a wear tester of the pin-on-disc variety was utilised. When the materials were loaded with 10 and 15 N at speeds of 54, 80, and 110 m/min respectively, a statistically substantial rise in the composites' wear rate was noticed.

All of the samples that were examined exhibited the same linear relationship between sliding distance and wear rate, which is consistent with the findings of other studies. Analyses of the GFRP were carried out with the aid of solid particle erosion tests, which Yang and Nayeb Hashemi [100] had previously reported in their research. For the purpose of the experiment, an erodent consisting of SiC particles with sizes ranging from 400 to 500 µm was used. In contrast to this, while the speed 42.5 m/s is kept throughout each and every experiment, the impingement angle as well as the amount of time that the object is exposed to it varies. The rate of erosion is greater if the material is exposed for 120 seconds at impinging angles of $60°$ and $90°$ than if the material is exposed for 60 seconds.

2.7 Effect of filler on composite erosion behaviour

Fillers can boost critical qualities of composites by adding bulk to the material, which is why they are used. Fillers are frequently added to composites in the hope of elevating the materials' overall quality. Polymer composites make use of filler materials to increase the material's strength and stiffness. Examples of filler materials include organic compounds, inorganic compounds, and metallic compounds. According to Patnaik and Satpathy [101], determining the durability of polyester composites with glass fibre reinforcement and fly ash filling can be accomplished through analysing the composites' reaction to erosion and wear. Even while there was a minor improvement to the mechanical qualities as a result of adding fly ash to polyester resin, there was an increase in erosive resistance.

The influence of erosion rate variables such erodent impact angle and velocity and the percentage of filler material weight and standoff distance, might be examined by employing a Taguchi experimental design [102]. Following elements were identified as potential contributors to the issue: When compared to the effects of the other components, the categorization indicates that the erosion rate is less affected by the impact velocity. When it comes to erosion wear, the results of a second look at the effects of impingement angle on various fly ash filled composite materials proportions demonstrate that these materials are semi-ductile. A particularly high rate of erosion occurs when the impingement angle is set at $60°$.

In a study carried out by Sinmazc and Taskiran [103], which was later published in the journal Composites, the researchers looked at the qualities of calcium carbonate-filled polyphenylene sulfide composites.

It was decided to carry out a number of different erosion experiments on the composites. These composites were reinforced with glass fibre that was dispersed at random, and they were exposed to a number of different testing settings. It was found, during the process of determining the rate of degradation of produced composites subjected to different impact velocities, that at an impingement angle of $60°$, the rate of degradation was much greater associated to the rate of degradation at other angles. The material displays ductile qualities when the impingement angles are brought down to their smallest possible amount; contrasted with the material displays brittle properties when impingement angles are raised to their highest possible value. As a result of being subjected to high rates of erosion, the filler-reinforced composites exhibited a behaviour that was semi-ductile. This behaviour was most apparent at

impact angles between and $45°$ to $60°$, as the trials showed. The material's mechanical properties were improved as a direct consequence of the incorporation of calcium carbonate particles into its composition. For all of the composite samples that were made, when the impact velocity was adjusted from 20, 40, and 60 m/s and the impinging angle was set to $60°$, the highest level of erosion was attained.

When the impact velocity was increased to 60 m/s, an unexpected rise in the erosion rate was detected. According to Ismail [104], chemosphere-filled carbon epoxy composites offer mechanical and erosion properties that warrant further study. When the two types of composites' mechanical and erosion properties are contrasted, filled composites come out on top. The amount of erosion that took place was significantly influenced by a number of different factors. Particle speed, impact angle, erodent time, and particle size were among the factors that were considered and examined. The relationship between erosion time and erosion rate is the one we can identify as having the smallest impact. When struck at an angle of $30°$, both composites degrade ductility, exhibiting ductile degradation. As the experiment progressed, It was immediately apparent that increasing the velocity increased the rate of erosion..

Glass/epoxy composites packed with alumina underwent a slurry erosion test for the objective of assessing how the composites will respond under a variety of environmental conditions. During both the carrying out of the experiments and the carrying out of the analysis, each and every one of these factors was taken into consideration. The study's findings also show that erosion is influenced by the slurry's concentration and speed in a multiplicative manner. Higher impact angles, up to $60°$, have been discovered; nevertheless, additional impact angle reductions have reduced erosion rates [105].

Jet erosion tests were used in further research to examine the slurry erosion of epoxy glass composites that included alumina fillers. According to the study, adding more alumina filler increased the composites' resistance to erosion. The impact angle also affected the erosion rate, with higher impact angles resulting in lower erosion rates [106]. Another study used impingement velocity and slurry concentration as variables to examine the effects of alumina fillers on the slurry erosion behaviour of glass epoxy composites. The findings demonstrated that increasing the filler content enhanced the composites' resistance to erosion. Higher slurry concentration and impingement velocity also led to greater erosion rates [107].

Cement bypass dust, also known as CMPD, is a residue that is left over from the manufacturing process. It is a by-product of the cement manufacturing process and includes forty percent lime

by weight. Our objective is to gain a deeper insight of the mechanical and eroding characteristics of an epoxy composite material that makes use of waste cement as filler. Bamboo reinforcement that has been subjected to chemical processing is used in a bidirectional reinforcement system. This reinforcement deteriorates with time. This was followed by the addition of three distinct quantities of filler material, each of which occupied a distinct portion of the overall capacity of the mould. After making modifications to five crucial aspects of an erosion test rig, the researchers utilised it to carry out an erosion experiment. The addition of polymers to the CMPD has a significant effect on the rate at which it breaks down. The modified bamboo fibres shown superior mechanical and erosion qualities, in addition to a manageable and straightforward handling experience. The maximum erosion rate of treated filler-reinforced composites, in addition to untreated composites, is subject to significant variation based upon this angle where the impingement takes place. The findings of the study indicated that the filler content and the angle of impingement had the most influence on the final result, more so than any of the other factors [108].

2.8 Effect of Red Mud Filler on the Mechanical and Tribo Performance of Glass Polyester Composites

According to Biswas and Satapathy [109], the prestigious scientific journal Tribology has published a report on the tribological behaviour of epoxy composites filled with industrial waste. The term "red mud" refers to a form of industrial waste that is frequently utilised in the construction industry as a filler in composites made of glass fibre matrix. The dry silica sand that was employed in the experiment served as the erodent, and the particle sizes of the erodent were altered as the experiment progressed (300, 450, and 600 µm). Several factors that affected erosion rate, such as the amount of filler, the temperature of the erodent, the erodent's velocity, the standoff distance, and the impinging angle, could be evaluated and understood thanks to this study. According to the discoveries that Taguchi came to in the course of his dissertation research, erosion rate is primarily unaffected by impact velocity, but it has a significant impact on the interface that exists between erosion rate and filler weight.

When conducting the experiment with a range of different filler contents it was found that the impact angles used had an impact on the composite's semi-ductile property. According to the findings of the research, the innovative composite material might potentially be used for a broad variety of other items, projects like sports equipment, fibre boats, housing, industrial fans, etc. In a previous study, Biswas and Satapathy [110] examined the mechanical and

tribological characteristics of composites made of red mud filled with fibre reinforced bamboo. It was found that composites possessed superior mechanical and tribological qualities. The Taguchi method was developed expressly for the purpose of parameter analysis, and an air jet-type testing apparatus was utilised so that the experiment could be carried out.

In terms of performance, composites made from bamboo performed far better than those made from glass fibre, as shown by the findings of the comparative study. The erosion wear resistance of composites made of bamboo and glass fibres was improved by the addition of filler material. As a result of their investigation, the experts came to the conclusion that filler-reinforced composites made with bamboo are suitable for usage in highly corrosive conditions. They made this recommendation at the conclusion of their study. The creation of the glass polyester composites with red mud filler in order to evaluate their erosion capabilities was the objective that Jena and Satapathy [111] set out to achieve, and they were successful in doing so. The newly created composites were put through their paces in a number of different testing conditions to ensure their quality.

Glass polyester composites' tensile and flexural strengths are reduced when red mud filler is added. However, the addition of the filler causes the filled composites' microhardness to rise. The integration of the filler into the material resulted in a reduce in the material's mechanical attributes; nevertheless, the material's tribo performance was improved as a direct result of the inclusion of the filler substance. On the other hand, the quantity of filler used is the sole variable that significantly affects the degree of augmentation that is achieved. In order to identify the erosion parameters that have a significant impact on the material's wear rate, Taguchi's experimental design approach was chosen. This was done in order to establish the optimal parameters for the material. The results of the Taguchi analysis showed that significant factors in lowering the wear rate included the weight percentages of filler and fibre, as well as the erodent velocity and impact angle. It was determined that the particle size had a less significant impact on the erosion rate of the filled polymer composites when compared to the other erosion parameters. This was the conclusion that was reached when the comparison was carried out. Attia and Ali [112] used sand blasting equipment to investigate the epoxy composites filled with synthetic oil to determine the composition of the composites. A number of experimental aspects, such as the influence of the experiment, the standoff distance, and the amount of filler that was contained in the matrices, were examined. The findings of the study show that raising the proportion of filler in a mixture can greatly boost its resistance to erosion.

2.9 Study of Erosive Wear Characteristics of Epoxy Composite

To evaluate the long-term robustness of an epoxy composite loaded with (Al2O3+ SiO2) particles, Bagci [113] studied the composite's erosive wear characteristics. In this experiment, three different impinging velocities of 23, 34, and 53 m/s were used together utilising three distinct impact angles of 30°, 60°, and 90°°s with an erodent particle size of 200 µm. The findings were achieved when the experiment was conducted out while the temperature was set at room temperature. Because Taguchi's experiment was designed the way it was, we are aware of the results of the experiment. In terms of its ability to resist erosion, it is abundantly obvious that a filled composite produced using the 45/45/45 fibre arrangement performs better than an unfilled composite. The study's conclusions state that delamination of the material's surface at different stages causes erosion wear. Microcracking appears on the substrate's surface after that. It makes no difference how rapid the impact is; the rate of erosion is anywhere from two to three times faster when the velocity of the impact is higher.

Researchers claim that Bagci and Imrek [114] developed a distinctive epoxy resin composite material with GFR. This material was put through a series of tests to determine how well it withstood wear after boric acid was added as a filler ingredient. Impact velocities, particle sizes of the erodent, and angles of the composite impingement were all varied along various fibre directions for the analysis of the composites. The orthogonal array that Taguchi created was applied to the problem of determining how the influence of various parameters may be employed to minimise the erosion rate. The specifications given in ASTM G76-07 were adhered to in order to carry out the erosion wear test. The addition of the boric acid particles caused a solid bond to form between the epoxy matrix and the boric acid particles, increasing the composite's hardness and strength and reducing the rate of erosive wear and erosion. The highest erosion rate of 30% was observed across all of the samples, regardless of the other variables. Erosion can be slowed down even more by increasing the angle of impingement. The significance of an object's impact velocity grew in direct proportion to its wear rate.

2.10 Impact of particle size and fibre orientation on erosion rate of polymer matrix composites

Recent studies have shown that larger abrasive particles wear out more quickly than smaller ones do. This was determined by comparing the two sizes of abrasive particles. Alterations in fibre orientation, along with a number of other factors, have the potential to have an impact on the rate of erosion experienced by polymer matrix composites. Refer to the second publication

that Bagci and Imrek [115] have written if you are interested in learning more about the solid particle erosion behaviour of a glass fibre epoxy (GF/EP) composite material filled with borax (B2O3) particles. Experiments were carried out utilising erodible Al2O3 particles in a selection of different working settings. These circumstances included 23, 34, and 53 m/s impact velocities, 30°, 60 and 90 impact angle and 0° fibre orientation. In this study, the impacts of a number of various operational factors on the erosion rate were explored using the Taguchi method. Taguchi analysis was used to determine the ideal values for the impact angle, erodent size, erodent velocity, and fabric orientation, which are all 90 °s, 200 µm, 23 m/s, and 45°, respectively. In line with Bagci and Imrek [115], their study examined the effects of erodent velocity, fibre direction, and impact angle on the performance of boric acid-filled composites. With the aid of a device that measures wear and erosion, the erosive behaviour of the polymer composite was assessed at impact angles of 30° and 90°.

The strength of GF/EP composites is significantly reduced when boric acid is added to the mix. The fibre matrix bonding limits in GF/EP composites filled with boric acid cause the filled composite to erode more quickly than the empty composite. Because of this, the filled composite is the one that is recommended. Comparing filled and empty composites, it has been discovered that the former exhibit lower rates of erosion. This is due to the material that is used to make these composites has a high bonding strength.

2.11 Investigating the Effect of Fillers on the Tribological Properties of Polymer Composites

Fly ash cenosphere, a thermal power plant by-product, was utilised as a filler in the production of lightweight high-density polyethylene composites, which were later put to the test in operational settings. These composites are intended for use in aerospace and defence applications. The effectiveness of a constant load of 10 N applied for 10-40 seconds at sliding distances between 9.42 m and 37.88 m was found to be useful in determining wear on pin-on-disc devices. The sliding distances ranged from 9.42 m to 37.88 m. The measured distances ranged from 9.42 metres (m) to 37.88 metres (m). According to the results of the wear tests, adding more cenosphere to the composite materials significantly enhances their mechanical properties. In addition, the cenospheres that had been treated with silane might be included into the matrix in order to achieve desirable mechanical and tribological properties [116]. Patnaik and his colleagues [117] studied the tribological characteristics of GFR polyester composites filled with alumina. They discovered that these composites have advantageous tribological

qualities when compared to composites made entirely of glass and polyester, those made with alumina as filler had superior tribological behaviour. On the other hand, the manufacturing process has no effect on alumina-filled composites because these composites are impenetrable to fibre and matrix debonding.

The results of Sudheer and colleagues [118] show that adding graphite and potassium titanate whisker improved the mechanical and tribo-performance characteristics of fibre-reinforced epoxy composites. In order to carry out the experiment and determine the rate of wear that composites experience, Pin-on-disc equipment was utilised. During the course of the experiment, the following parameters were in play: The experiment was planned to take place with the following weight values and sliding speeds: 30 N load values, 5 m/s sliding speeds, and an initial sliding distance of 4.2 km. Throughout the experiment, load values of 30 N were utilised.

The erosive wear characteristics of epoxy composites made with wheat flour as a filler ingredient were examined in this particular research project [119]. Researchers were successful in making the matrix material more robust by employing the use of e-glass fibres. In order to produce the specimens, Various filler materials were used in amounts varying from 1 to 4 g of each. It has been discovered that increasing the percentage of wheat flour in a glass-fibre reinforced plastic (GFRP) composite results in a reduction in the composite's erosion resistance while simultaneously boosting the composite's mechanical qualities. The fact that the filler material inhibits the fibre matrix from debonding is the cause for this behaviour.

It was found that two elements that affected the variation in the erosion rate of the glass epoxy specimen were the specimen's impingement angle and the particle velocity.

The by-product of agricultural production was utilised by Rout and Satapathy [120] in the production of an epoxy polymer in the capacity of an active filler. The epoxy polymer was developed so that it would not be harmful to the surrounding ecosystem. To make the GF/EP composite more resistant to abrasion, rice husk particles were mixed in with the composite material. Throughout the production and testing processes, rose husk-filled composites were put through various types of testing, including erosion and mechanical testing. Within the scope of this study, Taguchi's (DOE) methodology was utilised in order to investigate the authors' findings. The hardness and tensile modulus of the material are significantly increased when fillers are added; however, the flexural and shear properties along with the tensile strength are significantly decreased. Aside from that, the hybrid composite possesses an extraordinary

resistance to erosive damage. Sudarshan et al. [121] evaluated the wear response and the interaction between the two components by examining CFRP with and without graphite filling. This was done in order to compare the two scenarios. To determine the relationship between the amount of filler and the amount of composite that is impinging, the erosive wear rate of a composite was measured in an experiment [122].

When impinged from the same direction, polymer composites—both filled and unfilled—exhibited semiductile wear activities, with the erosion rate being higher at a 45° angle for both types of material. In comparison to unfilled composites, graphite-filled composites had significantly lower erosive wear resistance. According to the findings of the study, the most common causes of wear damage in graphite-filled composites were microcracking and cutting, matrix delamination, and the absence of a link between the matrix and the fibre. Zahavi and his colleagues [84] investigated the mechanical and erosion wear metrics of aluminum nitri defilled composites as a means of gaining a deeper comprehension of the properties of the material. When manufacturing composites with an epoxy matrix and filler inclusions, the use of glass fibre reinforcement was utilised in the process of providing reinforcement. The orthogonal array was developed by Taguchi in order to assist in the identification of the components that contribute to erosion wear [102].

In spite of the material having a lower tensile strength, increasing the filler material content improves the material's hardness as well as the erosion wear properties. The results of these investigations show that the impact velocity is the factor that most significantly affects the rate of erosion.

2.12 Summary

The literature review discusses erosion and degradation of glass fibre-reinforced polymer composites when exposed to seawater, leading to mass gain, loss of mechanical strength, and degradation of the fibre-matrix interface. To address this, the study suggests the use of erosive-resistant polymeric coatings, and novel materials that improve the erosion resistance of composite materials. The gap in the literature is the need for investigations on the application of hybrid composite coatings and even more technologically advanced materials for tidal turbine blades to achieve sustainable development.

Therefore, this thesis studied the effects of erosion on new toughened and standard UD-GFRP and coatings by examining different parameters such as impact angle, impact velocity, particle size, and fibre orientation. The erosion mechanism was investigated using SEM and advanced

optical microscope, and an erosion map was generated to fully understand how erosion affected the tidal turbine blades.

Chapter Three

Research Methodology

Chapter 3 Research Methodology

3.1 Introduction

This chapter on methodology thoroughly explains the procedures and strategies employed in this study. This chapter comprehensively discusses the research methods employed, including analysis, data collection, and meticulous observation. Planning ahead thoroughly will help ensure that the research's analysis, computations, data collection, and conclusions were all correct. Before diving into the actual methodology, the guiding principles of the study will be discussed. A practical approach to the research is then detailed. The research's procedures for testing hypotheses, obtaining background material, and compiling data are then described in depth. To top it all off, the method considers the study's overall reach and limitations, laying a firm groundwork for further exploration and development.

3.2 Research Approach

The main objective of this study is to identify the various causes of erosion in tidal turbine blades and propose practical strategies that can be implemented to address this issue. It is imperative to understand the reasons behind the erosion of turbine blades as they play a significant role in generating clean and renewable energy.

As part of this study, various activities were undertaken, and these activities have contributed towards the generation of relevant data and claims that are pertinent to the research. Due to the nature of the research, an inductive research approach is considered appropriate. This is because the research is exploratory in nature, and the primary aim is to generate new insights and understandings that can be used to develop practical strategies to address the issue of erosion in tidal turbine blades.

An inductive research strategy also enables the development of a more thorough understanding of the phenomena being studied. The approach is based on observation and the collection of data, which is then analysed to develop new insights and theories. This method is particularly useful when investigating new or unexplored areas of research, as it allows the researcher to develop a deep understanding of the issues under investigation.

In conclusion, the adoption of an inductive research approach is not only acceptable but also necessary for this study, given its exploratory nature. The study aims to develop practical strategies for addressing the issue of erosion in tidal turbine blades, which is crucial for the continued development and growth of clean and renewable energy sources.

3.3 Research Method

In this study, artificial erosion techniques will be employed to simulate the effects of erosion on tidal turbine blades. Polymers, which are commonly used as materials for turbine blades, are known to become more brittle when subjected to erosion. Therefore, in this study, the blade material will be subjected to artificial erosion techniques to mimic the effects of erosion on the blades. This will enable us to evaluate the effects of erosion on the blades and develop appropriate strategies to mitigate this issue.

It is essential to protect the base material of the tidal turbine blades, which is Glass Fibre Reinforced Polymer (GFRP), with a coating material to reduce the rate of deterioration caused by erosion. A study conducted by Rasool and Stack [11] found that the use of a suitable coating material can significantly reduce erosion on turbine blades. Therefore, in this study, we will apply a suitable coating material on the GFRP base material of the turbine blades and evaluate its effectiveness in reducing erosion.

To ensure the quality and reliability of the data obtained, erosion maps, depth profiling and experimental approaches will be utilised as research methods. Erosion maps are an essential tool for identifying the areas of the turbine blades that are most susceptible to erosion [123]. This information can be used to develop effective strategies to mitigate the effects of erosion. Experimental approaches, on the other hand, enable us to evaluate the effectiveness of different composite and coating materials and other protective strategies in reducing erosion.

By using both erosion maps and experimental approaches as research methods, a more thorough evaluation of the data sets can be achieved. This approach will enable us to develop a deeper understanding of the mechanisms that contribute to erosion in turbine blades and develop effective strategies to mitigate this issue.

In conclusion, the utilisation of artificial erosion techniques, the use of a suitable coating material to protect the base material of the blades, and the implementation of both erosion maps and experimental approaches as research methods have improved the quality of this study. These methods have allowed for a more comprehensive evaluation of the data sets, enabling to develop effective strategies to address the issue of erosion in tidal turbine blades.

3.4 Data

3.4.1 Data Collection

The aim of this study was to gather primary data through experimentation, which was essential to developing a deeper understanding of the issue of erosion in tidal turbine blades. To achieve this, a number of features of the experiment were evaluated, including the measurement of relevant variables and parameters that were critical to the success of the study. These features were carefully selected to ensure that they accurately reflected the conditions of erosion in the blades of a tidal turbine.

In addition to the primary data obtained through experimentation, this study also relied on secondary data sources, which were obtained through a literature review. This literature review included the specifications and qualities of the Glass Fibre Reinforced Polymer (GFRP) and the coating material that was utilised in the experiment. These secondary data sources were instrumental in providing additional context and information that was necessary for the research study.

The combination of primary and secondary data sources allowed for a more comprehensive analysis of the experiment and a deeper understanding of the issue of erosion in tidal turbine blades. The primary data obtained through the experiment provided detailed information about the effects of erosion on the blades, while the secondary data sources provided context and additional information about the materials and conditions being studied.

By combining primary and secondary data sources, this study was able to generate a comprehensive data set that was used to accomplish the purpose of the research study. This data set was then analysed to identify the causes of erosion in tidal turbine blades and propose practical strategies for addressing this issue.

In summary, the success of this research study required the use of both primary and secondary data sources. The primary data obtained through experimentation provided detailed information about the effects of erosion on the blades of a tidal turbine, while the secondary data sources provided context and additional information necessary for a comprehensive analysis of the data. This approach allowed for a more thorough evaluation of the data sets, enabling us to develop effective strategies to address the issue of erosion in tidal turbine blades.

3.4.2 Data Analysis

Once the process of generating the data was completed, the next step was to undertake an analysis of the data. Initially, the data was entered into a log sheet and then transferred into an Excel file. This was done to ensure that the data was accurately recorded and organised in a way that would facilitate further analysis.

To analyse the data, a variety of methods were utilised. First, the material was scanned under a scanning electron microscope and an optical microscope. This allowed for a closer examination of the erosion patterns and the structure of the material. The data obtained from the experiments were then analysed by MATLAB, to create erosion maps.

Additionally, the structure of the graphs obtained from the experimental data was examined to identify any trends or patterns. Statistical analysis was also performed on the data to further investigate the relationships between the variables being studied.

The combination of these analysis techniques allowed for a comprehensive evaluation of the data and provided a deeper understanding of the mechanisms of erosion in tidal turbine blades. By utilising a variety of tools and methods, we were able to identify the causes of erosion and propose effective strategies for mitigating its effects.

Finally, the analysis of the data involved multiple steps and techniques, including the use of microscopes, image processing software, and statistical analysis. By utilising a variety of methods, we were able to generate a comprehensive data set that was used to identify the causes of erosion in tidal turbine blades and propose practical solutions to address this issue.

3.5 3Procedure and Experiments

3.5.1 Impingement Rig Test Set-Up
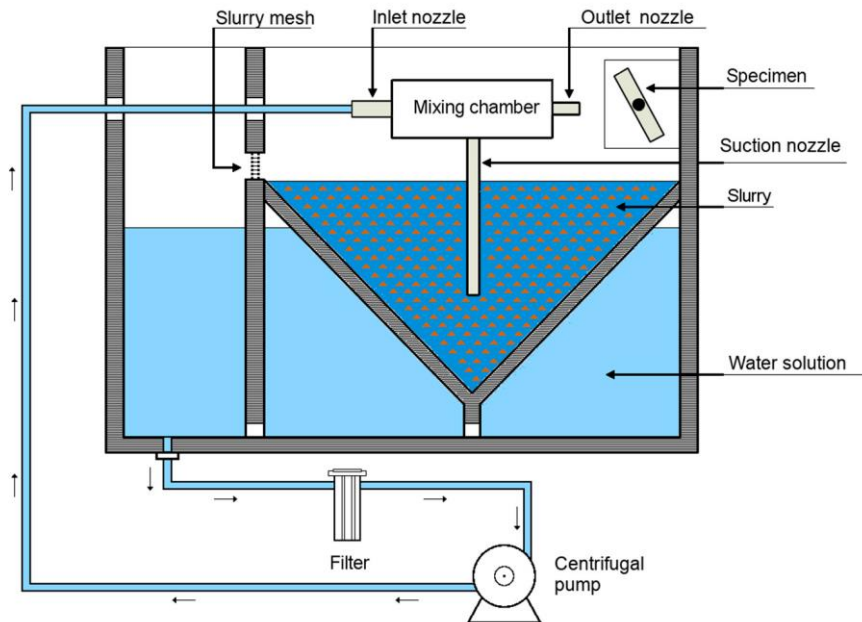
Figure 3. Impingement Rig Test Set-Up

For this kind of simulated testing, a slurry Jet rig is employed. The design principles presented by Hutchings [124] have been followed in the construction of the jet impingement rig. This testing apparatus is convenient for use in the laboratory or at home because it is easy to set up and use, takes little time, and allows for regulation of environmental factors. Fig. 3 shows how the rig is put together and how everything connects to one another.

The rig was built with efficiency in testing and results in mind. The rig's conical trapper is responsible for recirculating the sand once it has been impinged upon. As the slurry of saltwater and sand passes through the T-shaped nozzle, the negative pressure created by the nozzle causes the slurry to be sucked up, allowing for recirculation, and adjusting the ratio of seawater to sand. The cycle restarts when the sand and saltwater mixture are blasted through the nozzle and land in the trapper and the erosion products from the sample are retained within the filter. The sand in the rig system is circulated uniformly by 2 propellers that are connected to electric motors at the upper of the chamber and assist with mixing. Because of this, only need a small amount of sand for the 30 min test.

Both the conical trapper and the rig's framework are constructed from polypropylene. Because of its chemical resistance and its capacity to avoid corrosion of the rig from the repeated use of

saltwater, the use of this thermoplastic ensures the rig's longevity and allows for many testing cycles to be completed.

The sand and seawater in the rig can be separated with the use of a sieve sheet, allowing the water to be reused several times during the course of the test. For access to the saltwater storage tank, a hole is blasted out of the wall at the trapper's far end. The sheet of sieve is installed in the gap such that it corresponds to the gaps' unique dimensions. The holes in the sieve are large enough to let salt water through but too small for sand to get through. Yet, under actual circumstances, some sand particles quickly passed through the sieve as a result of the inter-particle collisions that occurred between the sand particles.

Because of this effect, the sand particles shatter and erode themselves, while the size of the erodent is reduced, resulting in smaller particles that are able to pass through the sieve. After going through the ejector, this salt water is delivered to the pumps using the network of pipes, and it is finally recycled. The use of polyvinyl chloride reinforced tubing in the production of pipes serves the purpose of preventing the pipe from becoming corroded.

Because of the way the rig was built, switching out the nozzles at the intake and outflow is much simpler than it would have been otherwise. Because of the need to exert precise control over the rate at which the slurry moves, the configuration of these nozzles is of the utmost importance. By utilising nozzles with a range of sizes, it is possible to adjust the flow velocity of the slurry at the rate that is needed. Because the speed of the pump that is being used is constant and cannot be adjusted as needed, the inlet and outlet nozzles that are being used in the rig have had their diameters adjusted. The difference in diameter between the nozzles needs to get bigger in proportion to the increasing ratio of D1/D2.

By drilling holes through the test material's holder and positioning the test material in the holder at the desired angle, the impingement angle can be controlled. This allows the holes to be drilled through the holder without affecting the test material. The screw in the holder allows the test material's position to be adjusted. As shown in the following fig. 4, this enables the holding of test material between the angles of $0°$ and $90°$, with the adjustment allowing for $15°$ increments.
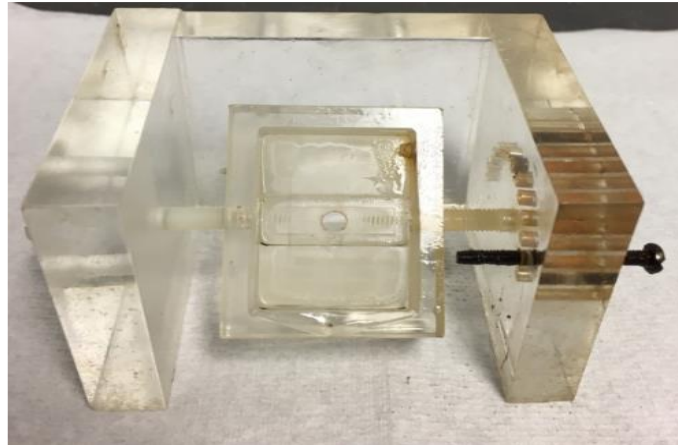
Figure 4. Sample Holder

In order to prevent the pump from overheating and failing the test, an uninterrupted running of the testing for no longer than 30 mins is the maximum amount of time that is recommended. Due to the fact that the pump won't get too hot during this recommended running time of 30 mins, it will be able to withstand being put through a battery of different kinds of testing. This keeps the mechanism of the pump and its motor in good working order, which protects the motor from malfunctions as well as faults caused by the pump in the test, and it ensures accurate measurement of the results of the test.

Because of this, there will be a significant temperature differential in the trapper, which is responsible for the modification of the composite properties. This will have an impact on the characteristics and type of erosion in the test material. As a result, the results of the test and the features of the erosion may not be accurate due to the presence of an accidental variable. Also, as a result of this, the simulated environment was in a deceptive state, and the coastal condition
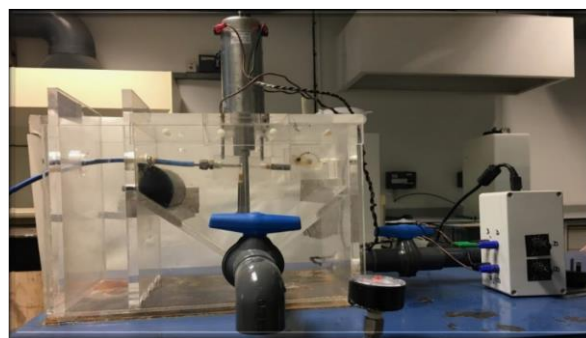
Figure 5. Impinging Jet rig setup

of the

sea water environment was different, both of which contributed to the potential for increased inadequacy in the erosion process.

Figure. 5 shows the impinging jet rig's configuration. Sand and salt water are trapped within the chamber by the V-shaped wall sides, which serve as a trap. The rig's top-mounted propellers maintain the flow of the sand-and-seawater mixture from the vertically positioned entrance of the T-piece ejector. The two connected electric motors at the top of the rig power these propellers. Each electric motor has its own speed control, as can be seen in Fig. 5. The position of the filter, which is at the very top of the sloping wall on the left, serves to prevent sand from reaching the pump so that only salt water can pass through it. After that, the sand travels through the slit to the following compartment, which is found on the extreme left side.

The hole acts as a passageway for the seawater flow, which passes through the compartment's bottom, travels to the pump via the pipes, and is then redirected by the blue piping. Figure 5 shows how the blue piping is passing through the compartment's perforations on its way to the T-shaped nozzle. Only 10 litres of water are added to the tank to prevent the mixture from overflowing the compartment openings. This will ensure that the overflowing of the mixture will stop.

Seawater flows through the horizontal portion of the T-piece ejector while a negative pressure is created in the vertical pipe. Because the T-horizontal piece's section is horizontal, this is the case. Sand is drawn out of the V-shaped catcher as a result of the vertical pipe's suction force being created by this negative pressure. After being sucked up, the sand moves into the T-horizontal piece's pipes where it combines with the salt water.

After the testing material has been positioned and secured within the rectangular specimen container, the nozzle will next discharge the slurry that has been thoroughly mixed onto the testing material. The angle of impingement is established by where the screw is positioned within the intended hole in the material. The screw also contributes to the holder's tightness by binding the material together and pressing it up against the holder's wall, preventing it from being pulled free by the force of the slurry. The rig is equipped with two roof parts to ensure that the testing chamber is hermetically sealed. These roof parts hold the T-piece ejector as well as the electric motors and are responsible for hermetically sealing the slurry.
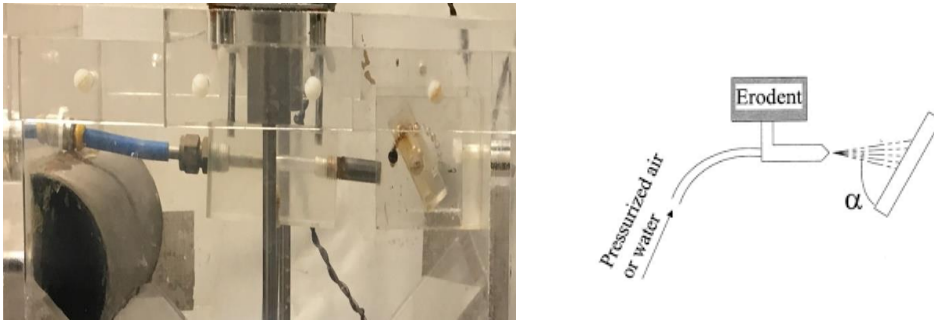
Figure 6. close-up of the sample holder and ejector nozzle

3.5.2 Rig Calibration

The rig was carefully calibrated to ensure that the desired velocities were achieved. This was done by first measuring the volume of water in the rig, and then using a timer to record the elapsed time and final volume of water in a separate container using a hose. By subtracting the initial volume from the final volume of water that flowed through the container, this determined the volume of water that passed through the rig.

The final step involved using the formula below to calculate the velocity of the water flow.

$$V = \frac{Q}{A} \qquad \textit{Equation (1)}$$

where is **'v'** is the velocity, **'Q'** is the flow rate and **'A'** is a cross-sectional area of the flow path. By dividing the flow rate by the flow path's cross-sectional area, the velocity of the water flow was determined. To increase the accuracy of the results, the steps above were repeated three times.

The ratio of D1/D2, which refers to the diameters of the inlet and outlet nozzles, plays a significant role in influencing the velocity of the slurry within the impingement rig. This ratio directly impacts the flow rate of the slurry through the system. To explain the relationship between the D1/D2 ratio and the velocity, it's important to note that the velocity of fluid flow is intricately connected to the cross-sectional area of the flow path. As indicated by Equation (1), the velocity 'v' is calculated by dividing the flow rate 'Q' by the cross-sectional area 'A'. In the context of the impingement rig, altering the nozzle diameters (D1 and D2) modifies the cross-sectional area of the flow path.

When the D1/D2 ratio is changed, the flow rate 'Q' remains constant due to the constant speed of the pump. However, by adjusting the nozzle diameters, the cross-sectional area 'A' of the flow path is altered. This directly influences the calculated velocity 'v'. As the D1/D2 ratio increases, the flow path's cross-sectional area decreases, resulting in an increase in velocity. Conversely, when the D1/D2 ratio decreases, the flow path area increases, leading to a decrease in velocity.

Overall, this careful calibration and measurement process allowed to obtain precise data on the velocity of water flow in the Jet rig.

3.5.3 Slurry

In the sixty years that have passed, numerous slurry erosion testing procedures have been developed and put into use [124]. The use of an impinging jet method is recommended as the appropriate approach for measuring the slurry erosion in the material due to all of the reasons that are outlined in this study. The impinging jet method's effective and adaptable process gives users control over the parameters and variables of erosion. Because of its effectiveness and adaptability, this method is dependable and ideal for testing purposes and studies of parameter effects. The impinging jet method can be propelled by either compressed gas or a pump. It consists of an ejector and nozzles, both of which assist in the regulation of the speed at which the slurry is moving. The ejector and the nozzles both have the responsibility of regulating the speed of the slurry so that it can be propelled at the desired speed. In the jet erosion test, it will come across three different types of erosion: surface erosion, bulk erosion, and erosion of flakes. If there are circular flakes that are less than 0.5 mm thick and a diameter between 1 and 3 mm strike the substance, erosion by flake occurs. This test is very useful because only the testing specimen, which is fixed and locked in the holder, is affected by erosion. At the chosen location, the material is stroked with the slurry, which confines erosion to that region.

The mass of erodent, the size of the test specimen, and the required energy are all kept to a minimum when conducting the ejector slurry test. The difference in size between the input and output nozzles is what allows the concentration of the particles to be managed.
The slurry moves quickly through the ejector, creating a negative pressure that causes the T-piece ejector to draw solid particles from the mixing chamber into itself. This ensures that the erodent is properly mixed with the slurry. The slurry that was utilised in the experiment was generated by combining the salt water and the silica sand in a mixing container. The running

saltwater with a salt concentration of 3.5% was combined with silica sand whose particle size ranged from 300 to 600 µm.

In addition, the parameters, such as velocity, slurry concentration, and impinging angle, can be easily adjusted and altered, which contributes to the repeatability of the equipment in an effective manner.

3.5.4 Sand Analysis

Before beginning the process of investigation, an image of raw sands was captured using a scanning electron microscope (SEM) so that the grain structure of the sand particles could be observed. In the experiment, the solid particle erodent that was employed was composed primarily of sand particles that contained a significant amount of silica. The sizes of the particles that made up the sand ranged anywhere from 150 to 900 µm. In accordance with ISO 3310-1 the sand were separated by sieving the sand with a Matest device fig. 7 to achieve the sand particles within the range of 300 to 600 µm. This was done so that the picture could accurately depict the condition of the Seawater.

Figure 7. Matest sieve shaker

Firstly, it was determined, based on Fig. 8 obtained from the SEM, that the sand particles have an irregular structure with sharp edges. When they come into contact with the surface of the material, these sharp edges cause erosion to occur. The material's surface develops dents and scratches as a result of the constant impact from these pointed and sharp sand particles, as well as the chipping away of material from the surface, which results in the erosion of the blades. In order to carry out the experiment, the sand particles were collected at a concentration of 3%. The pointed corners of the sand particles become rounded off as a result of repeated impact with the surface of the sample. Moreover, the size of the sand particles is often reduced as a

result of collisions that occur between the sand particles themselves. The reduction in the number of sharp edges may be seen in the following Fig. 8 scanning electron micrograph of the sand particles that was taken after the experiment.

Sand with a silica content of no. 60 was chosen to serve as the eroding agent for the series of tests (Minerals Marketing). To replicate the severe wear conditions that tidal turbines may be subjected to, particles with diameters ranging from 300 to 600 µm must be used.

It has been demonstrated that the simple and frequently used term "circularity" significantly correlates with wear rate. Developed by Riley in 1941 [125], the area and perimeter of the particle's two-dimensional representation are both considered by the circularity factor.

The equation for the circularity factor is as follows:

$$CF = \frac{4\,\pi A}{P2} \qquad\qquad \textit{Equation (2)}$$

where is P denotes the perimeter of the particle and A denotes the area of the particle's two-dimensional representation.

According to Equation (2), the circularity factor becomes closer and closer to the value of 1 as the shape of the particle gets closer and closer to being a perfect circle. The images of the particles, magnified to a factor of 100, were obtained. GIMP 2.8 was used to prepare the photos for study, and after that, Matlab was used to calculate the images' perimeter, area, and circularity factor (CF). The CF was averaged out to be 0.819 after the test. The angularity scale developed by Macleod [126] was utilised in order to tie the phrases "angular" and "rounded" to CF values. This was done because particles are frequently described as being either angular or rounded in wear studies without the use of a CF value.
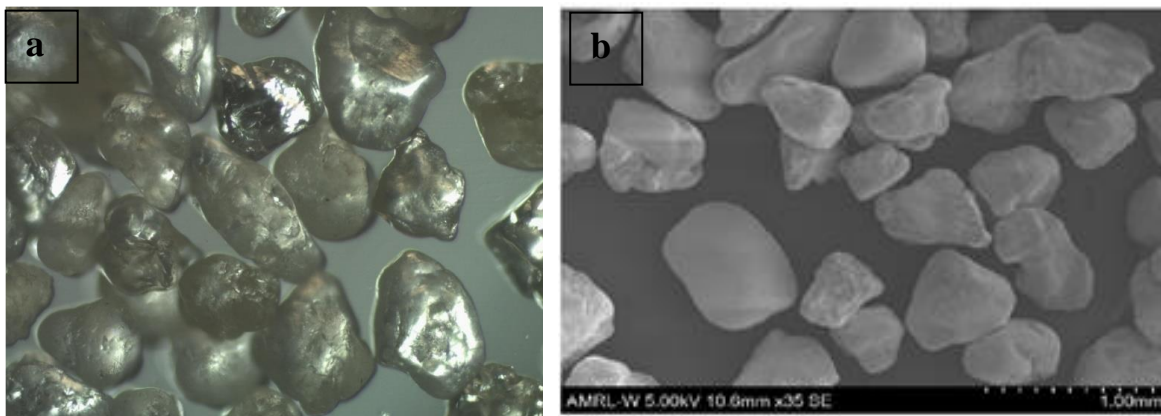
Figure 8. (a) Before, (b) After the experiment, image of sand particles

Drawings of particles are included on the angularity scale, and they match to descriptions that range from well-rounded to angular. The well-established technique for CF analysis was followed throughout the processing and analysis of these drawings.

The particles that are utilised in erosion tests are put through a series of hits, which causes them to frequently splinter and lose their angularity. These alterations in form and dimensions have the potential to have a major impact on the eroding mechanism [127]–[129]. In order to determine whether or not the aforementioned phenomenon was present in the experiments that were carried out and presented in this study, the particles that were used in the erosion tests that lasted for 30 minutes were collected, washed, and dried. At least 30 particles were examined using the standard operating procedure that had been developed beforehand to find out the CF factor and the change in particles shapes after the test.

42

Chapter Four

Investigating Erosion Characteristics of UD-GFRP Composites with Varied Fibre Orientations

Chapter 4 Investigating Erosion Characteristics of UD-GFRP Composites with Varied Fibre Orientations

4.1 Overview

The increasing demand for energy has prompted the exploration and utilization of various sources of energy generation. As solar and hydropower continue to dominate the renewable energy sector, efforts are being made to develop technologies that can effectively harness these energy sources. Marine energy, which uses the tides and pressure of the ocean, could become a good way to make electricity. However, there are significant challenges that need to be addressed before it can be fully utilised. One of the major challenges is the effect of erosion on tidal turbine blades, which remain underwater for prolonged periods of time [48].

The harsh ocean environment, characterised by salty sea air, presents a significant challenge to the durability of marine energy devices [130]. Even metals typically known for their strength and durability, such as iron, steel, and aluminium, can corrode and eventually fail in this environment [52]. Polymer and fibre composites have been proposed as a possible solution to reduce the likelihood of failure, but these materials are also susceptible to degradation that can impact their physical and chemical properties [12].

To make marine energy a viable option for energy generation, it is necessary to develop materials that can withstand the harsh ocean environment and the constant exposure to saltwater. Ongoing research is being conducted to develop novel materials that can effectively mitigate erosion and degradation in marine energy devices and enhance their overall durability and performance [131].

This chapter study aims to comprehend the erosion phenomenon on UD-GFRP materials and utilises empirical data obtained through experiments utilising sand particles as the eroding agent. The study employs a slurry impingement jet test device, as described in Chapter 3, to perform erosion tests on test specimens with different UD-GFRP fibre orientations at various impingement angles.

4.2 Experimental Setup

The experiment conducted to simulate the conditions experienced by tidal turbines used the Jet rig, which is shown in Figure 3 of Chapter 3. The aim was to assess the impact of various factors on the performance of tidal turbines. The study was conducted at various impact angles of 15°, 30°, 45°, 60°, 75°, and 90°, and at an impact velocity of 9.04m/s, the test duration was 30 min for each sample.

To replicate the natural environment, the experiment involved using a sand concentration of 3% and a salinity of 3.5%. The range of sand particles used in the test ranged between 300-600 μm, while the experiment was conducted at room temperature.

4.3 Results

The study examined how the UD-GFRP material resists erosion under different fibre orientations using a slurry of saltwater and sand of varying sizes. The results showed evidence of erosion, with most occurring between impingement angles of 45° and 60° at 0° fibre orientation.

The highest erosion rates were noted at an impact angle of 45° and peaked at 60°, indicating the significance of impact angle, particle size, and velocity. The examination also found many indentations and scrapes of varying depths [132]. Overall, the study provides insights into the erosion resistance of UD-GFRP at 0° and 90° fibre orientations and the factors that contribute to erosive wear [133].

Previous studies have indicated that submerging GFRP material can weaken its strength, as shown through tensile and compression tests [11]. Further research has also demonstrated that submerging the material increases erosion and defect count compared to unsubmerged samples [9], [12]. The experiment aimed to investigate erosion mechanisms, velocity patterns, and observation angles of solid particles. The results of this study could have big effects on the engineering field. Improving GFRP's ability to resist erosion while keeping its strength could make it a better choice for applications that need high strength, stiffness, lightweight, durability, and resistance to erosion. Overall, this study highlights the importance of developing erosion-resistant materials to meet the needs of tidal turbine blade applications [134].

4.3.1 Difference in Mass and Volume

The primary goal of this study was to investigate how erosion processes affect GFRP components used in maritime renewable energy systems. The research focused on solid particle erosion since previous literature had established that different types of erosion occur in marine environments [135], [136]. The study involved testing two types of GFRP samples, one with a 0° fibre orientation and the other with a 90° fibre orientation. Before conducting the experiment, the combined masses of the samples were determined. During the experiment, each sample was subjected to an impact velocity of 9.04 m/s one at a time.

4.3.1.1 Mass Difference
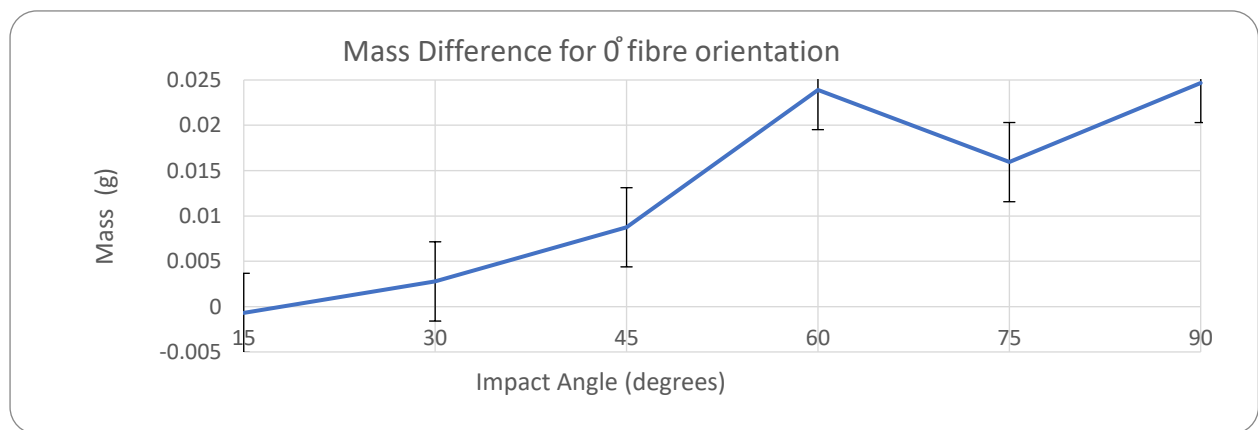
Figure 9. Mass Difference for 0° fibre orientation

The data presented in Fig. 9 reveals that the sample experienced a net increase in mass upon impingement at a 15°. This observation can be assigned to the high velocity of the collision, which resulted in the deposition of salt and other particles onto the surface of the GFRP specimen [10]. Further analysis of the erosion behaviour of 0° fibre oriented GFRP samples revealed that erosion occurred at a relatively slow rate when subjected to impingement at 15° and an impact velocity of 9.04 m/s. It is worth noting that impact velocity plays a crucial role in the phenomenon of erosion [137], [138], as demonstrated by the experimental findings. The preceding fig. 9 indicated the erosion frequency peaked at an impact angle of 60° to 90°. This phenomenon can be explained by both impact angle and surface strike rates. An increase in impact angle for the 0° fibre orientations led to a larger area being hit by particles, making the material more effective [139]. Particles stay on the surface for longer as a result of this increase, which subsequently removed material from the sample.
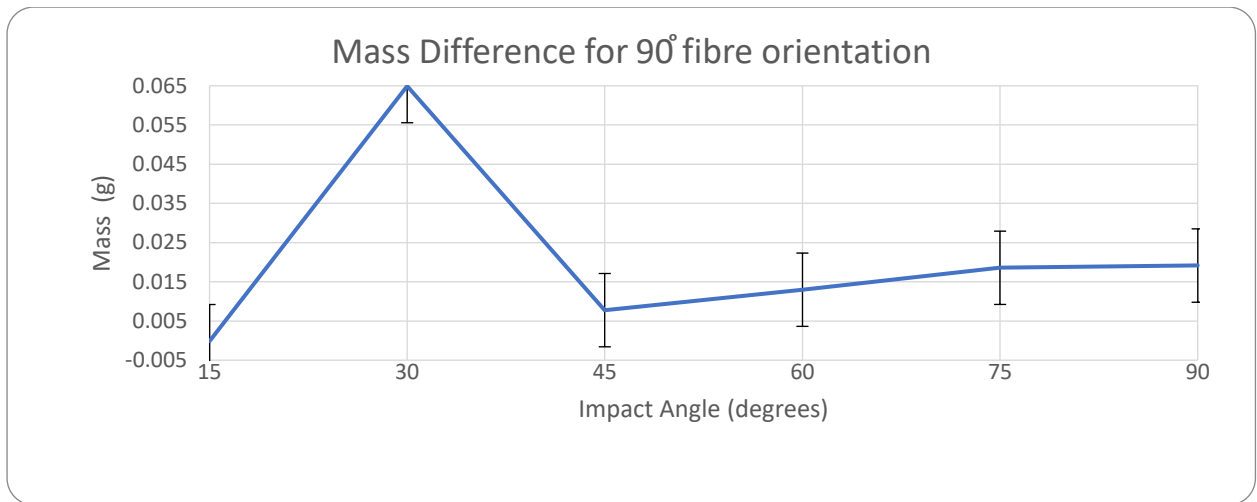
Figure 10. Mass Loss at various impact angles of 90° fibre orientation

From fig 10, it was observed that the sample with a 90° fibre orientation experienced a mass gain at an impingement angle of 15° due to the deposition of particles on its surface. This phenomenon can be attributed to the larger surface area that is struck by particles at this angle. Fig 10 shows that the rate of erosion for the 90° fibre orientation remains relatively constant between impingement angles of 45° and 90°.

4.3.1.2 Mass Difference 0° vs 90
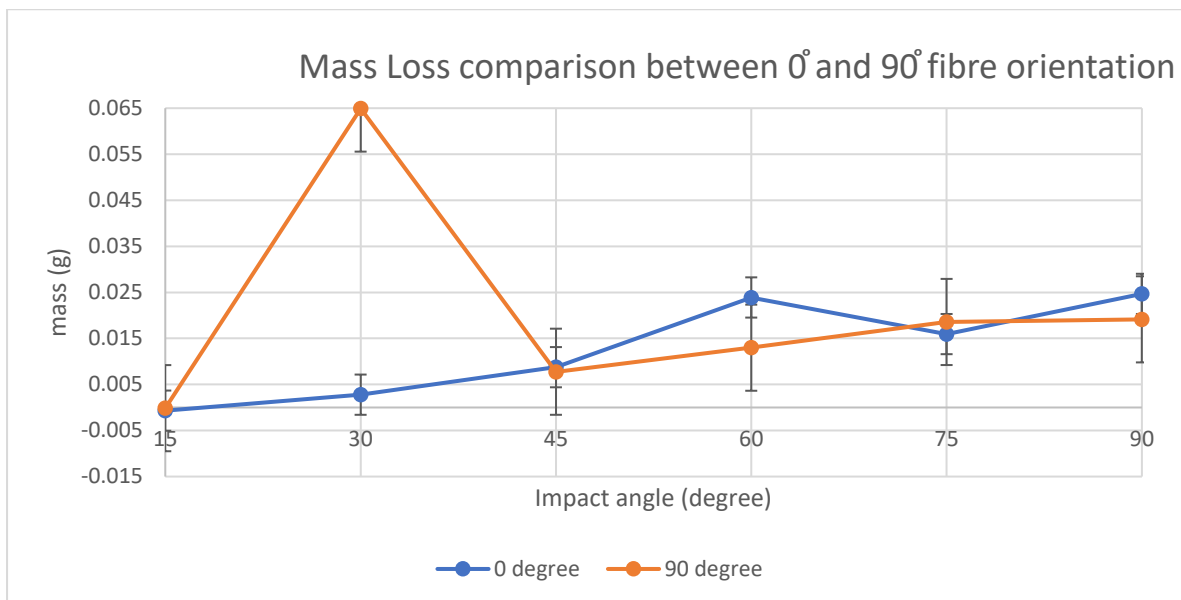
Figure 11. Mass Loss Comparison between 0° and 90° fibre orientation

Fig. 11 illustrates the erosion profile difference in 0° and 90° fibre orientation and compares their respective erosion mechanisms at different impingement angles. At an impingement angle of

15°, both types of GFRP experienced an increase in mass. The 0° fibre orientation exhibited a greater increase in mass compared to the sample with 90° fibre orientation. Neither sample exhibited any degradation at this particular angle.

The maximum mass loss for the 90° fibre orientation was found to be 0.65 g, while that for the 0° fibre orientation was 0.004 g. Furthermore, there was a notable variation in the mass loss between the two orientations. At an impingement angle of 45, both the 0 and 90 fibre orientations exhibited nearly identical mass loss, which was at its minimum for both types. Specifically, the mass loss for both orientations was 0.007 g.

Through a comparison of two types of UD-GFRP, it was found that at an impingement angle of 60, the mass loss for 0 fibre orientations was 0.023 g, whereas for 90° fibre orientations, it was 0.012 g. The difference in mass loss between the samples was found to be approximately 0.01 g. Moreover, the erosion rate for 0° fibre orientations was observed to approach the maximum value for that material at this particular angle.

When the angle of impact is 75°, the mass loss for both the 0° and 90° fibre orientations is similar. Specifically, the 0° fibre orientation experiences a mass loss of 0.016 g, while the 90° fibre orientation has a slightly higher mass loss of 0.0185 g. The overall trend of mass loss for UD-GFRP at this impingement angle is quite similar between the two fibre orientations. At the maximum impingement angle of 90°, the mass loss for the 0° fibre orientation is the highest, with a value of 0.0246 g. On the other hand, the mass loss for the 90° fibre orientation is 0.019 g, which is slightly lower. The higher mass loss for the 0° fibre orientation is attributed to its higher overlap. Despite this difference, the mass loss for the 90° fibre orientation is still very close to that of the 0° fibre orientation at this impingement angle.

Based on the findings on the relationship between mass loss and impingement angle and the comparison of erosion profiles between 0° and 90° fibre orientations, it can be concluded that the 90° fibre orientations exhibit a higher degree of mass loss compared to the 0° fibre orientations. This conclusion is supported by the available evidence. These results suggest that the mechanical properties of the 90° fibre orientations are relatively weaker than those of the 0° fibre orientations in UD-GFRP samples.

4.3.1.3 Volume Difference

At $0°$ fibre orientation and an impact velocity of 9.04 m/s experienced an increase in volume when impinged at $15°$. This can be attributed to the high impact velocity which led to the deposition of particles, particularly salt, onto the surface of the samples, expanding their volume and weight as a result. The formation of a crest on the impacted area provided evidence of the accumulation of solid particles originating from the erodent, leading to an increase in both mass and volume.

The data presented in Fig 9 allowed for the conclusion that the rate of volume loss is highest at impingement angles of $60°$ or $90°$, as erosion is the primary cause of volume loss. The impact angle and surface strike rate both contribute to this phenomenon [62]. The larger surface area struck by particles at higher angles leads to a more efficient erosion of the UD-GFRP material. This increased surface area also causes particles to remain on the surface for longer periods, further contributing to the material's removal [62]. Therefore, a larger volume of material is lost while covering a wider surface region.

Upon analysis, it was observed that at an impingement angle of $15°$, the sample with a $90°$ fibre orientation had increased in volume. This was attributed to the deposition of particles on the surface of the UD-GFRP sample, which occurred due to the higher impact velocity of 9.04m/s. Conversely, at an impact angle of $30°$, the $90°$ fibre orientation exhibited the highest volume loss during the erosion test, indicating that erosion was most severe at this angle. The volume loss observed at this angle was 0.025 cm3, which was significant in comparison to the other values of volume loss. These findings suggest that if UD-GFRP has a fibre orientation of $90°$ and is subjected to particles at an angle of $30°$, it would experience maximum erosion, rendering the material unsuitable for its intended application.

Based on the data presented in Fig 11, it was observed that for the $90°$ fibre orientation, the rate of deviation in volume remained relatively constant between impact angles of $45°$ and $90°$. Therefore, taking into consideration the characteristics of marine environments and the factors that contribute to erosion, it is recommended to use GFRP material in a way that minimises its impact on these environments.

4.4 Discussions

4.4.1 The influence of the angle of impact on erosion in saltwater containing particles.

The impact angle refers to the angle formed between the path of the particle and the surface of the sample [10], [83], [140], resulting in the turbine blades' normal angle of attack through the water. The investigation of impact angle is an essential and extensively researched parameter in the analysis of material erosion [124].

One practical application of this concept is in the study of tidal blades that are subject to erosion due to water impact. Research into the impact angle has been extensively conducted and has yielded important insights into the mechanics of material erosion.

4.4.2 Surface Analysis (SEM)

A scanning electron microscope (SEM) is a sophisticated imaging instrument that employs a high-energy electron beam to generate various signals from the surface region of a solid sample [141]. By providing excellent spatial resolution, SEM is a powerful tool for characterising specimens at length scales ranging from nanometres to µm. SEM is widely used in various fields of research, including materials science, biology, physics, and engineering [142]. With its ability to provide high-resolution images, SEM has become an indispensable tool for studying the morphology, structure, and composition of a wide range of samples [39].

4.4.2.1 Surface Analysis of 0° fibre orientation
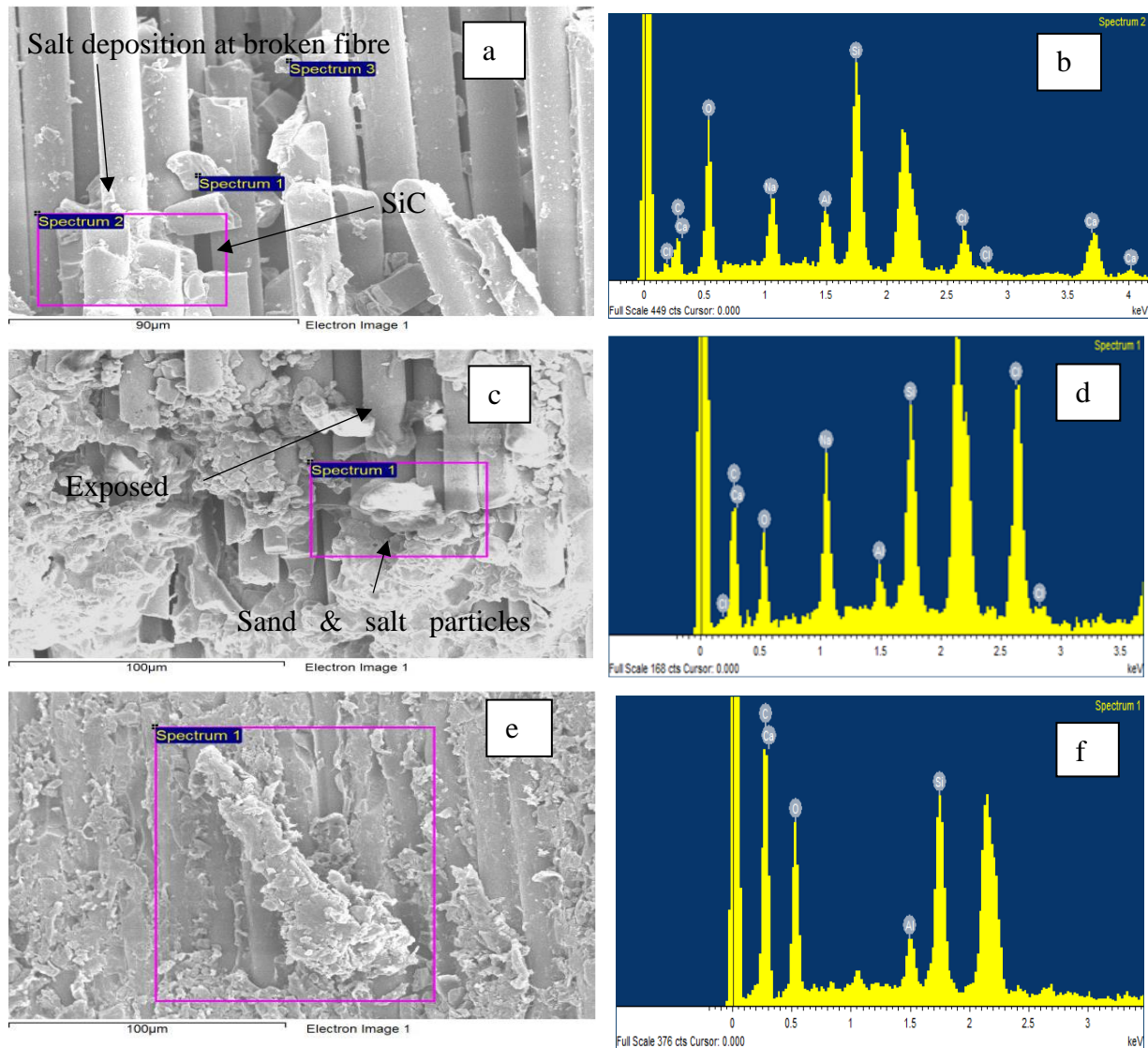
Figure 12. SEM & EDX of 0̊ fibre orientation at 45̊ impact angle

Figure 12 (a) provided evidence that the erosion of the 0̊ fibre orientation was caused by the degradation of the glass fibre matrix, which was established in the previous section. The displaced matrix further contributed to the erosion of the GFRP. The EDX Fig. 12 (b) indicated the presence of Silicon (Si) from silica sand and broken fibres in the fibre matrix interfaces. Additionally, the SEM image presented in fig. 12 (b) displayed the presence of Sodium (Na) and Chlorine (Cl) from Sodium Chloride (NaCl) salt.

Figure 12 (a) provides a clear illustration of the accumulation of salt within the damaged fibre. The image also reveals the presence of (SiC) from sand particles within the fibre matrix.

Figures 12 (c), illustrate the deposition of an external substance on the matrix. Through EDX analysis, it was discovered that sodium and chloride ions from the salt were present on the

49

fibre-matrix interface, as depicted in fig. 12 (d). The diffraction pattern of EDX confirmed this finding. On the other hand, Figure 12 (c) demonstrates the evidence of the erodent on the exposed matrix fibres due to erosion.

Figure 12 (e) depicts the deposition of silicon carbide (SiC) and a polymeric compound on the surface of the sample. The deterioration of the matrix was found to be a result of erosion, as evidenced by the presence of fine particles and a removed layer on the GFRP surface. The shredded structure of the composite fibres provided a location for the slurry particles to aggregate, which contributed to the deposition of SiC and the polymeric compound. This observation highlights the susceptibility of GFRP materials to erosion, which can lead to significant changes in their physical and mechanical properties.
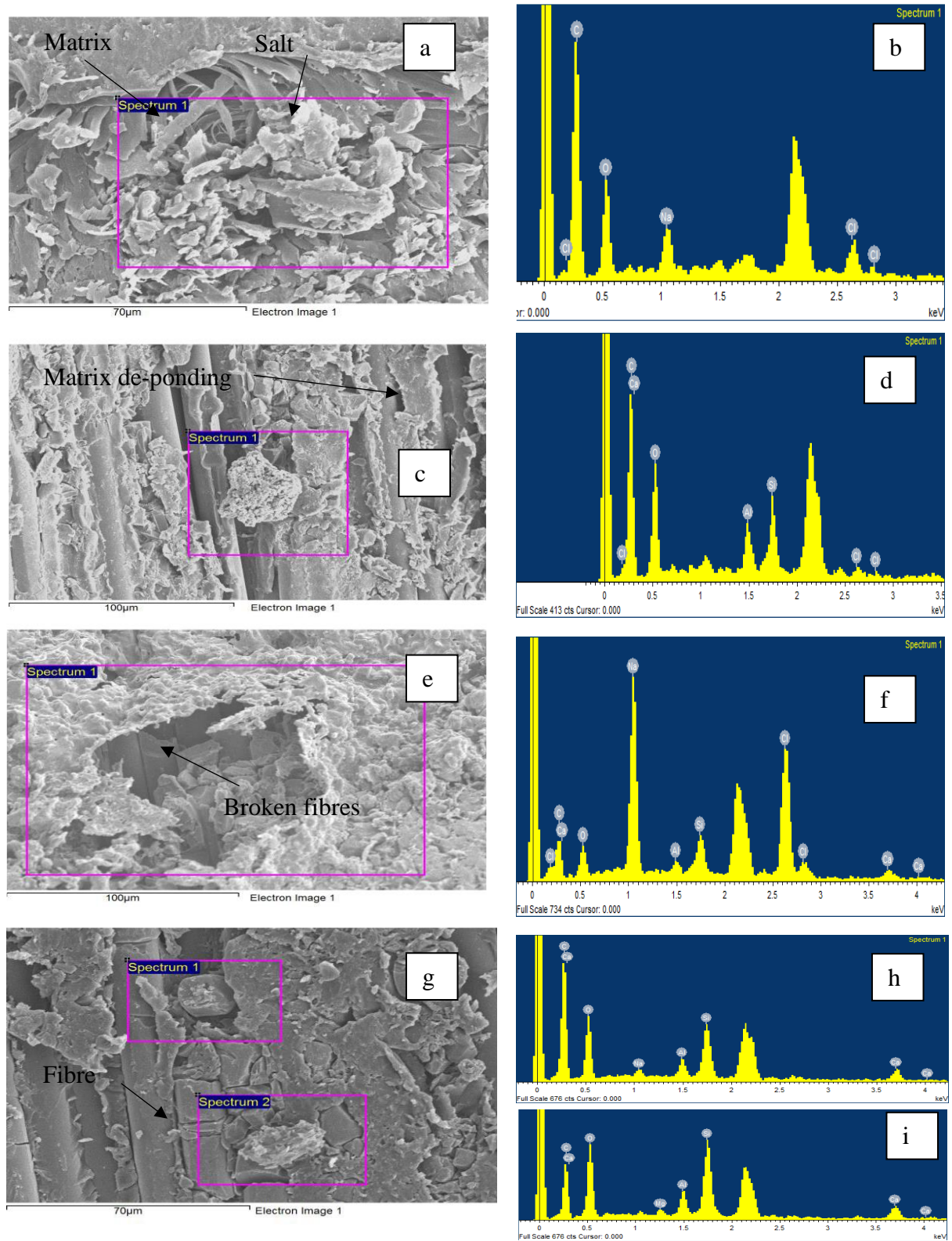
Figure 13. SEM & EDX of $0°$ fibre orientation at (a)(b) $60°$, (c)(d) $45°$, (e)(f)(g)(h)(i) $90°$ impact angle

Figure 13 (a) provides a detailed explanation of the erosion mechanism observed in the $0°$ fibre orientation sample. It was observed that the erosion caused the composites of the material to fracture, which was attributed to the erosive forces. The surface scraping revealed the inner

layer of the material, providing insight into the extent of erosion. This observation highlights the potential for erosive forces to cause significant damage to the composite structure of materials, which can ultimately affect their mechanical and physical properties [143].

Figure 13 (c) showed that the components in the erodent were what caused the glass fibres to scrape and erode laterally. Additionally, the deposition of salt particles on the surface of the (GFRP) composite is shown in Fig. 13 (d). The erosive forces exerted by the particles on the composite surface caused the fibre matrix to be de-boned, resulting in a separation of the fibres from the polymer composite[144]. This debonding effect made the glass fibres and the matrix vulnerable to damage and fracture, which could ultimately lead to a deterioration of the composite material's properties [145].

Figure 13 (e) clearly illustrates the extensive damage caused by solid particles to the surface layer of the UD-GFRP material, resulting in the exposure of its interior fibre matrix. Erosion caused the fibres located within the surface to break, and the protective outer layer of the polymeric composite underwent complete erosion. This, in turn, led to ductile erosion of the matrix layer of glass fibre linked to the surface[146], in the direction of the fibre's transverse axis. The breakdown of the fibres was followed by lateral erosion of the fibre matrix, resulting in the formation of voids and hollows within the matrix. This observation highlights the severe impact of erosion on the mechanical and structural properties of composite materials, which can lead to their deterioration and ultimately impact their performance in various applications [61].
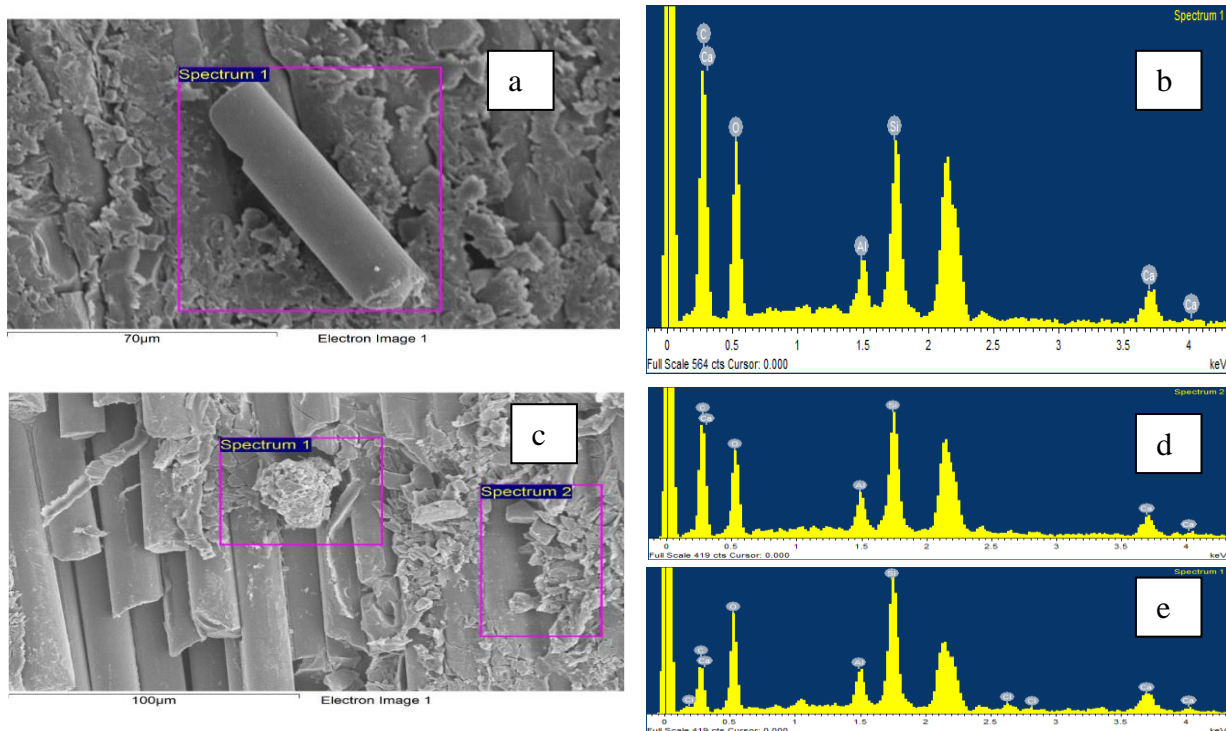
Figure 14. SEM & EDX of 0˙ fibre orientation at 75˙ impact angle

Figure 13 (g) depicts the deposition of erodent particles on the surface of the sample. Fig 13(h) shows the presence of salt particles at the interface, while fig. 13 (i) shows the composition of sand particles. During the erosion process, a fracture was identified on the glass fibres running in a transverse direction. The sharp-edged erodent particles caused the development of the fracture and erosion of the surface of the glass fibre. These cracks could potentially result in faults in the fibre composite material at a later stage, emphasising the need for a better understanding of the mechanisms involved in erosion processes in composite materials.

Figure 14 (a) illustrates the fragmentation of the fibre resulting from erosion. Figure 14 (b) displays evidence of the SiC particles' presence, which were found to have caused the fracture of fibre on the surface because of impingement on the GFRP.

The results presented in Fig. 14 (c) indicate that the impingement of particles on GFRP caused the complete breakage of the fibre matrix. Figure 14 (d) illustrates the presence of sand particles, while Figure 14 (e) reveals the complete breakage and de-bonding of the glass fibre, along with the presence of Chlorine (Cl).

The findings suggest that the impingement of particles on GFRP can cause significant damage to the fibre matrix, leading to complete breakage and de-bonding of the glass fibre [147]. The detection of Chlorine in Figure 14 (e) indicates the nature of the environment in which the

material is being used, which can play a crucial role in the type of particles that impinge on the material's surface. The results highlight the importance of considering the potential impact of impinging particles on the structural integrity of GFRP materials in various applications [123].

4.4.2.2 Surface Analysis of 90° fibre orientation
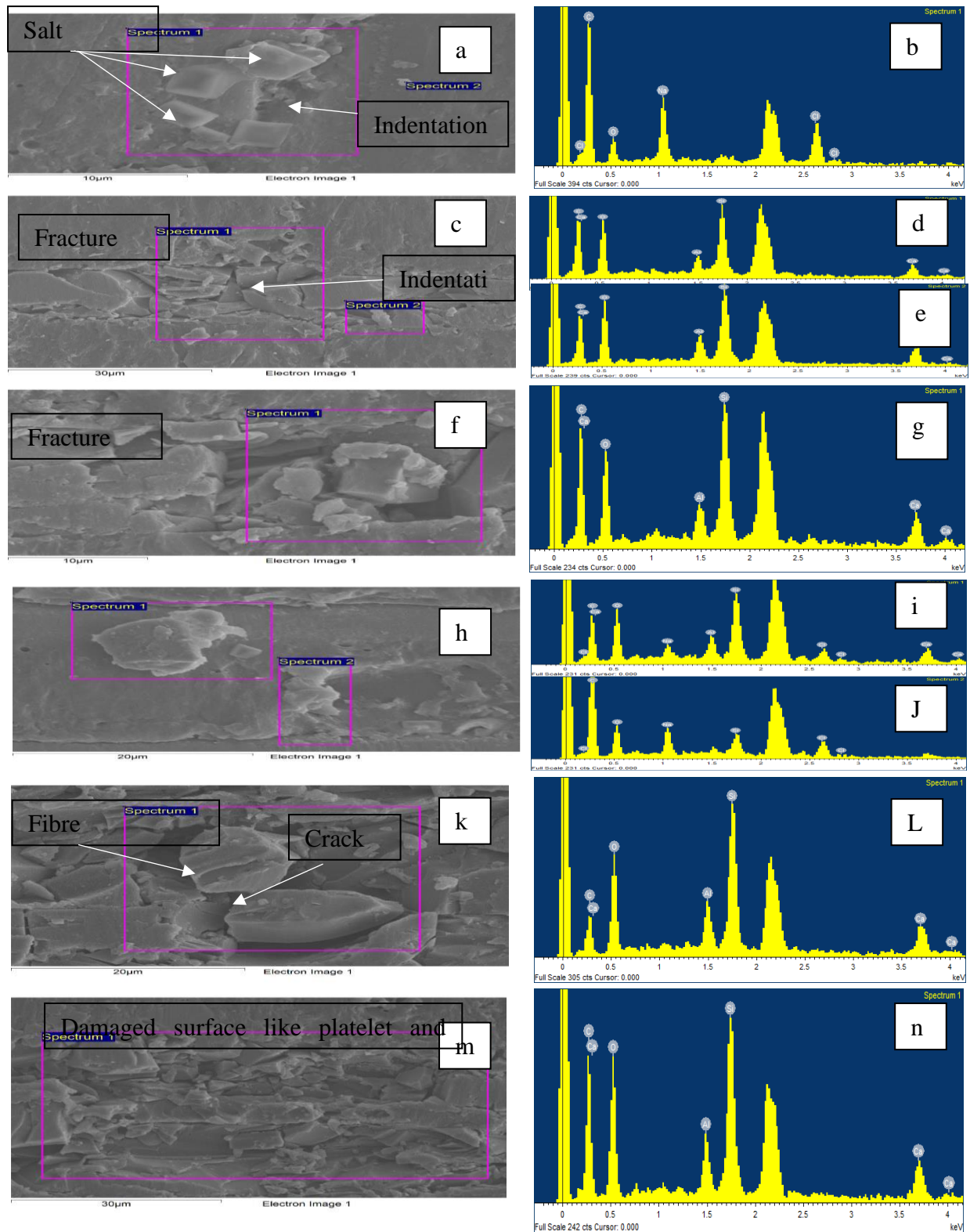
Figure 15. SEM & EDX of 90 fibre orientation, fig 15 (a)(b)(c)(d)(h)(i)(j)(m)(n)15 impact angle ; Fig 15 (f)(g) 4 impact angle Fig. 15 (k)(l) 90 at 15 impact angle

Figures 15 (a) and (b) illustrate the accumulation of salt crystals on the surface, let to the increase in the mass of the sample. To validate this occurrence, the test was repeated on two additional samples. These findings suggest that salt crystal deposition on the surface of composite materials could result in an increase in their mass, which may have implications for their performance and durability in various applications.

Based on fig. 15 (c), the erosion mechanism for the 90° fibre orientation occurred due to the breakage of the layer on the impinged area, which resulted in a brittle erosion mechanism [80], [146]. The figure clearly illustrates the erosion of the surface and the fracture of the surface, which supports this mechanism. Fig. 15 (d), (e) shows the presence of sand particles, indicating an increase in mass at 15°. These observations suggest that the presence of sand particles can contribute to erosion and mass gain in UD-GFRP composites, which could affect how long they last and how well they operate in different applications.

Figure 15 (f) provides a clear depiction of the scraping off materials during erosion in the UD-GFRP composite. Fig. 15 (g) supports this observation, showing the formation of particle chunks in the eroded area. The figure also demonstrates that the eroded particles remained in the cavity, suggesting that erosion can cause significant damage to the composite material, affecting its structural integrity and mechanical properties [12].

Figure 15 (h) provides a clear illustration of the erosion caused by salt particles. The figure shows the deposition of salt crystals on the surface layer with a 90° fibre orientation on the plain layer. Fig. 15 (i) provides evidence of the presence of salt particles at the interface. On the other hand, Fig. 15 (J) shows the presence of a cavity caused by the erosion of the material. The erosion caused by the salt particles led to the deposition of salt crystals on the cavity area, further damaging the material [51].

Figure 15 (k), (L) reveal the existence of Silica particles within the fracture of the composite. Additionally, the eroded section's crest exhibited shattered laminates of the UD-GFRP composite material. These observations suggest that the erosion mechanism caused a brittle fracture in the laminates, leading to the intrusion of sand particles [97].

Figure 15 (m) presents a clear description of the erosion phenomenon in the 90° fibre orientation. The erosion process causes multiple breakdowns of the matrix and the composite constituents. Fig 15 (n) confirmed the presence of sand particles, indicating a gain in mass in the 15° samples. The presence of sand particles is evidence of the erosion process, which causes the breakdown of the material.

4.4.3 Discussion

The results presented in Figures (12)(14) provide evidence that erosion can cause significant damage to GFRP materials, ultimately impacting their physical properties(Fouad et al., 2011). The findings suggest that the erosion of the GFRP material is caused by the degradation of the glass fibre matrix and the accumulation of salt, sand, and other particles on the material's surface. The presence of Silicon (Si), Sodium (Na), Chlorine (Cl), and Silicon carbide (SiC) particles in the fibre matrix interfaces and on the surface of the GFRP material indicates the nature of the environment in which the material is being used, which can play a crucial role in the type of particles that impinge on the material's surface [9], [148].

The results further demonstrate that erosive forces can cause the composites of the material to fracture, resulting in the exposure of the inner layer of the material. The breakdown of the fibres was followed by lateral erosion of the fibre matrix, resulting in the formation of voids and hollows within the matrix. The detection of Chlorine in Figure 14 (e) indicates the nature of the environment in which the material is being used, which can play a crucial role in the type of particles that impinge on the material's surface [149].

The observations highlight the severe impact of erosion on the mechanical and structural properties of composite materials, which can lead to their deterioration and ultimately impact their performance in various applications. Therefore, it is crucial to better understand the mechanisms involved in erosion processes in composite materials to develop effective strategies to minimise the impact of erosive forces on the structural integrity of these materials [132].

Based on the results presented in figure 15, it can be inferred that erosion, caused by both salt and sand particles, can significantly affect the structural integrity and mechanical properties of composites. The erosion mechanism in the $90°$ fibre orientation is found to be brittle, leading to the intrusion of sand particles and the deposition of salt crystals on the cavity area [62].

Furthermore, the increase in mass due to the deposition of salt crystals on the surface of composite materials could have implications for their performance and durability in various

applications. The presence of sand particles can also contribute to erosion and mass gain in UD-GFRP composites, further affecting their durability and performance [10].

The observation of eroded particles remaining in the cavity suggests that erosion can cause significant damage to the composite material, further affecting its structural integrity and mechanical properties. The erosion process causes multiple breakdowns of the matrix and composite constituents, leading to brittle fractures in the laminates and intrusion of sand particles[150].

Overall, these findings are crucial for understanding the behaviour of UD-GFRP composites in various applications and environments, particularly in coastal areas or locations with exposure to saltwater [151]. Engineers and designers can use this information to improve the performance and durability of composite materials by considering erosion-resistant designs and selecting appropriate materials for specific applications. Further research could investigate the impact of erosion on other types of composite materials and explore erosion-resistant coatings or treatments to mitigate the effects of erosion on composite materials[152].

4.5 Erosion Maps

In order to perform an erosion map of the UD-GFRP, a simulation was conducted using MATLAB. The purpose of this simulation was to generate an erosion map and patterns in UD-GFRP samples. To achieve this goal, a code was developed. This code allowed for the analysis and evaluation of the erosion process in UD-GFRP, providing valuable insights into the behaviour of the material under different conditions. The use of maps can be beneficial in providing a deeper understanding of the erosion mechanisms in composite materials [153], which can ultimately lead to the development of more robust and durable composite structures.

The findings from the erosion map in figure 16 demonstrate that the highest erosion occurs in the composite material when subjected to an impact angle in the range of $45°$ to $90°$ at an impact velocity of 9 m/s. This suggests that the UD-GFRP material is particularly vulnerable to erosion at high impingement velocities and angles. The dark blue colour in the image indicates the area that suffered the least amount of material loss during the erosion tests. This suggests that there are areas in the composite material that are less vulnerable to erosion and that these areas could potentially be reinforced to improve the overall erosion resistance of the material [154].
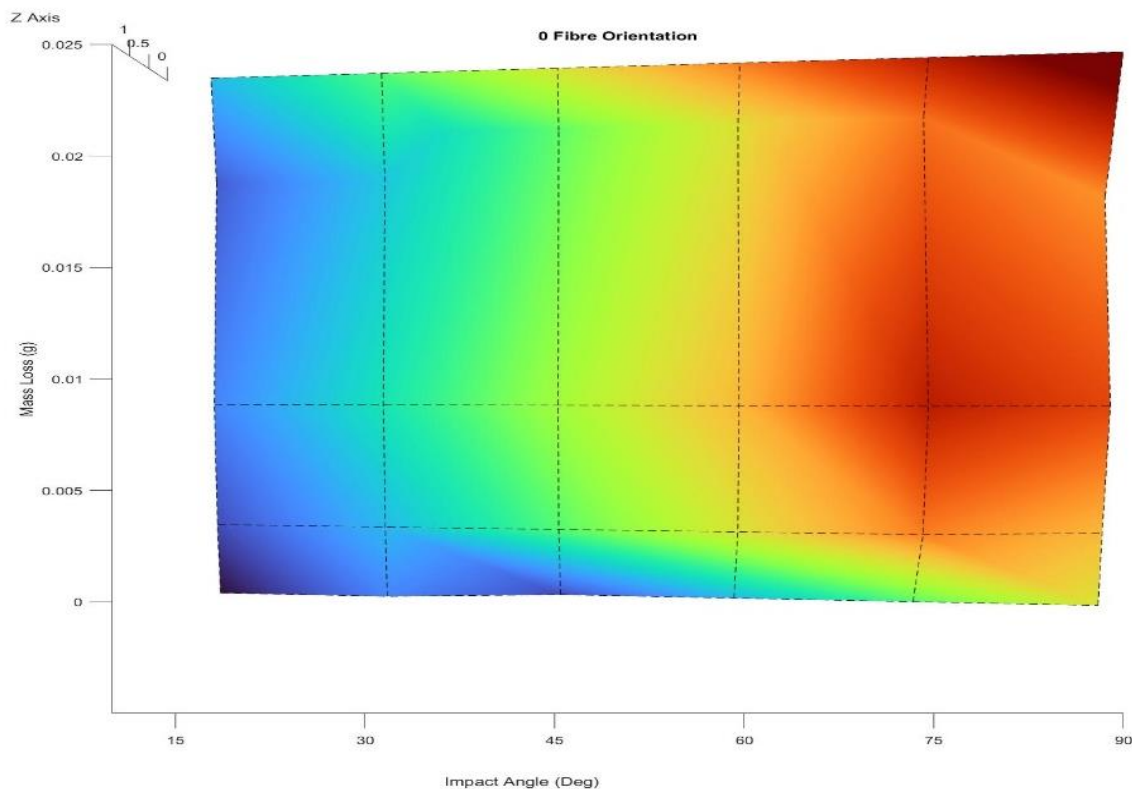
Figure 16. Erosion map of 0 fibre orientation

Additionally, the discovery that the GFRP material suffers the least amount of material loss when subjected to an impact with a velocity of 9.04 m/s and an impingement angle of either $15°$, $30°$, or $45°$ is significant because it suggests that there is an angle that can help to minimise erosion damage in the material. This information can be useful in the design of blades that are exposed to erosion, as it can help to identify the conditions under which erosion damage is most likely to occur, and the conditions under which the material is most resistant to erosion.
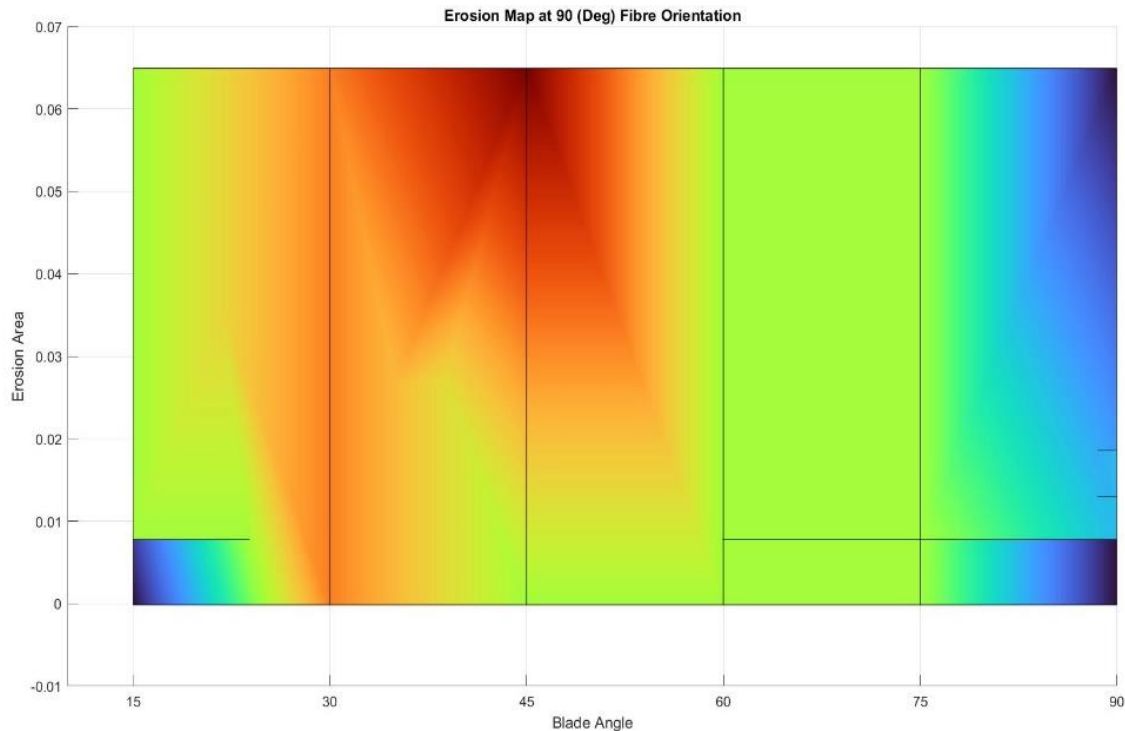
Figure 17. Erosion map of 90˚ fibre orientation

The finding from figure 17 of the erosion map is a significant result in the study of the erosion behaviour of UD-GFRP material. The maximum erosion observed in the material at the impingement angle range of 15˚ to 45˚ and impingement velocity of 9 m/s implies that the material is highly vulnerable to erosion under these conditions. This is an important consideration when designing and implementing structures that are subjected to high-velocity impacts or abrasive environments [155].

Further investigation is necessary to understand the underlying mechanisms that contribute to this erosion behaviour. Factors such as the material's composition, fibre orientation, and matrix properties may play a role in its susceptibility to erosion [133], [156]. Additionally, the effects of erosion on the mechanical properties of the material should be examined to assess its overall durability and reliability in practical applications.

Overall, this result underscores the importance of erosion-resistant materials in tidal turbine industries where structures and components are exposed to harsh environments. The development of new materials and coatings with improved erosion resistance is an active area

of research, driven by the need for high-performance and long-lasting materials in these industries.

4.6 Main conclusions and Summary of Findings

The study provides valuable insights into the erosion mechanism in UD-GFRP materials and the impact of seawater immersion on their mechanical properties, which could be useful for the development of more durable and reliable materials that can withstand the harsh marine environment. The erosion maps revealed the erosion mechanism and highlighted the performance differences between $0°$ and $90°$ fibre orientation, with $0°$ showing ductile erosion.

The study's summary of findings revealed that the impingement angle of $15°$ caused the least amount of erosion in UD-GFRP material. Additionally, the $0°$ fibre orientation UD-GFRP was less affected by erosion compared to the $90°$ fibre orientation UD-GFRP. The erosion mechanism in GFRP was the result of the fibre matrix being eroded away, with the surface composite cracking and the fibres being removed, exposing the matrix due to the surface's broken glass fibres. Seawater immersion reduced the overall strength of the material because of the ability of saltwater to de-bond the glass fibres in the composite matrix. However, it was determined that the GFRP material's tensile and flexural strengths can be regained by the desorption process. Notably, the $0°$ fibre orientation displayed ductile erosion. Further research is needed to explore the feasibility and effectiveness of the proposed solutions and to address the limitations and challenges of the study.

Chapter Five

Mapping the Erosion Performance of Toughened GFRP Plates for Tidal Turbine Blades Under Slurry Conditions.

Chapter 5 Mapping the Erosion Performance of Toughened GFRP Plates for Tidal Turbine Blades Under Slurry Conditions.

5.1 Overview

Tidal turbines experience significant material risk from high thrust and torsional loads on their spinning surfaces, resulting in erosion in the marine environment that reduces the potential for tidal energy harnessing. Polymer-matrix composites are susceptible to blade erosion when exposed to salt and substantial sand fragments in sea flows. Coatings that prevent erosion can be applied to the blade surface[11], but their transition with the composite can become a weak spot.

To address this, a matrix made of polymers that varies in toughness is preferred[157], where a more robust, ductile polymer matrix is located at the blade surface and steadily transitions to the high stiffness matrix required for excellent mechanical properties of composites.

This research contrasted several powder epoxy systems, and only two systems were selected for use in the production of UD-GFRP plates with a toughening gradient created by varying epoxy ratios for surface and inside plies. Mechanical analysis of gradient plates and historical analogues subjected to rigorous erosion tests in a model of the British marine environment showed significant changes in materials with varying stiffness under these conditions, resulting in erosion maps. The use of a polymer matrix with a toughness gradient allows for more precise manipulation of the composite's mechanical properties.

5.2 Materials and Methodologies

This study aimed to investigate the mechanical and erosion properties of different laminate configurations. The process of experimentation comprised of three stages. First, the mechanical properties of various toughened epoxies were evaluated to pick the most suitable one for the composite matrix. Next, a study was conducted to assess the compatibility between standard and toughened epoxies. Finally, the erosion of both pure standard epoxy laminates and through-thickness gradient epoxy laminates was studied.

To conduct mechanical testing, laminates were produced using one type of resin system or a consistent proportion of standard and toughened powder epoxy. On the other hand, to carry out the erosion tests, the toughness of the resin system was altered within the laminate by incorporating epoxy powders, leading to a gradient.

Mapping the Erosion Performance of Toughened GFRP Plates for Tidal Turbine Blades Under Slurry Conditions.

In this research, two different kinds of glass fibres were utilised, one for mechanical testing and another for erosion testing. GFRP was chosen due to its excellent strength, stiffness, and endurance to fatigue in water in comparison to metallic materials.

The mechanical tests in this paper rely on test standards developed for composite materials in which the resin system is homogeneous through the thickness of the test specimens. For the mechanical testing specimens, the laminates were manufactured with either one resin system or a constant ratio of toughened and standard powder epoxies. This is not the case for the erosion tests, however, where the resin system toughness was varied through the thickness. Working with epoxy powders allows the user to change the toughened to standard epoxy ratio in a discrete manner, resulting in a gradient through the laminate thickness, which is impossible to achieve with a liquid infusion system. This gradient allows for a much better continuity of the toughened and un-toughened substrate layers and allow the user to avoid the interlayer decohesion that can happen with standard toughened protection systems (especially for underwater applications). The gradient samples in Figure 1 were compared to standard PE6405 epoxy samples to assess the benefits of the novel processing method.

5.3 Fibres

Composite materials are the optimum choice for making the most efficient types of tidal turbine blade, due to their specific strength and stiffness, along with a high fatigue resilience in water in comparison to metallic materials [158]. In this scope, glass fibre reinforced polymer (GFRP) is usually a good candidate for marine turbine blade applications due to its relatively low cost [159]. One drawback of GFRP, however, is its tendency to corrosion in the marine environment[160], making erosion protection even more important for glass fibre FRP compared to basalt and carbon FRP [12]. In this project, two types of glass fibres were used, one for mechanical testing and one for erosion testing. A quasi-UD (10% weight in transverse direction) glass fabric was used for mechanical testing (SAERTEX® E-Glass U-E-591g/m2-1200mm), representative of standard structural composite systems. A 100% UD-glass fibre fabric (StarRov LFTPlus 871 E-Glass) was used for erosion testing purpose, as transversal fibres would have otherwise affected the erosion behaviour independently to the epoxy powder matrix properties.

5.4 Epoxy powders

A powder-based epoxy (PE6405) from FreiLacke & Swiss CMT AG was used in this study as the un-toughened, baseline epoxy resin. Due to a heat-activated catalyst technology, the powder

epoxy provides significant advantages compared to its liquid equivalents: low minimal viscosity, low exotherm [157], [161], ability to pre-shape different parts and co-cure them in a one shot process and stability at ambient temperature (no refrigeration requirement). These advantages result in lower manufacturing costs and quicker production of mechanically superior composite parts [157], compared to standard liquid epoxy based composites.

Additionally, a set of experimental toughened epoxy powders (VPB-22, VPB-25, VPB-26 and VPB-27) were provided by FreiLacke & Swiss CMT AG to the University of Edinburgh and compared with the commercial PE6405. Plates were tested using the mechanical testing procedure described further below. First, an initial screening of the toughened powder epoxies mechanical properties as GFRP in tension (ISO 527-5) and 4-point bending (ISO 14125) was performed in order to select the best candidate, as well as to compare to the standard powder epoxy GFRP (PE6405). Then, the most suitable toughened epoxy candidate was mixed with the standard epoxy system at 50% and 25% toughened epoxy volume ratios and mechanical properties were investigated. The compatibility of both epoxy systems was also investigated using a differential scanning calorimetry (DSC) temperature sweep, to determine both their melting and curing temperatures.

5.5 Manufacturing Procedure of the GFRP

The process of manufacturing GFRP laminates involved creating symmetric and balanced plies with either UD or CP fibre orientation. The fabric layers were cut and weighed, and the inter-ply layers were sprinkled with epoxy powder to achieve a 45% overall laminate fibre volume fraction. The steel frame with the layers was positioned for consolidation in an oven under vacuum pressure, without applying any external pressure. The curing process consisted of three steps: drying the powder, melting it to allow it to permeate the fabric, and then curing it fully at 185°C for two hours. Subsequently, the temperature was slowly decreased over five hours until it reached room temperature. The thickness of the laminates was altered depending on the type of test being conducted; for mechanical compatibility study, the standard thickness was 2mm, while for erosion testing, it was increased to 6mm.

Mapping the Erosion Performance of Toughened GFRP Plates for Tidal Turbine Blades Under Slurry Conditions.

Sample code	Categories
St0	Standard GFRP with 0° fibre orientation
St45	Standard GFRP with 45° fibre orientation
St90	Standard GFRP with 90° fibre orientation
Grd0	Gradient GFRP with 0° fibre orientation
Grd45	Gradient GFRP with 45° fibre orientation
Grd90	Gradient GFRP with 90° fibre orientation

Table 1 Specimen codes for erosion testing

Parameter	Value
Impact velocity ms^{-1}	9.04
Solutions	Salt and Sand
Sand concentration wt%	3
Impact angle	15°, 30°, 45°, 60°, 75°,90°
Salinity wt%	3.5
Sand particle size μm	300 - 600
Test duration (min/sample)	30

Table 2 Test Conditions

Test Description	Nominal sample length (mm)	Nominal sample width (mm)	Nominal sample thickness (mm)
Tensile 0˚ and 90˚ (ISO 527-4 and ISO 527-5)	250	25	2
Compression 0˚ and 90˚ (ASTM D6641)	140	13	2
4 point bending 90˚ 0˚ and (ISO 14125-Class III)	60	15	2
Fibre volume fraction (ASTM D2734)	10	10	2

Table 3 Mechanical test standards and dimensions

5.6 Erosion Test

The erosion performance of six GFRP grades was evaluated by subjecting them to slurry impingement jet rig tests at impact angles ranging from 15° to 90°, as depicted in Figure 3. Table 1 listed the various types of specimens and sample codes produced from unidirectional (UD) glass-fabric reinforced laminates, which were machined with a 0˚, 45˚, or 90˚ fabric orientation

Mapping the Erosion Performance of Toughened GFRP Plates for Tidal Turbine Blades Under Slurry Conditions.

to investigate the impact of fibre angle on erosion behaviour, as shown in Figure 19. The erosion behaviour was evaluated by analysing mass loss using an analytical scale with an accuracy of +/-0.01mg and conducting a surface inspection with a Scanning Electron Microscope (SEM).

 The Slurry impingement jet rig was designed based on Hutchings' principles and comprised a slurry chamber containing the erodent and a water chamber containing 3.5% saline water, which was circulated by a centrifugal pump.
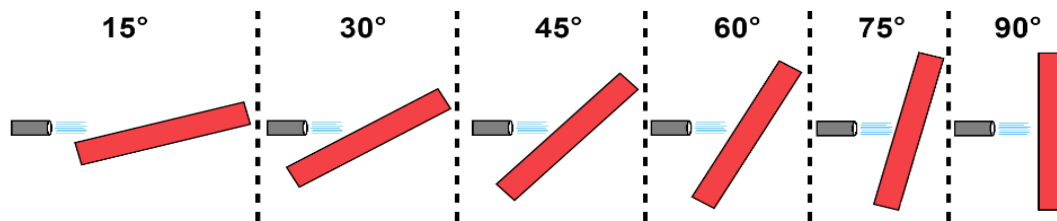
Figure 18. Schematic of the test specimen position in respect to the exit nozzle for the range of impingement angles tested.

The impingement speed and concentration of particles were regulated by modifying the inlet and outlet nozzles' diameter and location of the T-shaped venturi chamber.

The experiments were conducted using an impingement speed of 9.04 m/s and a sand particle concentration of 3%. The flat specimen was mounted on a flexible bracket, allowing testing at different impingement angles ranging from $15°$ to $90°$. Following impingement, the slurry flowed back into the slurry chamber, and surplus water drained into the water chamber, while a mesh trapped the particles in the slurry chamber for reuse over the 30-minute testing period. SEM was used to examine surface defects to obtain a more detailed understanding of the type of erosion occurring in UD-GFRP [142]. Figure 18 Schematic of the test specimen position with respect to the exit nozzle for the range of impingement angles tested.

Mapping the Erosion Performance of Toughened GFRP Plates for Tidal Turbine Blades Under Slurry Conditions.

To replicate the harsh wear conditions that may be encountered by tidal turbines, high silica sand with a diameter of 300-600µm and a grade of No. 60 from Minerals Marketing was utilised. The sand particles were sorted based on ISO 3310-1 standards using stainless steel mesh sieves with 600 µm and 300µm grids.
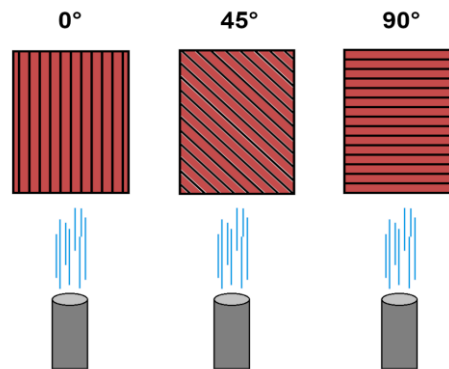
Figure 19. Schematic representation of fibre orientation with respect to the impingement jet

To ensure the accuracy and consistency of the test results, the erosion experiments were repeated three times. This was done to minimise the impact of any potential random variations or errors that may have occurred during the testing process. By repeating the experiments multiple times, a more reliable and robust set of results was able to be obtained, which would allow more confident conclusions to be drawn about the underlying phenomenon being studied.

Additionally, the experiments being repeated also helped in identifying and addressing any potential sources of bias or confounding factors that could have affected the results. Overall, the decision to repeat the erosion experiments multiple times was an important step in ensuring the scientific rigor and validity of the research findings.

Mapping the Erosion Performance of Toughened GFRP Plates for Tidal Turbine Blades Under Slurry Conditions.

5.7 Result and Discussions

5.7.1 Gradient vs Standard GFRP

The direction of fibres in unidirectional glass fibre-reinforced plastic (GFRP) has a significant impact on the erosion rate [85], [162], with 90° fibre orientation being more vulnerable to erosion compared to other orientations. Figure 20 shows that when subjected to a 15° impingement angle, all three standard plate specimens exhibited a small increase in weight to a similar degree, while the specimen with 45° fibre orientation experienced weight loss. This weight loss occurred because particles were deposited on the surface of the sample due to the high impingement velocity of 9.04 m/s combined with the acute angle of attack and ductile
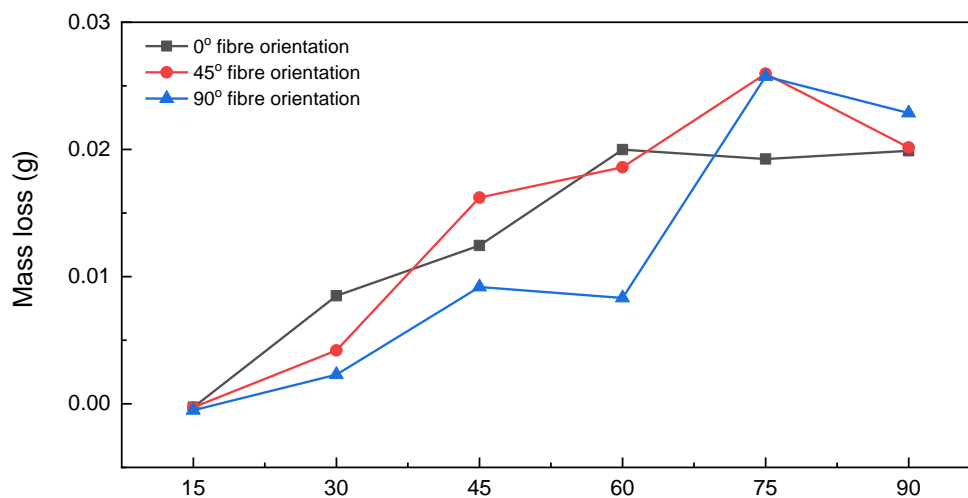
Figure 20. Mass loss of GFRP Standard plates with three different surface fibre orientations 0˚, 45˚ and 90˚ subjected to erosion at 15˚, 30˚, 45˚, 60˚, 75˚ and 90˚ at 9.04 m/s impact velocity.

nature of the composites. As the impingement angle increased, there was a significant increase in weight loss across all types of specimens.

For varying erosion time and Impact pressure, the most significant erosion occurred at a 60° impact angle, and the mass loss of Std0 increased steadily with an increase in the impact angle, reaching a maximum at 60° before stabilising [85]. Std45 and Std90 experienced their highest mass loss at 75°, followed by a drop at 90°. Grd0 experienced a nearly linear increase, with a maximum mass loss occurring at a 90° impact angle, while Grd90 also had its highest mass loss at 90° but exhibited a considerable decrease in a mass loss at 75° after a linear increase up to 60°. Grd45 had a more irregular pattern, with mass loss increasing at 30° and then decreasing at 45°, followed by a steep increase to its maximum at 60°, a drop at 75°, and a minor increase

Mapping the Erosion Performance of Toughened GFRP Plates for Tidal Turbine Blades Under Slurry Conditions.

at 90°. Polymers, despite being relatively ductile, can behave in a brittle manner and have their highest erosion rate at an impact angle of 90° as reported by [163].

The research also discovered that the behaviour of gradient plate GFRPs varied depending on
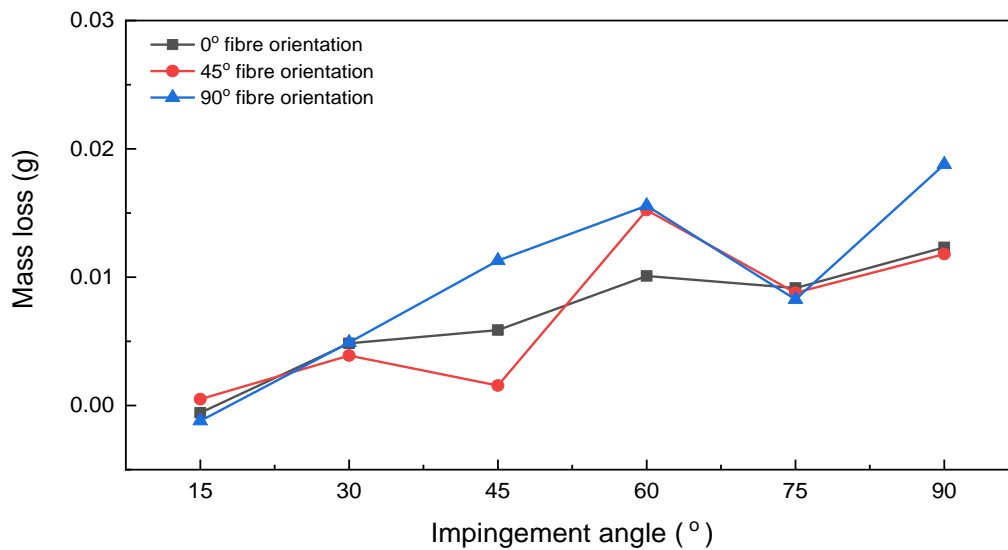
Figure 21.Mass loss of GFRP Gradient plates with three different fibre orientations 0˚, 45˚ and 90˚ subjected to erosion at 15˚, 30˚, 45˚, 60˚, 75˚ and 90˚ at 9.04 m/s impact velocity.

their fibre orientation [156]. Grd0 showed a nearly linear increase in mass loss, with the highest mass loss occurring at a 90˚ impact angle. On the other hand, Grd90 had its maximum mass loss at 90˚ after a linear increase in mass loss up to 60˚, followed by a significant decrease in a mass loss at 75˚. Grd45 had a more unpredictable pattern, with mass loss increasing at 30˚ and then decreasing at 45˚, followed by a sharp rise to the highest mass loss at 60˚, a decline at 75˚, and a small increase at 90˚.

Overall, findings suggest that fibre orientation and impingement angle play significant roles in the erosion rate of unidirectional GFRP [164]. The study provides insights into the behaviour of different types of GFRP under erosive conditions, which can inform the design and selection of materials for applications that are exposed to erosion.

5.7.2 Effect Of Fibre Orientation on Erosion

Based on Figure 22, the mass loss of the gradient specimens with 0˚ fibre orientation is generally lower than that of the standard specimens with 0˚ fibre orientation for most impingement angles, although both types of GFRP exhibit a similar trend. At an impingement angle of 15˚, both types of specimens experience a gain in mass due to the deposition of sand and salt particles, which is supported by SEM analysis in Figure 25(a). Previous research has also reported similar findings of mass gain due to erodent deposition [53]. The sand particles

Mapping the Erosion Performance of Toughened GFRP Plates for Tidal Turbine Blades Under Slurry Conditions.

were deposited mechanically in the more ductile epoxy, while the high-pressure water jet from
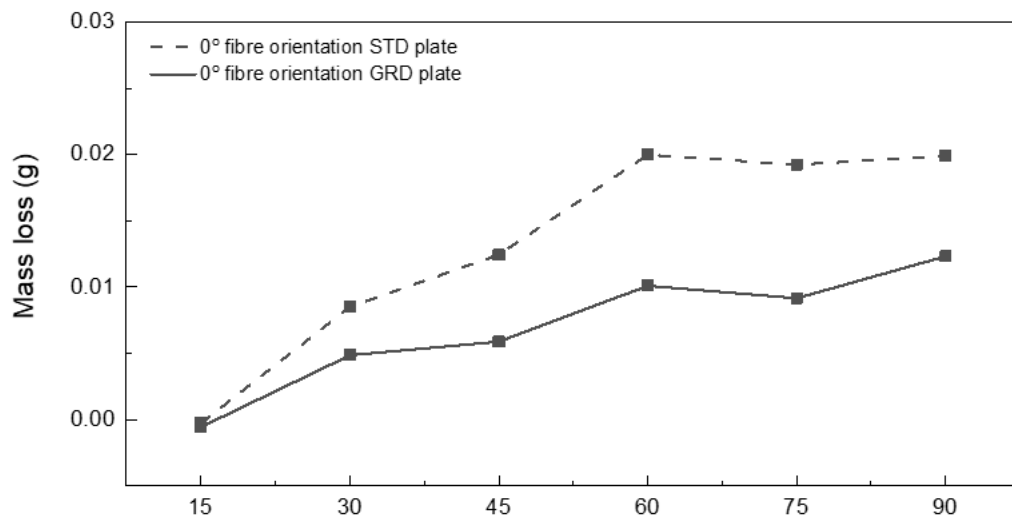
Figure 22. Mass loss of STD0 and GRD0 subjected to erosion at 15˚, 30˚, 45˚, 60˚, 75˚ and 90˚ at 9.04 m/s impact velocity.

the salt facilitated the diffusion of saline water through the matrix, which enabled the glass fibres in the composite matrix to de-bond. This phenomenon is visible in Figure 25 (d). As the impingement angle increases, there is a noticeable difference in erosion behaviour between the two GFRP types. At 30˚, the Std0 exhibits a 75% higher mass loss than Grd0, and this difference increases to 112%, 98%, and 110% at 45˚, 60˚, and 75˚, respectively. At 90˚, the difference decreases to 61%.

The results presented in Figure 23 show that, similar to Std0, Std45 experiences an increase in mass at an impingement angle of 15˚. However, Grd45 only shows a minor mass loss of 0.00049g. This difference in behaviour can be attributed to the denser epoxy used in Grd45, which reduces the amount of sand particle embedding. At an impingement angle of 30˚, there is almost no difference in the erosion performance between the two specimens, with Grd45
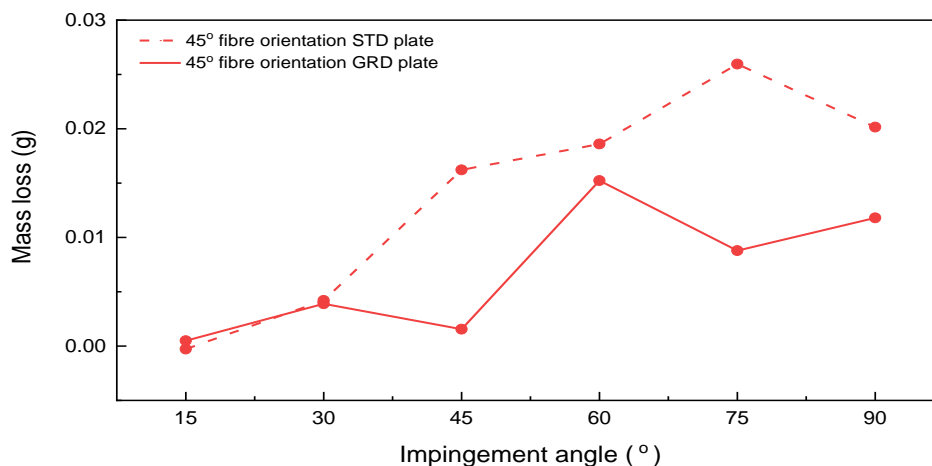
Figure 23. Mass loss of STD45 and GRD45 subjected to erosion at 15˚, 30˚, 45˚, 60˚, 75˚ and 90˚ at 9.04 m/s impact velocity

71

slightly outperforming Std45 by only 7%. However, at 45˚, the difference becomes significant, with Std45 showing a much higher mass loss of 945% compared to Grd45. The SEM analysis in Table 6 revealed that the fibres of Std45 were broken away, resulting in significant mass loss, while the damage to Grd45 was mostly on the matrix, indicating some degree of fibre protection by the polymer. At higher impingement angles of 60˚, 75˚, and 90˚, Std45 had mass loss values 22%, 195%, and 70% higher than those of Grd45, respectively. These results suggest that the toughened epoxy used in Grd45 has a better ability to absorb the kinetic energy of the impacting erodent at higher impact angles.

The results shown in Figure 24 indicate that while Grd0 and Grd45 have better erosion resistance than their standard counterparts, the same cannot be said for Grd90. At 15˚, both Grd90 and Std90 experience mass gain, while at 30˚, 45˚, and 60˚, Grd90 has higher mass loss than Std90, with differences of 113%, 22%, and 87%, respectively. However, at 75˚ and 90˚, Grd90 outperforms Std90, with mass losses being 68% and 18% lower, respectively. Overall, the best-performing specimen was Grd45, which not only had the lowest average mass loss over the range of impingement angles but also performed best at 15˚, 45˚, and 90˚ impingement angles.

The toughness of the matrix appears to play a dominant role in erosion when the jet force is perpendicular to the fibres (90˚ fibre orientation), while the erosion resistance of the fibres dominates mass loss when the jet force is parallel to the fibres (0˚ fibre orientation). The GRD materials exhibit less mass loss at 0˚ and 45˚ fibre orientations, where there is a perpendicular component of the jet and impinging particles with respect to the fibre direction. However, the GRD materials do not perform better than the STD materials at 90˚ fibre orientation, where there is no perpendicular component of the jet force with respect to the fibre direction. To provide a clear representation of the discussed results, maps were drawn, which could also aid

Mapping the Erosion Performance of Toughened GFRP Plates for Tidal Turbine Blades Under Slurry Conditions.

in accurately predicting damage and ensuring a sufficient level of safety during tidal turbine blade operation. [11]
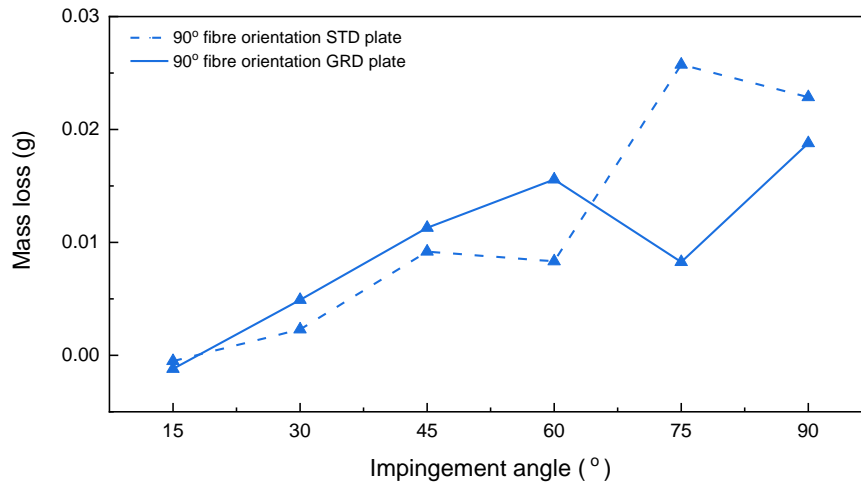
Figure 24. Mass loss of STD90 and GRD90 subjected to erosion at 15˚, 30˚, 45˚, 60˚, 75˚ and 90˚ at 9.04 m/s impact velocity.

5.8 SEM Analysis

To gain a deeper understanding of the erosion mechanisms involved, surface analysis is required in addition to mass loss measurements. In this study, after being coated with a 5 µm layer of gold to facilitate SEM examination [39], all specimens underwent optical analysis using a (W-SEM). Table 4 identifies and lists the types of surface damage that each specimen experienced. The results show that all GFRP specimens, regardless of fibre orientation or epoxy type, experienced sand particle embedment on their surface when subjected to erosion at 15˚, which explains the low mass loss or even mass gain recorded in this scenario [10]. Figure 25a shows an illustration of a particle embedded in a GFRP specimen's surface. The damage process altered as the impingement angle increased. The STD specimens displayed fibre damage in the form of cracking and fracture at 30, while the matrix of the GRD specimens was harmed. At this point, no embedded particles were visible. The damage types and intensities between STD and GRD specimens were remained different at 45, with STD specimens exhibiting fibre breakage and cracking and GRD specimens mostly experiencing matrix

73

damage. Higher impact angles (60°, 75°, and 90°) resulted in substantial damage for all specimens, with GRD and STD type specimens suffering notable matrix and fibre damage without any discernible pattern separating their erosion behaviour depending on epoxy type or fibre
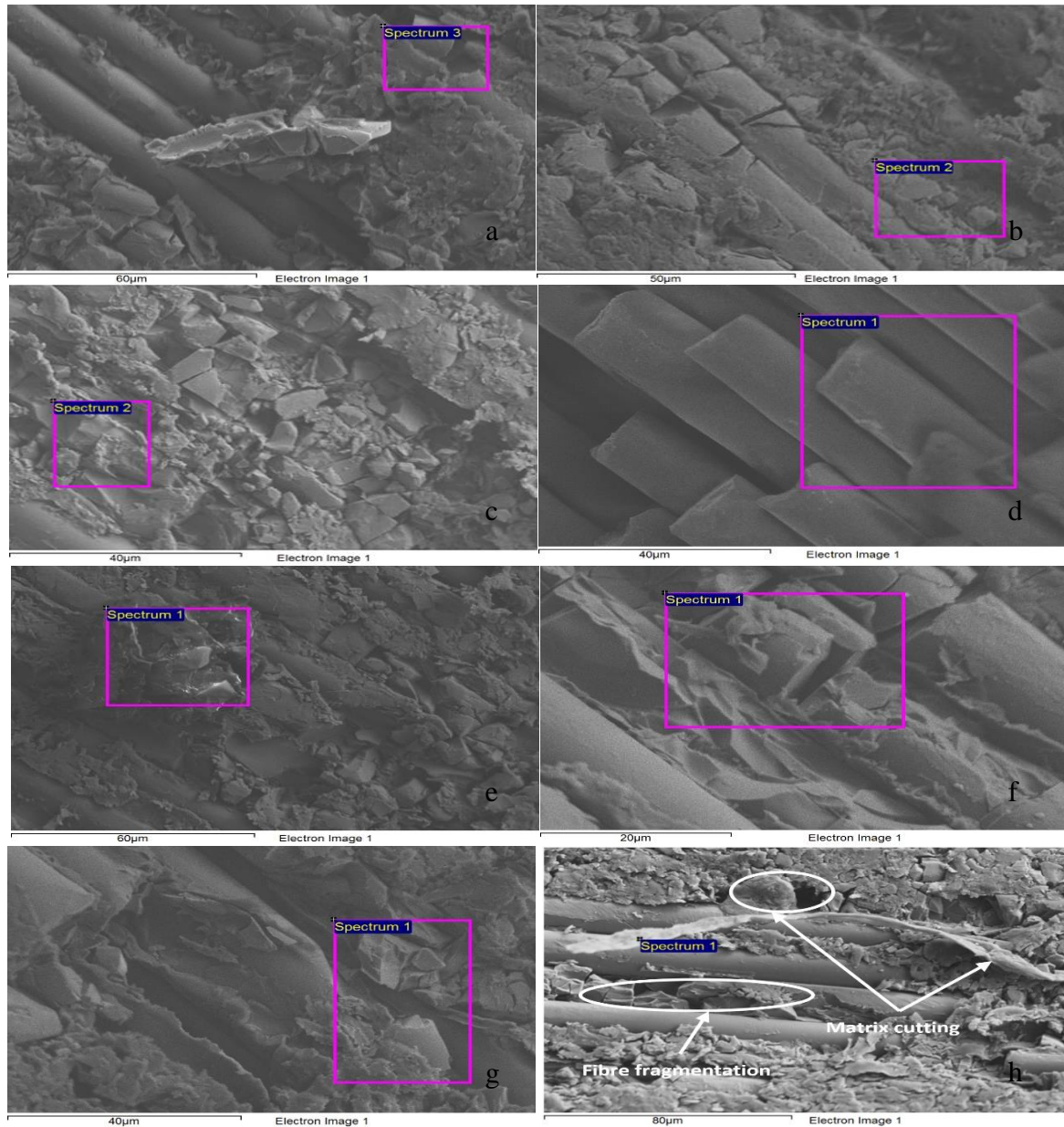
Figure 25. SEM of GRD45 at 15° impact angle (a), STD45° at 30° impact angle (b), GRD45 at 30° impact angle (c), STD45 at 45° impact angle (d), GRD45 at 45° impact angle (e), GRD45 at 60° impact angle (f), GRD45 at 75° impact angle (g), STD90 at 90° impact angle (h)

orientation.

The surface damage types observed in the specimens indicate the occurrence of both ductile and brittle erosion. Ductile erosion occurs when a material deforms and stretches under the applied force, while brittle erosion occurs when the material fractures and breaks into pieces.

Mapping the Erosion Performance of Toughened GFRP Plates for Tidal Turbine Blades Under Slurry Conditions.

Table 4 List of defect types based on SEM analysis.

Impingement angle	Defect type
STD 0˚ fibre orientation	
15°	Exposed fibre, Fibre fracture, Particle Embedment
30°	Fibre fracture
45°	Fibre fracture
60°	Fibre cracking
75°	Particle embedment, Matrix cutting, Fibre fracture
90°	Fibre fragmentation, fibre cracks
STD 45˚ fibre orientation	
15°	Particle embedment, Matrix cutting
30°	Fibre fracture, Fibre cracking
45°	Fibre fragmentation
60°	Matrix cutting, Fibre fragmentation
75°	Fibre fragmentation
90°	Fibre fracture, Fibre cracking
STD 90˚ fibre orientation	
15°	Particle embedment
30°	Matrix cutting, Fibre exposure
45°	Matrix debonding, Fibre exposure, Fibre cracking
60°	Fibre cracking
75°	Matrix cutting, Fibre fracture
90°	Matrix cutting, Fibre fragmentation
GRD 0˚ fibre orientation	
15°	Fibre exposure, Fibre cracking, Particle embedment
30°	NaCl deposition, Fibre cracking, Matrix debonding
45°	Matrix cutting, Fibre exposure
60°	Fibre cracking, Matric cutting
75°	Fibre cracking
90°	Fibre fracture, Matrix cutting
GRD 45˚ fibre orientation	
15°	Particle embedment
30°	Matrix debonding
45°	Matrix cutting, Matrix debonding
60°	Fibre fracture
75°	Matrix debonding, Fibre cracking
90°	Particle embedment, Matrix cutting, Fibre fracture
GRD 90˚ fibre orientation	
15°	Fibre exposure, Particle embedment
30°	Matrix cutting, NaCl deposition
45°	Fibre exposure, Matrix debonding,
60°	Fibre cracking, Matrix cutting
75°	Fibre fragmentation
90°	Matrix cutting, Matrix debonding, Fibre fragmentation, Fibre cracking

At the 15˚ impingement angle, the specimens suffered from ductile erosion as sand particles embedded in the surface of the specimens, which caused minimal mass loss. At 30˚, no imbedded particles could be seen, and the specimens began to erode brittlely. While the GRD

specimens' fibres were largely unharmed while the matrix was affected, the STD specimens' fibres experienced damage in the form of cracking and breaking.

Both ductile and brittle degradation were seen at 45°. While the damage in the GRD specimens was primarily on the matrix, indicating ductile erosion, the STD specimens experienced fibre fracture and cracking, indicating brittle erosion. At 60°, 75°, and 90°, all specimens suffered substantial damage from ductile and brittle erosion, but there was no obvious pattern differentiating their erosion behaviour based on the orientation of the fibres or the type of epoxy.

Therefore, it can be concluded that the erosion behaviour of GFRP is complex, and the occurrence of ductile and brittle erosion depends on the impact angle, fibre orientation, and epoxy type [61], [62], [146]

5.9 Erosion Wastage Maps

An alternative method for visualising damage, called wastage maps, was created based on protocols outlined in previous studies [9], [11], [165]. These maps can be used to forecast how safely tidal turbine blades will operate. The map indicated the erosion mechanism for the standard and gradient plates with three distinct fibre orientations (0°, 45°, and 90°), at a constant speed of 9.04 m/s, and impact angles varying from 15° to 90°. Blue denotes minimal erosion, green indicates medium erosion, and yellow denotes high erosion on the maps.

In Figure 26, for instance, the STD plate with a 0° fibre orientation encounters medium waste at 30° and 45° impingement angles, with the amount of wastage rising as the impingement
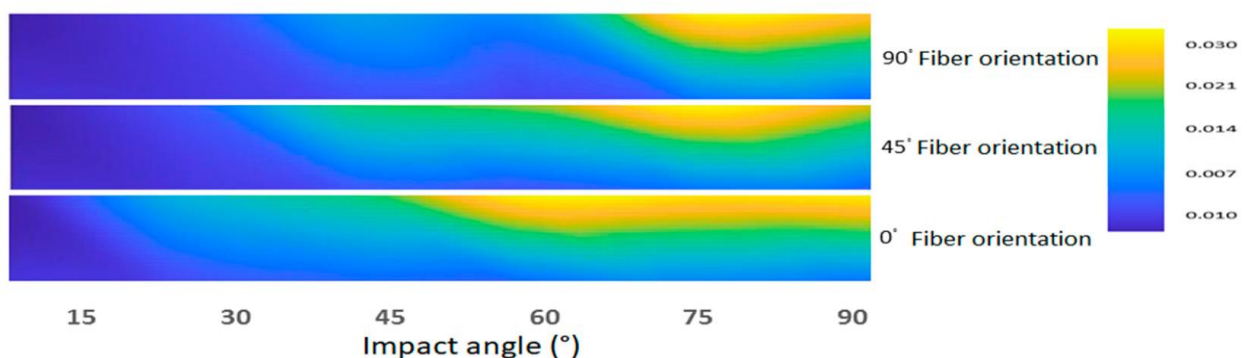
Figure 26. STD Erosion wastage map

angle rises. For the STD plate with a 45° fibre orientation, there is medium wastage at an impingement angle of around 45°, high wastage at an angle of more than 60°, and maximum wastage at 75°. The STD plate with a 90° fibre orientation, in contrast, exhibits low wastage at impingement angles between 15 and 65°, with a sharp rise at 75 and 90°.

Mapping the Erosion Performance of Toughened GFRP Plates for Tidal Turbine Blades Under Slurry Conditions.

The wastage maps for the GRD plates are notably different from those for the STD plates, as seen in the figure 27. For the GRD plate with a 0° fibre orientation, the wastage rises with the impingement angle, becoming high at 60° and peaking at 90° with a slight decline at 75°. The wastage for the 45° fibre orientation GRD plate is minimal for acute impingement angles, rising to a high level at 60° and then levelling off at higher impingement angles. The wastage is uniformly low for the 90° fibre orientation GRD plate, with occasional peaks of substantial wastage at 60° and 90° impingement angles.

The impingement angle at which the peak erosion occurs varies significantly between the STD and GRD plates. Peak erosion for STD plates occurs at 75°, whereas it occurs at 60° for GRD plates. Additionally, across the range of studied impingement angles, GRD plates demonstrate generally lower wastage and more uniform erosion. Since the GRD plates' erosion is uniform, damage to the blades will also be more predictable, making damage prediction easier.
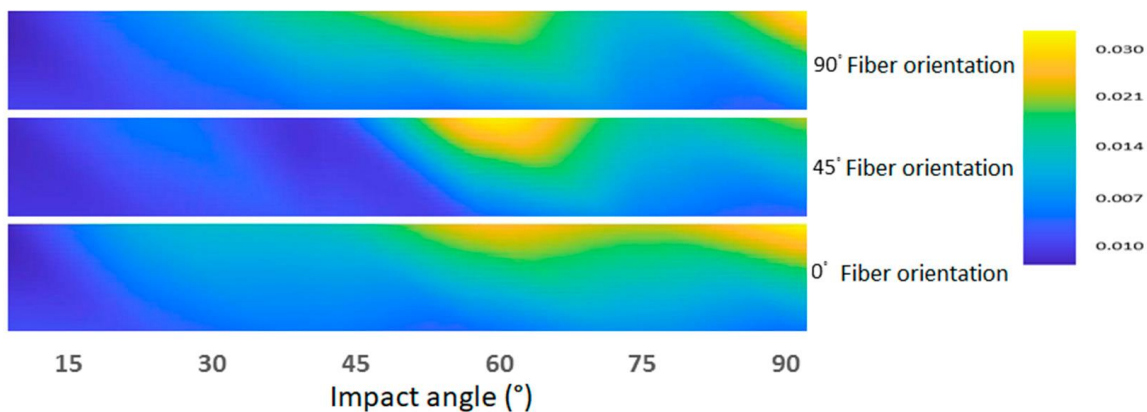
Figure 27. GRD Erosion wastage map

5.10 Main Conclusion and Summary of Findings

The study aimed to develop a glass-fabric-reinforced laminate with a gradient in epoxy matrix toughness to increase its resistance to surface erosion in tidal turbines. The use of a powder-epoxy fabrication method allowed for the creation of a laminate with a harder but weaker epoxy matrix for the remainder of the material and the strongest epoxy matrix on the sea-eroded surface. The study also aimed to identify the optimal toughened powder epoxy system for blade protection in tidal turbines.

The study found that at a 15° impingement angle, both standard (STD) and gradient-toughened (GRD) epoxy plates showed no significant mass loss or sand particle embedding. However, the GRD plates outperformed the STD plates in general, and the mass loss increased with

increasing impingement angle. The GRD plates had a more ductile response to erosion than the STD plates, with the greatest amount of mass loss occurring at an impact angle of $60°$, compared to the STD plates, which experienced the highest amount of mass loss at an impact angle of $90°$. The erosion performance of the GRD plates was more constant across the range of impingement angles examined, simplifying lifetime estimations. The material's surface fibre orientations of 0 and $45°$ had the most performance differences between GRD and STD plates. The study successfully demonstrated the potential of the powder-epoxy fabrication method to create a gradient-toughened composite with varying proportions of standard and toughened powders to increase the resistance of glass-fabric-reinforced laminate to surface erosion in tidal turbines.

Chapter Six

Erosion Mapping of Coated Composites in Simulating Conditions for Tidal Turbines Blades.

Chapter 6 Erosion Mapping of Coated Composites in Simulating Conditions for Tidal Turbines Blades.

6.1 Overview

In earlier chapters, an examination of UD-GFRP was conducted through the use of a jet rig to imitate the environments in which the blades operate. The chapters then explored the assessment of the tested GFRP under a range of erosion conditions. The results indicated that the UD-GFRP was confronted with various tribological difficulties, including fibre fractures, cracks, indentations, matrix debonding, and salt and sand depositions, which resulted in an increase in the mass of the GFRP [1]. These findings suggest that the UD-GFRP may require additional protective measures or alternative materials to enhance its performance and durability in similar operating environments. Ahmed and Rasool addressed the tribological challenges faced by GFRP [10], [11].

In order to investigate the tribological mechanisms of potential composite materials that could be used in tidal turbines, advanced experimental research was conducted. This research considered the effects of various erosion parameters on the degradation modes, both with and without particles, in still and seawater conditions [1], [2]. The chapter aims to investigate the effectiveness of a specialised epoxy erosion-resistant coating for glass fibre-reinforced plastic (GFRP) in resisting the impact of slurry erosion. Slurry erosion is a process by which solid particles suspended in a fluid medium impinge on a surface, causing material loss due to repeated impacts [3, 4]. The coating's efficacy will be evaluated through a series of tests in which it will be subjected to various erosion causes, including three different speeds and six different impinging angles.

To assess the coating's resistance to erosion, the tests will simulate different levels of erosion by varying the speed and angle of impingement of the slurry on the coated GFRP samples. The aim is to analyse the coating's ability to withstand a range of erosion mechanisms under different conditions. The study will provide valuable insights into the durability and effectiveness of the epoxy erosion-resistant coating, which can help identify potential applications in various industries where slurry erosion is a common issue. The results of the study will provide guidance for optimising the use of the coating in tidal turbine blade industries where resistance to erosion is crucial for long-term performance and safety.

Erosion Mapping of Coated Composites in Simulating Conditions for Tidal Turbines Blades.

6.2 Materials and Methodologies

6.2.1 Materials

The materials used in this study include FR4-G10 GRP, which serves as the base for the erosion-resistant coating being evaluated. These materials were selected for their unique properties and suitability for the intended purpose of the study. Technical specifications for each of these materials are provided in Table (5), which includes information on their mechanical, thermal, and water absorption properties.

To ensure consistent and accurate testing, the materials were prepared by cutting sheets of plate arranged in a specific size of 36mm by 25mm and 3mm thickness. The sheets were cut to fit into the Jet rig specimen holder as shown in fig. 4, which is used to direct the slurry at the coated samples. The uniformity and precision of the sample size and arrangement ensure that the results of the tests are reliable and repeatable.

The FR4-G10 GRP materials are commonly used in the manufacturing of marine components, while epoxy and plastic glass is used in a variety of industrial and consumer applications [166]. The selection of these materials as a base for the coating is based on their durability, strength, and erosion resistance, which are essential properties for withstanding the impact of slurry erosion.

Overall, the use of these materials in the study ensures that the results obtained are applicable to real-world scenarios and can provide insights into the efficacy of the epoxy erosion-resistant coating for protecting materials from slurry erosion in various industries. The technical specifications of the materials used in the study also serve as a reference for future research and development of similar materials and coatings.

Technical Data	Units	Test Method	Values
Colour	NA	NA	Light Green
Specific Gravity	g/cm³	ISO 1183	1.95
Water Absorption	mg	ISO 62	5.5
Flexural Strength	MPa	ISO 178	500
Tensile Strength	MPa	ISO 527	450

Table 5 Technical Specifications of FR4-G10 GRP

6.2.2 Coating

Belzona 2141 is a high-performance, erosion-resistance polymeric coating manufactured by Belzona International Ltd, which was selected for testing in this study due to its mechanical properties and high erosion resistance as described in table 6. This coating is commonly used in a variety of industrial and marine applications to protect equipment from the effects of wear, corrosion, and erosion[13].

To apply the Belzona 2141 coating to the FR4-G10 GRP samples, the surface of the samples was first prepared using 80-grit sandpaper as in Fig 28 (a), which helps to ensure good adhesion between the coating and the composite material. The Belzona 2911 activator was then mixed with the Belzona 2141 coating to achieve the required polymeric coating form. This mixture was carefully prepared according to the manufacturer's instructions to ensure the correct ratio of components and consistency of the coating [13]as shown in Fig 28 (b).

Once the samples were prepared and the coating mixture was ready, the coating was applied as a one-coat system by brush [11], [13]to achieve the desired thickness as shown in Fig 28 (c,d). The coating application process was carried out under the supervision of Belzona representatives to ensure that it was performed correctly and according to the manufacturer's guidelines [13].

After application, the coated samples were left to dry for 24 hours in ambient temperature conditions to allow the coating to cure and reach its full mechanical properties. The coating thickness was measured to ensure that the average thickness of 0.8mm was achieved for all samples.

Overall, the application process for the Belzona 2141 coating involved careful preparation and application to ensure that the coating was evenly applied and had the required thickness and mechanical properties. The use of this high-performance coating in the study provides valuable insights into its effectiveness in protecting composite materials from slurry erosion in various industrial applications.

PROPERTIES	UNIT
COLOR	Green
HARDNESS	ASTM typical value 87
HEAT RESISTANCE	40°C
TENSILE STRENGTH	ASTM D412 15.2 MPa
TEAR STRENGTH	ASTM D624 380 pli
DENSITY	1.1 g/cm3
WATER ABSORPTION	nil

Table 6 Coating specifications.
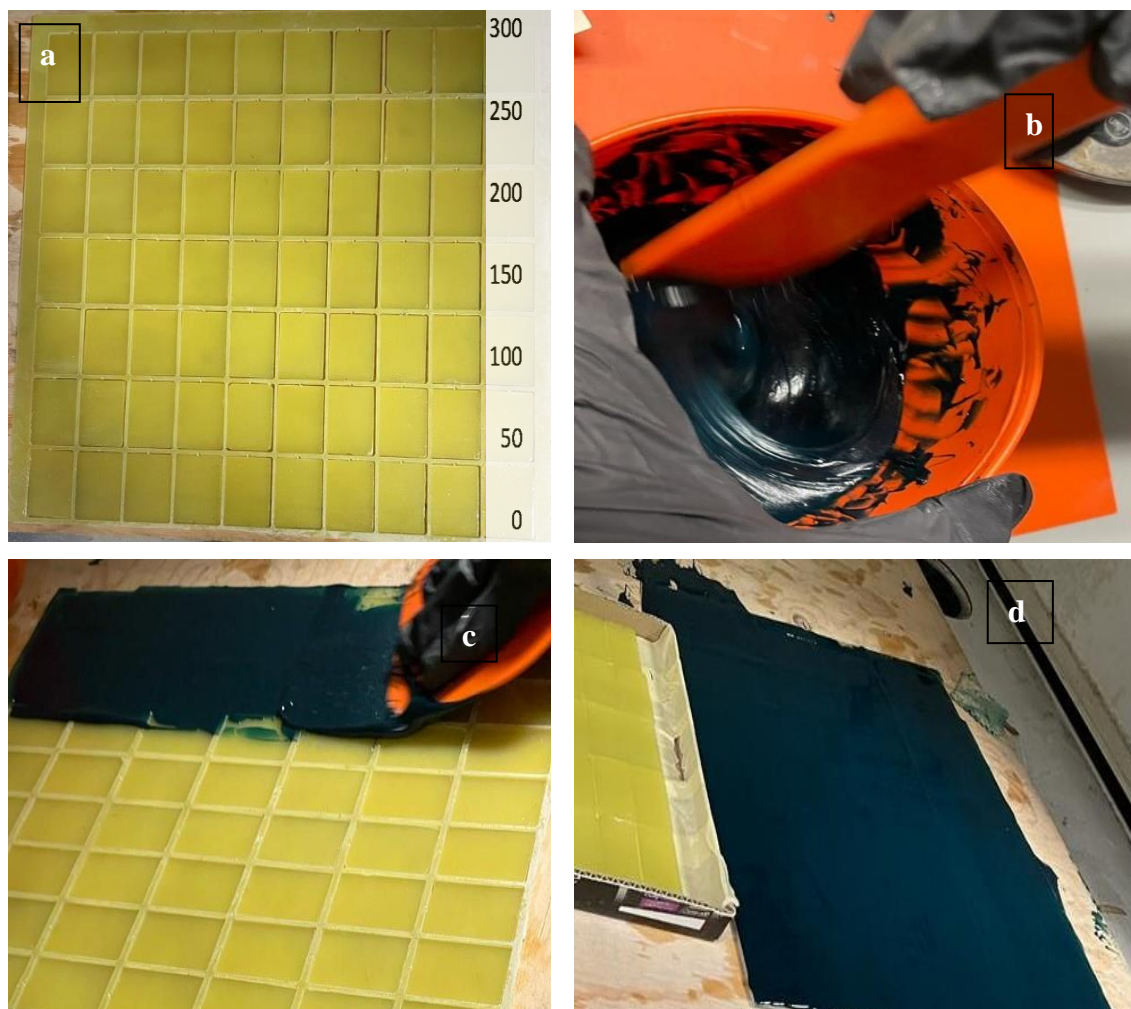
Figure 28 Coating application steps – Fig 28(a) in mm

Erosion Mapping of Coated Composites in Simulating Conditions for Tidal Turbines Blades.

6.2.3 Test Conditions

The experiment conducted to simulate the conditions experienced by tidal turbines used a device called the Jet rig, which is shown in Figure 3 of Chapter 3. The aim was to assess the impact of various factors on the performance of tidal turbines. The study was conducted at various impact angles, including 15°, 30°, 45°, 60°, 75°, and 90°, and at three different impact velocities of 6.25m/s, 8.42m/s, and 10.16m/s, the test duration was 30 min for each sample.

To replicate the natural environment, the experiment involved using a sand concentration of 3% and a salinity of 3.5%. The range of sand particles used in the test ranged between 300-600 µm, while the experiment was conducted at room temperature.

INLET DIA (MM)	VELOCITY (M/S)
2	6.25
2.5	8.42
3	10.16

Table 7 Nozzles vs Velocities

The velocities used in the test were regulated by the inlet nozzles diameter, as specified in table 7. The rig was carefully calibrated to ensure that the desired velocities were achieved. This was done by first measuring the volume of water in the rig, and then using a timer to record the elapsed time and final volume of water in a separate container. By subtracting the initial volume from the final volume of water that flowed through the container, this determined the volume of water that passed through the rig.

The final step involved using the formula below to calculate the velocity of the water flow.

$$V = \frac{Q}{A} \qquad \textit{Equation (3)}$$

where is **'v'** is the velocity, **'Q'** is the flow rate and **'A'** is a cross-sectional area of the flow path

By dividing the flow rate by the flow path's cross-sectional area, the velocity of the water flow was determined. To increase the accuracy of the results, the steps above were repeated three times.

Overall, this careful calibration and measurement process allowed to obtain precise data on the velocity of water flow in the Jet rig.

Erosion Mapping of Coated Composites in Simulating Conditions for Tidal Turbines Blades.

6.3 Results and Discussions

6.3.1 Results
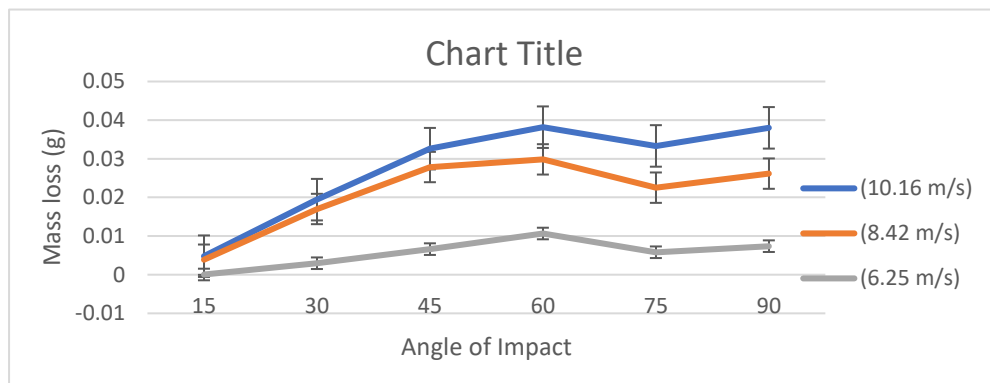
Figure 29 Mass Difference of Coated samples at 6.25m/s, 8.42m/s and

The erosion of the coating material was significantly influenced by the impact angle and water flow velocity, according to Fig. 29 it was noted that the coating experienced higher mass loss at impact angles of 60° and 90°, regardless of the velocity. This suggests that these angles are more critical for the durability of the coating and should be considered in the design and operation of turbines.

Additionally, the results showed that lower velocities of 6.25 m/s caused less damage to the coating material than the higher velocities of 8.42 m/s and 10.16 m/s. This suggests that a crucial element in the erosion of the coating material is velocity. Moreover, it was noticed that at an impact angle of 45°, the coating experienced mass loss at velocities of 8.42 m/s and 10.16 m/s.

The results of this experiment could have significant implications for the design and operation of tidal turbines. Erosion of the coating material can lead to reduced efficiency and a shorter lifespan of the turbines, which could result in significant financial losses [143].

6.4 Effect of Velocities and Impact Angle on Coating

The performance of the tidal turbine relies on the rotor blade, which is a critical component for extracting kinetic energy from the tide stream [167]. The blade is similar in concept to a wind turbine blade, but its design and reliability assessment cannot be based on those of the wind turbine due to differences in seawater density and other factors [11]. However, the efficiency and reliability of the blades are key indicators for a tidal current turbine[168]. The tribological issue, such as leading-edge erosion due to sand particles' impact, cavitation erosion, and the

85

combined effects of seawater and solid particles, can compromise the performance and reliability of the rotor blade [11], [39]. Researchers have investigated the erosion of the rotor blade caused by the impact of erodent under marine simulated conditions, i.e., saltwater plus sand particles, but ignored erosion due to cavitation [11], [169]. [48] also notes that the use of thermoplastic composite blades in a large-scale tidal power turbine is a potential game-changer for the marine energy industry, improving performance and sustainability, while also making the manufacturing process faster and more energy efficient.

The impact angle and velocity can significantly affect the erosion of polymeric coatings applied to tidal turbine blades [10], [12]. The erosion losses were evaluated at various impingement angles (15°-90°) and with the change of impact velocity 6.25 m/s, 8.42 m/s and 10.16 m/s, which reflects typical velocities experienced at the leading edge of the blade [10]. The polymeric coating acts as a barrier between the substrate and NaCl solution, slowing the ingress of moisture in composite materials [11]. The impact frequency can affect the ability of a coating to absorb and distribute the energy from an impact [170], which is typically taken into account in current blade coating systems.

The results indicate that the impact angle and velocity have a significant effect on the erosion of the samples [171]. At all velocities, the coating experienced higher mass loss at 60° and 90° impact angles. This can be attributed to the fact that at these angles, the impact energy is concentrated on a smaller area, leading to a higher erosion rate. At 6.25 m/s, the coating experienced a lower mass loss compared to 8.42 m/s and 10.16 m/s, indicating that lower velocity leads to a lower erosion rate. However, at higher velocities of 8.42 m/s and 10.16 m/s, the coating experienced higher mass loss, indicating that higher velocity leads to a higher erosion rate. At 45° impact angle, the coating experienced mass loss at velocities 8.42 m/s and 10.16 m/s, indicating that at this angle, higher velocities lead to a higher erosion rate. These results highlight the importance of considering impact angle and velocity when studying erosion and can be useful in designing coatings or materials that are more resistant to erosion [172]

Moreover, the coating material's ability to absorb and distribute the energy from an impact can also vary [170]. This further emphasises the importance of selecting the appropriate coating material and application process that can withstand the impact and erosion caused by the water flow. Overall, it is crucial to consider various factors, such as impact angle, velocity, and

Erosion Mapping of Coated Composites in Simulating Conditions for Tidal Turbines Blades.

coating material properties [53], [173], when designing and operating tidal turbines to ensure the longevity and efficiency of the system.

6.4.1 SEM Analysis
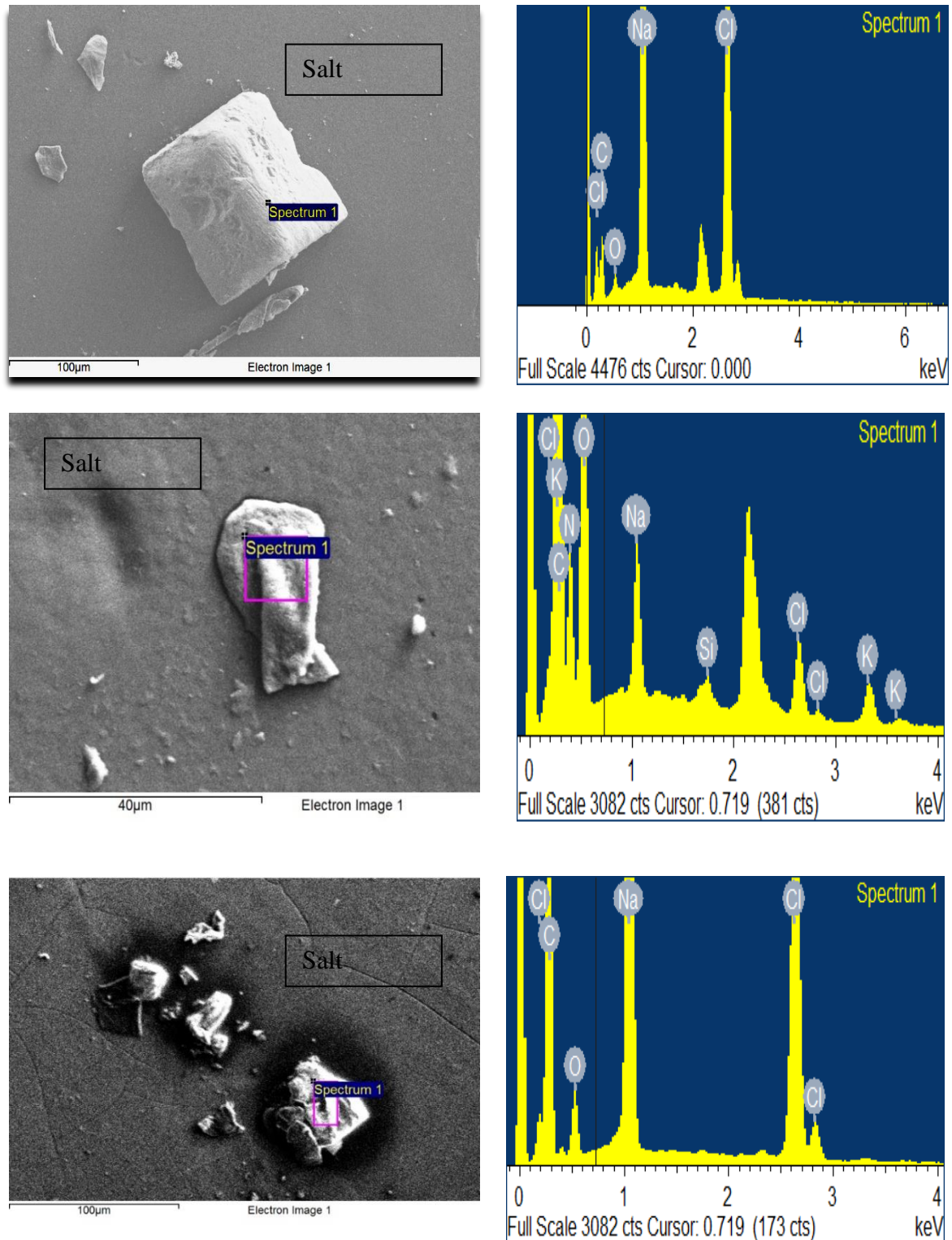
Figure 30 SEM micrograph and EDX coated sample at 15˚ Impact angle and 6.25 m/s velocity

Erosion Mapping of Coated Composites in Simulating Conditions for Tidal Turbines Blades.

A focused beam of high-energy electrons is used in a scanning electron microscope (SEM) to image the topography and learn about the material composition of conductive specimens. [141]. The SEM consists of an electron gun, a system of magnetic lenses, a scan control, and a detector, which work together to focus the electron beam on the sample and generate high-resolution images of its surface [141].

SEM was used to analyse the surface of an FR4-GRP coated with Belzona 2141. Fig. 30 of the SEM provided evidence of salt deposition on the coating surface, which occurred at an impact angle of 15 and 6.25 m/s velocity.

Figure 31 coated sample at 75 Impact angle and 8.42 m/s

The combination of the SEM image and the observation of an increase in mass in Fig. 30 provide strong evidence that the impact of the erodent caused salt deposition on the surface of the coating. This finding is important because it can have implications for the performance of the coating in tidal turbine operation, as salt deposition can have detrimental effects on the integrity and durability of coatings [12].

Fig. 31 shows the results of an erosion test on a coating surface, specifically at a 75° angle and a velocity of 8.42 m/s. Fig.31 indicates that this impact caused significant damage to the coating, as evidenced by the presence of voids, cavities, and loose debris scattered around the eroded surface.

The specific impact angle of 75° and a velocity of 8.42 m/s are significant because they provide information about the strength and durability of the coating. The voids and cavities in the figure indicate that the impact caused the coating material to fracture and break apart. This type of damage can weaken the structural integrity of the coating and may compromise its ability to

provide protection to the underlying material or surface [80]. The loose debris from sand and broken fibres scattered around the impact site suggests that the force of the impact was strong enough to dislodge and scatter coating material beyond the immediate vicinity.

Fig 5 confirms the presence of loose debris and coating erosion due to deformation and cutting
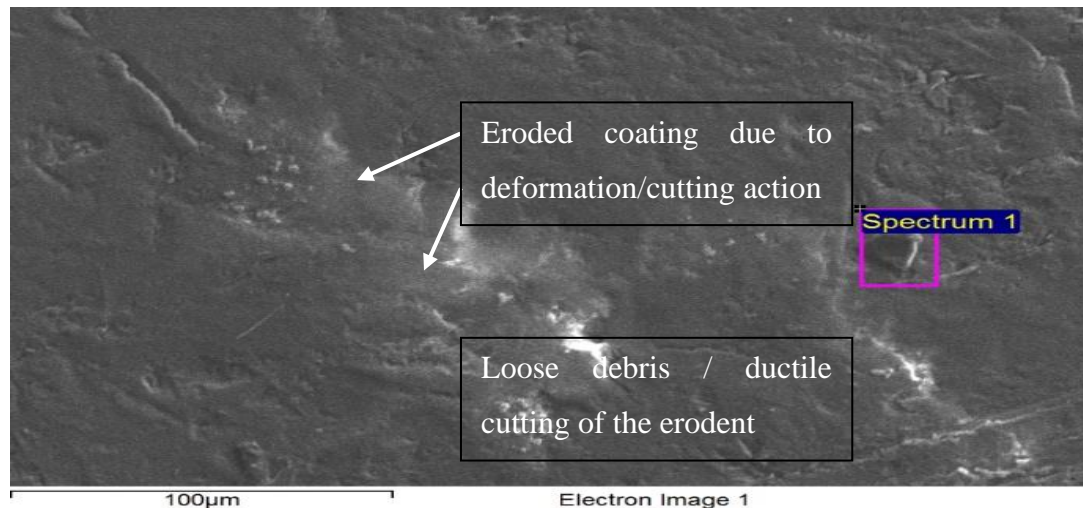
Figure 32 Coated sample at 90 Impact angle and 10.16m/s

action at a higher impact velocity of 10.16 m/s and an impact angle of $90°$. The figure also confirms the ductile cutting in the coating at these test conditions [134].

The presence of loose debris indicates that the impact caused some material to be dislodged or broken apart, similar to what was observed in Fig. 31. The confirmation of loose debris and coating erosion at higher impact conditions suggests that the coating may not be able to withstand high-speed impacts at these conditions. The presence of ductile cutting in the coating further confirms that the coating is a ductile material, as was observed in Fig. 32 at lower impact conditions [146].

The combination of loose debris, coating erosion, and ductile cutting observed in Fig. 32 provides evidence of the extent of damage caused by the impact at these higher impact conditions. The deformation and cutting action caused significant damage to the coating, resulting in the removal of material and the formation of loose debris.

The confirmation of ductile cutting at higher impact conditions is significant because it suggests that the coating may undergo significant plastic deformation before fracturing [61].

Erosion Mapping of Coated Composites in Simulating Conditions for Tidal Turbines Blades.

This information is important for understanding the behaviour of the coating under high-speed impact conditions and for determining the potential applications of the coating in environments with high-speed impacts.
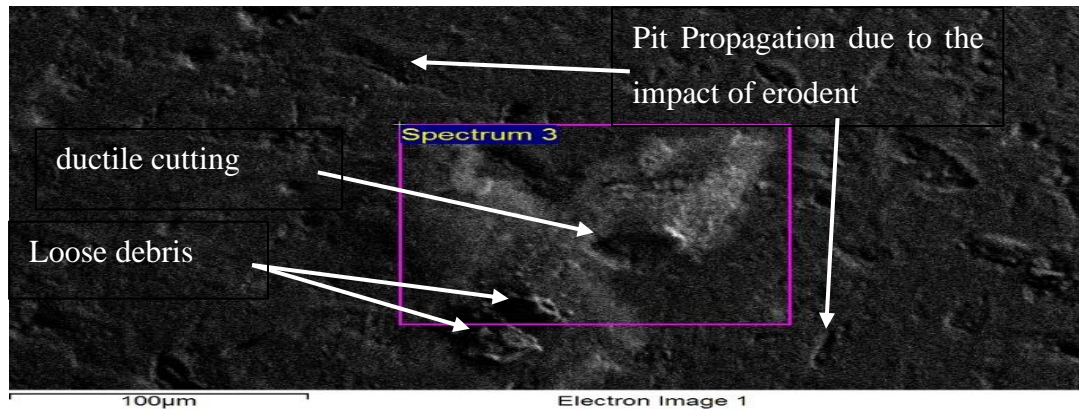
Figure 33 Coated sample at 75 Impact angle and 10.16m/s velocity.

Fig. 33 shows that at an impact angle of 75° and a velocity of 10.16 m/s, the coated surface suffered from pit propagation due to the impact of the erodent. The figure also shows the presence of loose debris and ductile cutting.

The observation of pit propagation is significant because it suggests that the impact caused the coating to undergo significant material removal in the form of pits. The presence of loose debris and ductile cutting further confirms that the impact caused damage to the coating surface [11], [61].

The combination of pit propagation, loose debris, and ductile cutting observed in Fig 6 provides evidence of the extent of damage caused by the impact under these conditions. The deformation and cutting action caused significant damage to the coating, resulting in the formation of pits and the removal of material, which formed loose debris.

The observation of ductile cutting in Fig. 33 is consistent with the observation in Fig. 32, which suggests that the coating is a ductile material. This information is important for understanding the behaviour of the coating under high-speed impact conditions and for determining the potential applications of the coating in environments with high-velocity impacts [174].

6.5 Erosion Mapping of Surface Coating
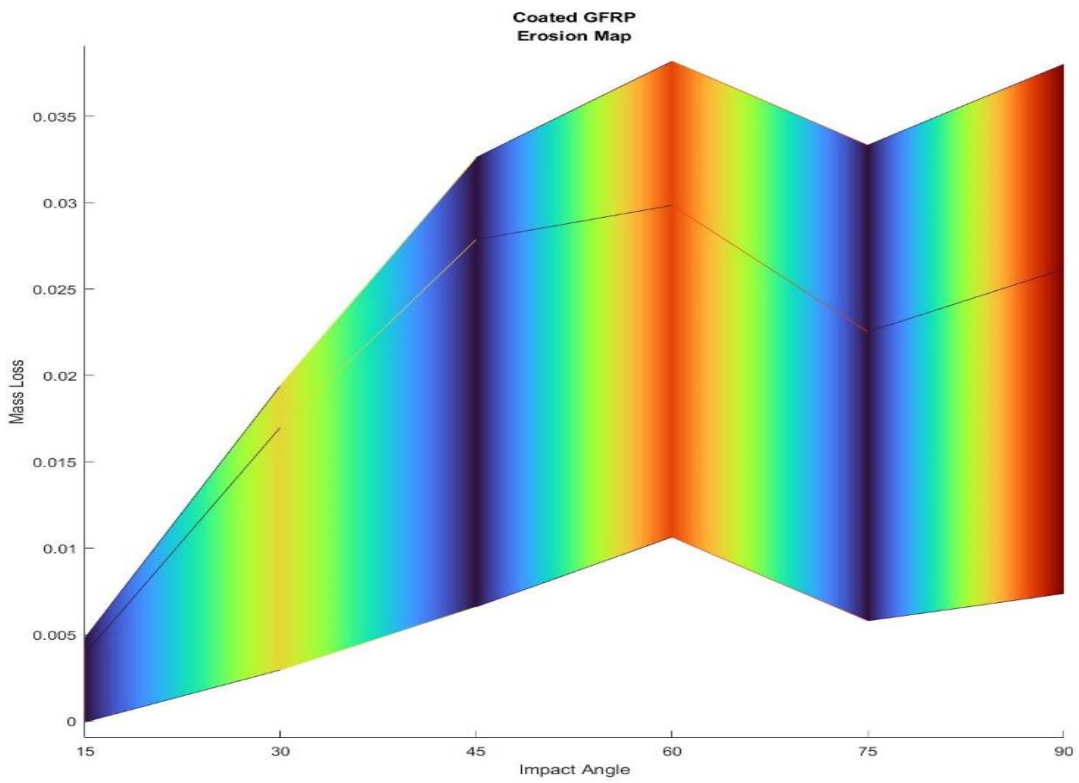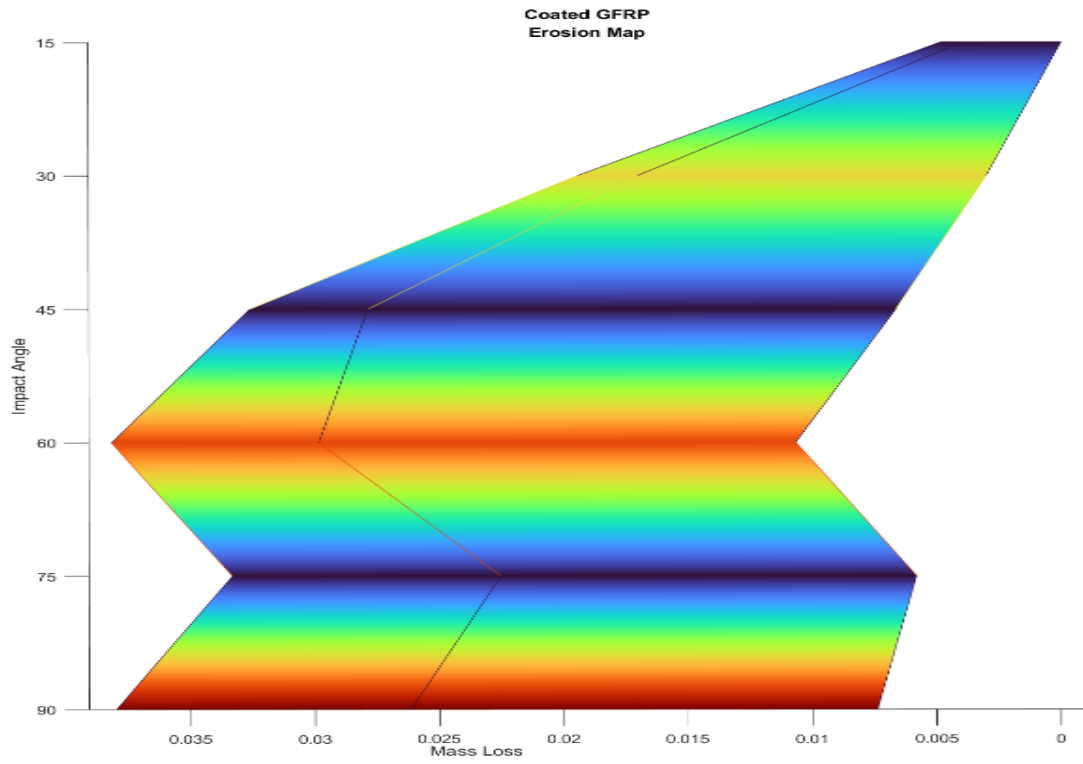
Figure 34 Erosion map of surface coating

Erosion Mapping of Coated Composites in Simulating Conditions for Tidal Turbines Blades.

To visualise damage, erosion maps were created as an alternative method. These maps were constructed using the procedures outlined by [123].

The aim of the study was to produce erosion maps and patterns in coated samples using a developed code written in MATLAB. This map allowed for the analysis and assessment of the coating erosion process, giving valuable insights into material behaviour under different conditions. Utilising the maps can aid in comprehending erosion mechanisms in coating and composite materials, which can assist design engineers in forecasting safety levels during operation and lead to the creation of a more sturdy and long-lasting coating for tidal turbine blades [165].

The erosion map provides a graphical representation of the level of material loss experienced by the coating under different impact velocities and angles [52]. The map in fig. 34 indicates that the coating is most resistant to erosion when tested at impact angles of $15°$, $30°$, $45°$, and $75°$ and velocities of 6.25 m/s, 8.42 m/s and 10.16 m/s, suggesting that the coating's design is most effective at deflecting the force of the impacting particles when it is applied at these angles.

In contrast, the coating experiences higher levels of erosion when tested at impact angles of $60°$ and $90°$ and velocities of 6.25 m/s, 8.42 m/s and 10.16 m/s, indicating that the design may not be as effective at deflecting the force of particles at these angles. This suggests that design modifications may be necessary to enhance the coating's performance under these impact conditions[175].

Fig 34 revealed that the coating performed best at a velocity of 6.25 m/s compared to velocities of 8.42 m/s and 10.16 m/s. This data can be used to optimise the design of the tidal turbine blades to reduce the impact of ocean currents and tides, potentially reducing erosion and improving the durability of the coating.

Overall, the erosion map provides valuable insights into the behaviour of the coating under different impact conditions [132]. By analysing the map, design engineers can determine the optimal impact angles and velocities for the coating, enabling them to optimise the design of the tidal turbine blades for increased durability and longevity. The map's findings can be used to enhance the efficiency and sustainability of harnessing the power of ocean currents and tides through tidal turbines[9].

6.6 Main conclusion and Summary of Findings

The study aimed to address the erosion challenges of the coating material used in tidal turbine blades. The coating design proposed in the study proved to be effective in reducing material loss due to erosion compared to GFRP addressed in previous chapters. The study also emphasised the importance of using erosion maps to visualise and analyse the level of material loss under different impact conditions. The erosion map produced in the study provides valuable insights into the behaviour of the coating and can be used to optimise the design of tidal turbine blades for increased durability and longevity [39].

The coating material showed better performance compared to GFRP addressed in previous chapters, with the lowest erosion rate observed at an impact velocity of 6.24 m/s. The highest erosion was observed at 75° and 90° impact angles at all impact velocities. The erosion maps displayed the level of material loss experienced by the coating under different impact conditions, providing valuable insights for the design of tidal turbine blades.

In addition to the erosion rate and impact velocity, the study also identified the type of erosion observed in the coating material. The erosion mechanism was found to be ductile erosion, which is a type of erosion where the material undergoes plastic deformation before it fails. Ductile erosion is a desirable type of erosion as it allows the material to withstand more wear and tear before it breaks down. The study's finding that the coating material underwent ductile erosion suggests that it can better resist the wear and tear caused by the harsh underwater conditions present in tidal turbines. By understanding the type of erosion that the coating material undergoes, engineers can better design the coating to improve its durability and longevity.

94

Chapter Seven

Investigation of Depth Profiling and Erosion Behaviour in Composite Materials and Polymeric Coatings

Chapter 7 Investigation of Depth Profiling and Erosion Behaviour in Composite Materials and Polymeric Coatings

7.1 Introduction

Erosion is a complex process involving the degradation of a material due to the impact of particles on the surface, leading to the loss of material and changes in the surface morphology and microstructure [176]

The erosion depth profiling analysis of the blades materials used in previous chapters will be studied in this chapter by comparing the depth profiling of uncoated and coated samples. The benefit of using erosion mapping and depth profiling techniques to investigate erosion behaviour on the material used in tidal turbine blades will be highlighted.

Erosion behaviour on materials, particularly in harsh environments like those encountered in tidal turbine blades, is better understood through the use of erosion mapping and depth profiling techniques. By conducting erosion depth profiling, a better understanding of how materials are affected by erosion and how their durability and resistance to wear and tear can be improved is obtained.

The benefits of using these techniques and the importance of studying erosion behaviour in tidal turbine blades are explored in this chapter. By gaining a better understanding of erosion in these blades, their performance can be improved, their lifespan can be increased, and ultimately, they can become more cost-effective and sustainable.

7.2 Erosion Maps vs Depth Profiling

Erosion mapping and depth profiling are two different techniques used to analyse the erosion behaviour of materials. [123] explain that erosion mapping is a technique used to visually represent the distribution of erosion on a material surface. This is typically done using a color-coded map that indicates the severity of erosion at different points on the surface. Erosion mapping can provide valuable information about the pattern and extent of erosion on a material surface and can be used to identify areas that are particularly vulnerable to erosion [177].

Depth profiling, as explained by [150], is a technique used to determine the depth of penetration of the erosion on the material surface. This technique involves measuring the erosion depth at different points on the material surface, typically using a high-resolution microscope or profilometer. Depth profiling provides valuable information about the extent of the damage to

the material and can be used to determine the effectiveness of different materials and coatings in resisting erosion.

However, erosion mapping does not provide information about the depth of penetration of the erosion, which is important in determining the overall damage to the material. Similarly, depth profiling does not provide information about the pattern or distribution of erosion on the material surface.

In summary, erosion mapping and depth profiling are two different techniques used to analyse the erosion behaviour of materials. Both techniques are important in understanding the erosion behaviour of materials and can be used to inform the development of more erosion-resistant materials and coatings.

7.3 Depth Profiling Analysis

7.3.1 Keyence VHX-7000

The Keyence VHX-7000 is a high-resolution microscope that is commonly used for depth profiling analysis of materials. This instrument allows for precise measurements of erosion depth and characterization of surface features such as cracks, pores, and other defects. The VHX-7000 uses a unique optical system to provide high-resolution, three-dimensional images of materials with sub-micron accuracy.

According to [178], the Keyence VHX-7000 has a number of advantages over other techniques for depth profiling analysis. For example, the instrument is capable of measuring the depth of erosion at very high resolution, which is important for accurately characterising the damage to materials. Additionally, the VHX-7000 can be used to detect and analyse small-scale features on the material surface, such as micro-cracks and pores, which can contribute to erosion damage.

Keyence VHX-7000 is a powerful tool for depth profiling analysis of materials and is capable of providing high-resolution images and precise measurements of erosion depth and surface features. This instrument has been used by researchers in a variety of fields to analyse the erosion behaviour of different materials.

7.4 Characterization of erosion penetration depth

Characterization of erosion penetration depth is an important aspect of studying erosion mechanisms in materials. The erosion penetration depth can provide information about the material's ability to resist erosion and can help in the identification of the most vulnerable

regions of the material surface [179]. One commonly used method for characterization of erosion penetration depth is depth profiling, which involves measuring the depth of erosion by removing thin slices of the eroded material and analysing them using various techniques such as microscopy and spectroscopy [180].

In recent years, advanced techniques such as confocal laser scanning microscopy and atomic force microscopy have been used for the characterization of erosion penetration depth. These techniques provide high-resolution images and can reveal information about the morphology and topography of the eroded surface.

Depth profiling is a powerful tool used to understand the extent and nature of damage caused by erosion. One of the most advanced and commonly used tools for this purpose is the Keyence VHX-7000 microscope, which offers high-resolution imaging and 3D visualization capabilities. By analysing the depth profile of eroded surfaces, the characterization of erosion penetration depth and the identification of defects can be performed with high accuracy and precision. This information is critical for understanding the erosion mechanisms and improving the design and performance of materials subjected to erosive environments.

Numerous studies have utilised the optical and scanning electron microscope for depth profiling of various materials subjected to erosion. For example, a study by [181] used the Keyence VHX-7000 to investigate the mechanism of degradation of porous metal-organic frameworks.

7.5 Results and Discussion

In GFRP composites, the wear mechanism is influenced by various factors, including the fibre-matrix interface, the orientation of fibres, and the type of matrix material [182]. The use of depth profiling analysis has become increasingly common in the characterization of materials, particularly in the study of surface damage caused by mechanical wear, corrosion, or both. In

recent years, depth profiling analysis techniques have been widely applied in the study of erosion damage in GFRP composites [183]

The 3D depth profiling analysis presented in Fig. 35 reveals the extent of erosion damage experienced by a GFRP composite sample tested at an impact angle of 60° and a fibre orientation of 90°. The depth profiling analysis captures the erosion damage across the entire
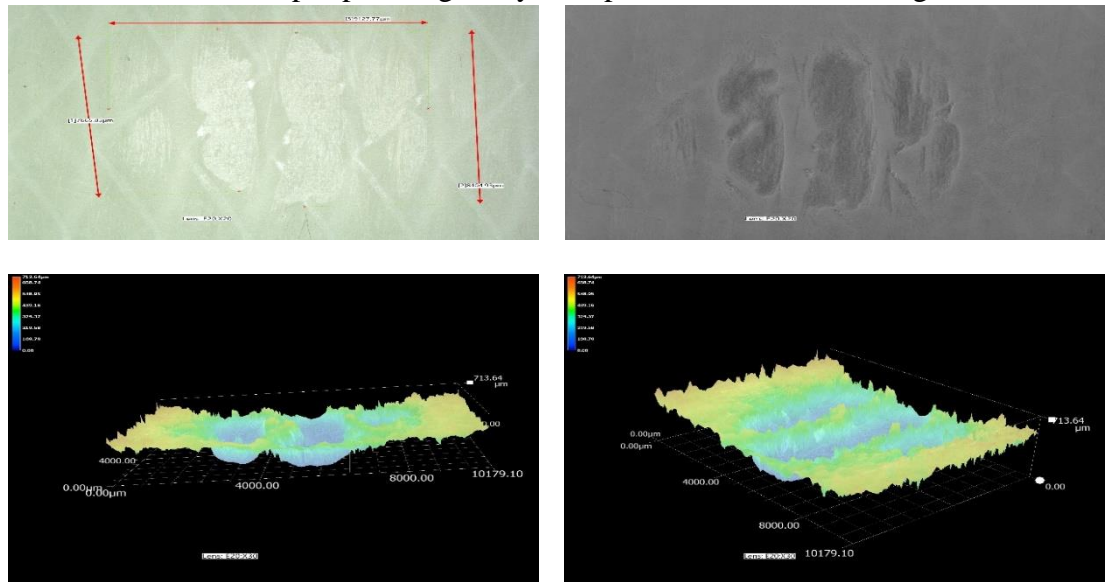
Figure 35. 3D profile for uncoated GFRP at 60° impact angle and 90° fibre orientation and 9.04 m/s

surface of the sample, allowing for a comprehensive assessment of the damage sustained. The results show that the eroded sample experienced a loss of 713.64 µm in depth, indicating severe erosion damage.
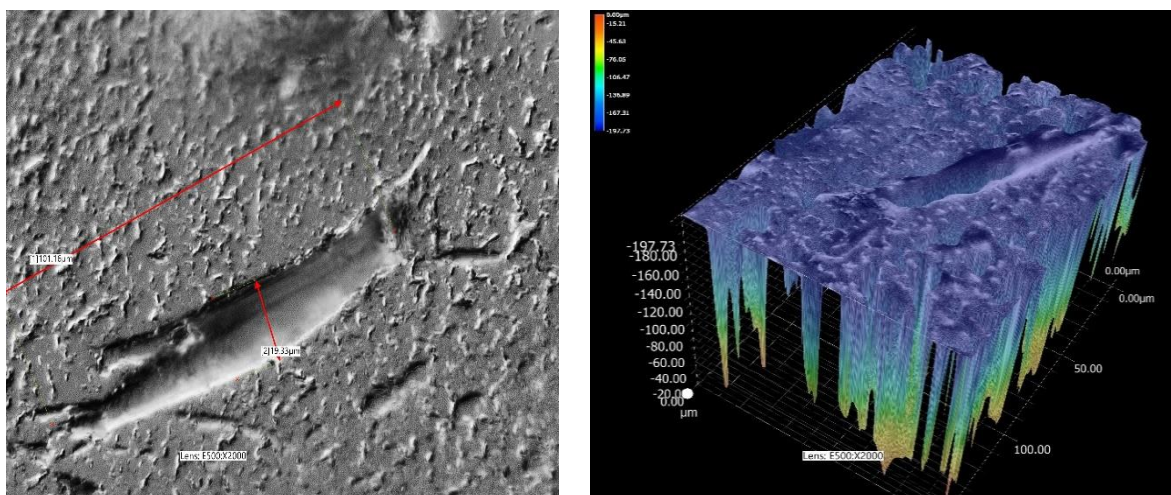
Figure 36. 3D Depth profile of the coated sample at an impact angle of 60° and impact velocity of 10.16 m/s

The depth profiling analysis in Figure 35 reveals that the erosion damage in the GFRP composite sample was primarily due to material loss resulting from the impact of particles. The

impact of the particles caused surface defects, such as cracks and pits, which led to the loss of material and changes in the surface morphology [184]

Figure 36 presents a 3D depth profile analysis of a Belzona 2141 coated sample described in section 4.3, subjected to solid particle erosion at an impact angle of $60°$ and impact velocity of 10.16 m/s. The results indicate that the material suffered a maximum loss of 197.73 µm in depth due to the erosion caused by solid particles. Moreover, the 3D depth analysis clearly shows the formation of voids and cutting of the coating when the silica particle hit the coated surface.

The presence of voids and matrix cutting suggests that the coating has undergone significant deformation during the impact event. Voids can be caused by the detachment of the coating from the substrate or the collapse of the coating due to the force of the impact. Matrix cutting occurs when the coating material is sheared or sliced by the projectile or by the deformation of the coating during the impact event.
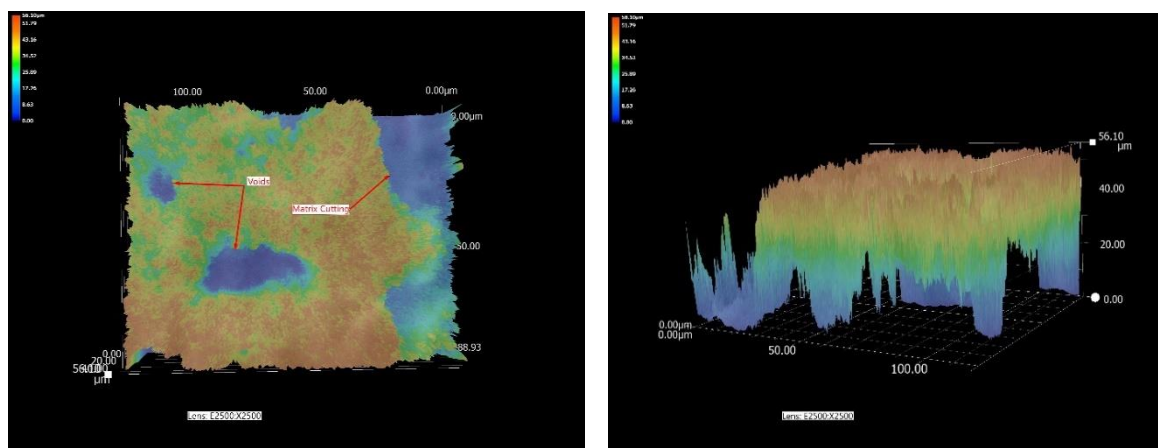
Figure 37. UD-GFRP sample at an impact angle of $75°$; $90°$ fibre orientation and velocity of 9.04 m/s

Fig. 37 depicts the impact of erosion on a unidirectional glass fibre reinforced polymer (UD-GFRP) sample at an impact angle of $75°$ and an impact velocity of 8.42 m/s. The analysis of the sample indicates that it has suffered a loss of 56.10 µm in depth, with the presence of voids and matrix cutting. the presence of voids and matrix cutting suggests that the erosion process was predominantly ductile. The resin matrix of the composite is a relatively brittle material compared to the glass fibres and is therefore more susceptible to fracture upon impact. The presence of voids and matrix cutting indicates that the resin matrix has fractured or detached from the glass fibres upon impact, resulting in the rapid and removal of material from the composite surface.
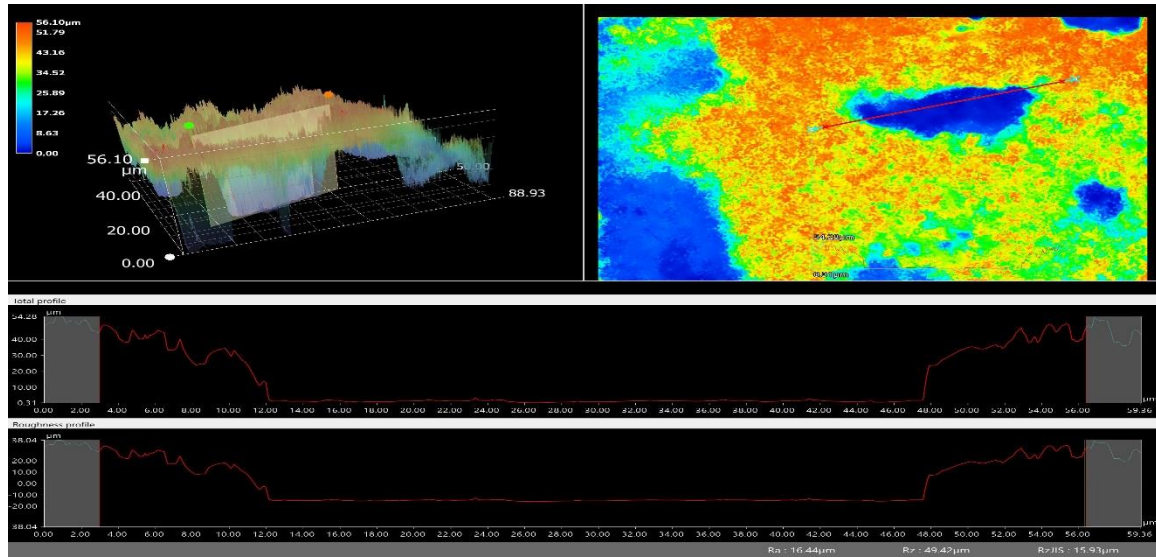
Figure 38 UD-GFRP at 45° impact angle and 45° fibre orientation and 9.04 m/s velocity

Fig. 38 and Fig. 39 show the analyses of the surfaces of eroded UD-GFRP and eroded coated samples, at 45° impact angle respectively, under the influence of solid particle erosion. While both figures depict surfaces that have undergone erosion by solid particles, there are some differences between the results shown in Fig. 38 and Fig. 39.
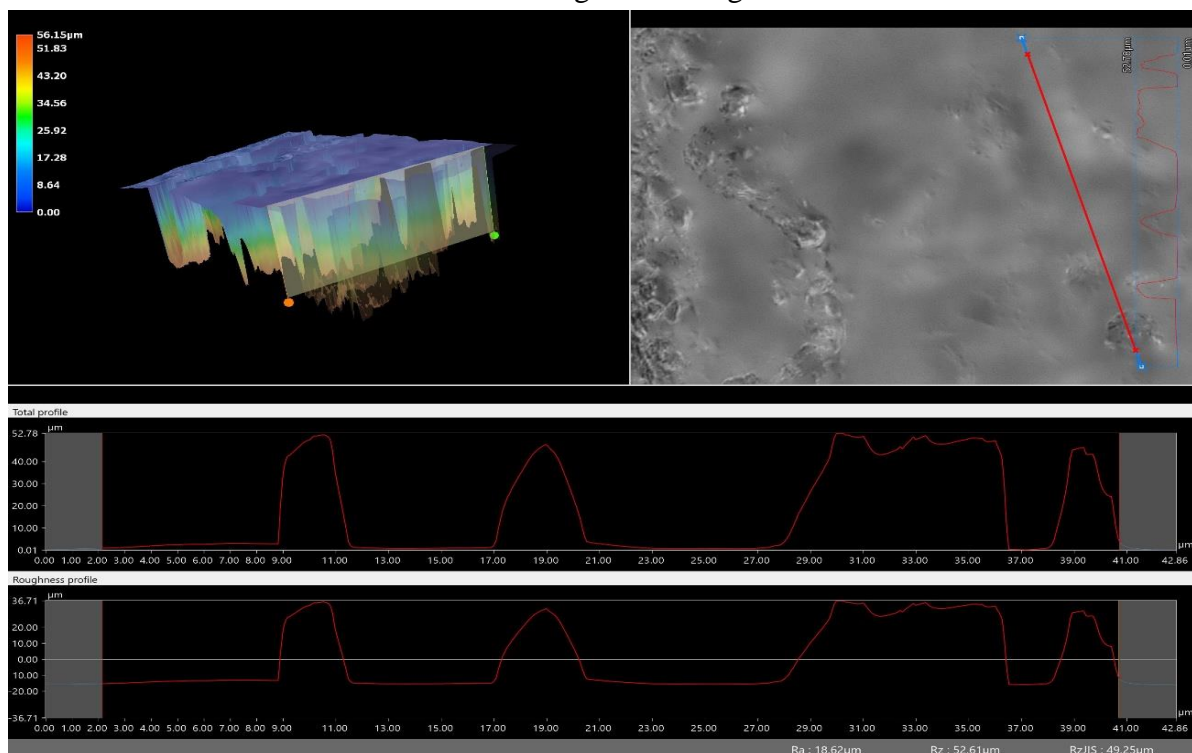
Figure 39. Coated sample at 45° impact angle and 10.16 m/s velocity.

Fig. 4 shows the analysis of an eroded UD-GFRP sample, indicating an average surface roughness value of 14.44 µm. This suggests that the erosion process has caused a significant

amount of material loss and surface damage, resulting in a rough and irregular surface. The roughness value may be attributed to the detachment of the resin matrix, exposing the glass fibres, and resulting in surface roughness.

Fig. 5 shows the analysis of an eroded coated sample, indicating an average roughness value of 18.61 µm. This value is higher than that of the eroded UD-GFRP sample in Fig. 4, indicating a rougher surface. The presence of the coating may provide a layer of protection against solid particle erosion, but the coating itself may also contribute to surface roughness if it is not properly adhered to the substrate or if it is susceptible to erosion. The higher roughness value in Fig. 5 may suggest that the coating has suffered from erosion and detachment, resulting in a rougher surface.

Fig. 6 shows the analysis of a coated sample that has undergone solid particle erosion at an impact angle of 60° and a velocity of 6.25 m/s. The analysis reveals that the sample has been exposed to severe erodent hitting, resulting in the formation of scars and voids on the surface. The scars and voids indicate that the coating has been partially removed from the surface, exposing the underlying substrate to further erosion.
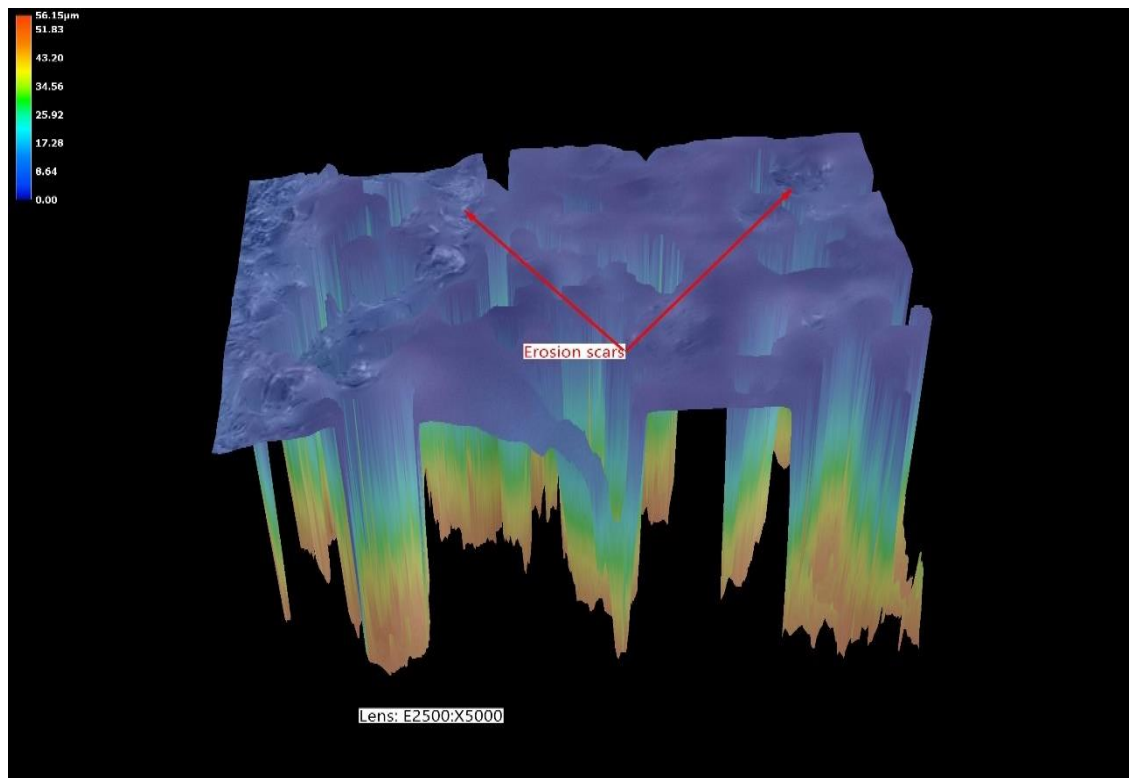
Figure 40.3D depth profiling for coated sample at 6.25 m/s velocity

101

Investigation of Depth Profiling and Erosion Behaviour in Composite Materials and Polymeric Coatings

The results presented in Fig. 41 indicated that two distinct techniques were employed to investigate the erosion mechanism resulting from solid particles on turbine blades subjected to an impact angle of 75. One of the techniques involved generating a figure denoted as (a), which demonstrated the depth of the defect incurred from erosion. This figure (a) shows that the erosion caused a loss of 56.20 µm in depth due to the existence of voids on the sample surface. The second technique entailed the creation of an erosion map Fig. 41 (b), which provided concrete evidence of the erosion damage sustained at the same impact angle of 75 degrees. The erosion map revealed the distribution of the eroded material on the blade's surface, thereby enabling to pinpoint areas that are especially vulnerable to erosion. The application of both techniques is critical in comprehending the erosion mechanism resulting from solid particles and its impact on turbine blades. The figure 41(a) furnishes quantifiable data on the depth of the defect attributable to erosion, while the erosion map fig. 41 (b) offers a visual representation of the extent of the erosion damage. Together, these techniques enabled us to identify the contributory factors of erosion and formulate effective strategies for mitigating its impact on turbine blades. The findings reported here provide empirical evidence that erosion resulting from solid particles can significantly affect the efficacy and longevity of turbine blades. A thorough understanding of the erosion mechanism and the development of effective strategies for mitigating its effects are vital for enhancing the efficiency and dependability of tidal turbines.
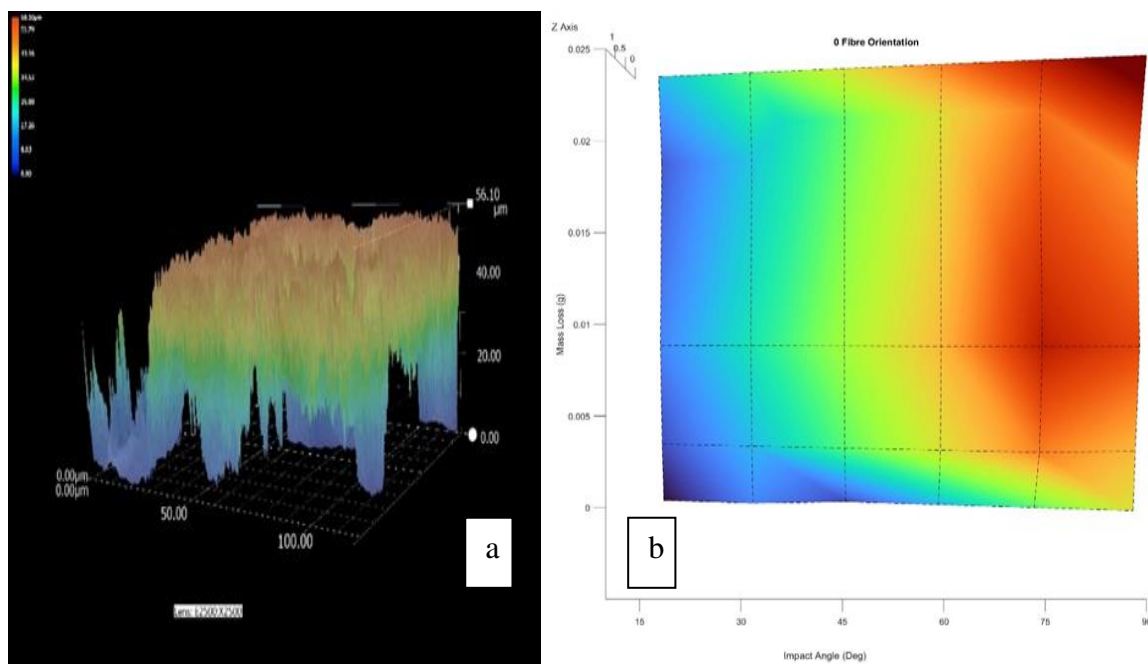
Figure 41. (a) Depth profiling (b) Erosion maps of UD-GFRP with 90 fibre orientation and 75 impact angle

7.6 Main conclusion and Summary of Findings

The study highlights the importance of investigating the erosion mechanism of materials used in tidal turbine blades, and how depth profiling techniques can provide valuable insights into the surface morphology, microstructure, and chemical composition of the material. The depth profiling technique combined with erosion maps was found to be an effective method for investigating the erosion mechanism in coated and uncoated materials. By using this technique, researchers can identify the underlying wear mechanism, develop effective strategies to improve wear and erosion resistance, and optimise the design of tidal turbine blades for increased durability and longevity.

The presence of a coating may offer some protection against erosion, but if it is not properly adhered or if it is susceptible to erosion itself, it can contribute to surface roughness and damage. The severity of erosion and surface damage depends on several factors, including the properties of the erodent particles, the impact angle, and the velocity of the particles.

The analysis reveals that the sample has been exposed to severe erodent hitting, resulting in the formation of scars and voids on the surface. The erosion process caused a significant amount of material loss and surface damage, resulting in a rough and irregular surface. The severity of the erosion and surface damage increased with increasing impact angle and velocity. The coating provided some protection against erosion, but it was observed that the surface roughness was higher for the coated sample compared to the uncoated sample.

Chapter Eight

General Conclusions & Future Work

Chapter 8 General Conclusions and Future Work

8.1 Overview

Tidal turbines are a renewable energy technology that uses the power of the tides to generate electricity. The harsh marine environment in which tidal turbines operate presents significant challenges, including erosion of the blades caused by the abrasive forces of the water. Erosion can cause significant damage to the blades, reducing their efficiency and increasing maintenance costs. Therefore, there is a need for more durable and erosion-resistant materials to increase the lifespan of tidal turbines and reduce maintenance costs.

The study focused on investigating erosion and tribological concerns in tidal turbine blades, which are subject to severe erosion due to the harsh marine environment. Specifically, the study aimed to understand the erosion mechanism in unidirectional glass fibre-reinforced polymer (UD-GFRP) and coating materials and the influence of seawater immersion on their mechanical properties. In his thesis a series of experiments conducted to investigate the effect of different impingement angles, impact velocities, particles size and fibre orientations on erosion, as well as the effect of seawater immersion on the mechanical properties of the materials.

8.2 Erosion Mechanism in UD-GFRP Materials with Varied Fibre Orientations

It was found that the impingement angle of $15°$ caused the least amount of erosion in UD-GFRP material. Additionally, the $0°$ fibre orientation UD-GFRP was less affected by erosion compared to the $90°$ fibre orientation UD-GFRP. The effect of erosion was greatest for $90°$ fibre orientation when solid particles impinged at a $30°$ angle. The erosion mechanism in GFRP was the result of the fibre matrix being eroded away, with the surface composite cracking and the fibres being removed, exposing the matrix due to the surface's broken glass fibres.

8.3 Strategies to Increase Durability and Longevity of Tidal Turbine Blades:

The study explored strategies to increase the durability and longevity of tidal turbine blades, which are subject to severe erosion due to the harsh marine environment. One approach was the use of gradient-toughened composites with varying proportions of standard and toughened powders. The gradient-toughened composite with varying proportions of standard and

toughened powders showed better erosion performance than the standard epoxy plates, providing a potential solution to the erosion challenges faced by tidal turbine blades.

The use of a powder-epoxy fabrication method allowed for the creation of a laminate with a harder but weaker epoxy matrix for the remainder of the material and the strongest epoxy matrix on the sea-eroded surface. The study found that at a $15°$ impingement angle, both standard (STD) and gradient-toughened (GRD) epoxy plates showed no significant mass loss or sand particle embedding. However, the GRD plates outperformed the STD plates in general, and the mass loss increased with increasing impingement angle. The GRD plates had a more ductile response to erosion than the STD plates, with the greatest amount of mass loss occurring at an impact angle of $60°$, compared to the STD plates, which experienced the highest amount of mass loss at an impact angle of $90°$.

8.4 Erosion Mechanism in Coating

The study also addressed the erosion challenges of the coating material used in tidal turbine blades and highlighted the importance of using erosion maps to visualise and analyse the level of material loss experienced by coatings under different impact conditions. The severity of erosion and surface damage depends on several factors, including the properties of the erodent particles, the impact angle, and the velocity of the particles.

The coating material showed a good performance, with the lowest erosion rate observed at an impact velocity of 6.24 m/s. The highest erosion was observed at $75°$ and $90°$ impact angles at all impact velocities. Additionally, the type of erosion observed in the coating material was ductile erosion, which is desirable as it allows the material to withstand more wear and tear before it breaks down.

In conclusion, the study highlighted the importance of using erosion maps to visualise and analyse the level of material loss experienced by coatings under different impact conditions. The severity of erosion and surface damage depends on several factors, including the properties of the erodent particles, the impact angle, and the velocity of the particles. By erosion maps, the mechanisms of erosion can be better understood, and more effective materials and coatings can be designed to withstand harsh environments.

8.5 Depth Profiling and Erosion maps Analysis

Depth profiling techniques have been found to be effective in providing insights into the surface morphology, microstructure, and chemical composition of the material. These

techniques, when combined with erosion maps, can be used to identify the underlying wear mechanism, and develop effective strategies to improve wear and erosion resistance.

One finding of the study is that the presence of a coating may offer some protection against erosion, but if it is not properly adhered or if it is susceptible to erosion itself, it can contribute to surface roughness and damage. The severity of erosion and surface damage depends on several factors, including the properties of the erodent particles, the impact angle, and the velocity of the particles.

The study further reveals that the sample under investigation has been exposed to severe erodent hitting, resulting in the formation of scars and voids on the surface. The erosion process caused a significant amount of material loss and surface damage, resulting in a rough and irregular surface. The severity of the erosion and surface damage increased with increasing impact angle and velocity.

While the coating provided some protection against erosion, it was observed that the surface roughness was higher for the coated sample compared to the uncoated sample. Therefore, it is important to ensure that the coating is properly adhered and is resistant to erosion to avoid contributing to surface roughness and damage.

8.6 Contribution to Knowledge

This research has made significant contributions to the understanding of erosion mechanisms in composite materials used in tidal turbine blades, as well as strategies to enhance their durability and longevity. The key contributions can be summarized as follows:

The study has provided valuable insights into the erosion mechanisms of unidirectional glass fibre-reinforced polymer (UD-GFRP) materials and coating materials under various environmental conditions. Specifically, it identified the impact of impingement angle, fiber orientation, and particle size on erosion in UD-GFRP materials. This knowledge enhances our understanding of how these factors influence erosion and helps in designing more erosion-resistant composite materials. Furthermore, the research highlighted the importance of ductile erosion in coating materials, indicating that these materials can withstand wear and tear before breaking down. This finding is crucial for designing coatings that can better protect tidal turbine blades from the harsh marine environment.

The study explored innovative strategies to increase the durability and longevity of tidal turbine blades, including the use of gradient-toughened composites with varying proportions of standard and toughened powders. This approach demonstrated improved erosion performance, offering a potential solution to the erosion challenges faced by these blades. This broader understanding is critical for developing materials that can withstand a wider range of erosion sources.

The research has opened up avenues for exploring the impact of environmental factors such as temperature and humidity on erosion mechanisms and mechanical properties of composite materials. This expanded scope can lead to the development of materials that are resilient across a broader range of environmental conditions. Furthermore, the study emphasised the importance of proper adherence and erosion resistance in coatings. Future investigations into coating materials and application methods can contribute to the development of more effective coatings for erosion reduction.

In conclusion, this research has made substantial contributions to the field of tidal energy technology by advancing our understanding of erosion mechanisms, proposing innovative strategies for durability enhancement, and paving the way for future research on environmental factors, coatings, and self-healing materials. These contributions collectively contribute to the development of more resilient and reliable materials for tidal turbine blades, ultimately supporting the growth of sustainable energy generation from tidal sources.

8.7 Future Work

Based on the current study's findings and limitations, several potential future research directions can be pursued to enhance our understanding of erosion mechanisms in composite materials and develop more robust and dependable materials for tidal turbine blades.

One area of focus could be on the investigation of the impact of different types and sizes of erosion particles on composite materials. The current study only examined solid particles, but other erosion particles such as sand and silt are also prevalent in marine environments. Investigating the effects of these erosion particles on composite materials can provide valuable insights into the erosion mechanism and help in the development of materials that can withstand a wider range of erosion particles.

Another area that requires further investigation is the erosion caused by cavitation. Cavitation occurs when low-pressure zones are formed in the water, causing bubbles to form and implode

on the surface of the blade, leading to surface erosion. To better understand this phenomenon, future studies can investigate the effect of different cavitation conditions on the erosion mechanism and the mechanical properties of composite materials.

In addition to the proposed future research directions mentioned above, the use of non-destructive testing (NDT) methods such as ultrasonic and X-ray diffraction (XRD) can also contribute significantly to the understanding of erosion mechanism in composite materials. These methods can detect subsurface defects resulting from erosion, such as delamination, which cannot be observed through visual inspection alone. By using these methods, researchers can gather valuable data on the extent and nature of the erosion damage and its effect on the mechanical properties of the material. This data can then be used to optimise the design of the material and develop more effective coatings to reduce erosion. Furthermore, a new approach such as bubble mapping could be used to demonstrate the analysis of the defect on the blade surface. This approach can provide a clear visual representation of the size and location of the defect, allowing for a more precise analysis of the erosion mechanism. Therefore, incorporating NDT methods and new approaches such as bubble mapping can enhance the accuracy and reliability of erosion analysis in composite materials, leading to the development of more durable and reliable materials for tidal turbine blades.

Another avenue for future research is the exploration of the impact of various environmental factors such as temperature and humidity on the erosion mechanism and mechanical properties of composite materials. Understanding how these factors affect erosion and mechanical properties can help in the development of materials that can withstand a wider range of environmental conditions.

In addition, future studies can examine the effectiveness of various coating materials and application methods in reducing erosion in composite materials. While the current study revealed that coatings can provide some protection against erosion, their effectiveness is contingent on their adherence and susceptibility to erosion themselves. Further research can explore the use of new materials and methods to develop coatings that are more durable and effective in reducing erosion.

Lastly, future studies can investigate the feasibility and effectiveness of incorporating self-healing mechanisms in composite materials to reduce erosion damage. Self-healing materials have the ability to repair themselves when damaged, which can significantly increase the durability and longevity of the materials. Investigating the use of self-healing mechanisms in

composite materials for tidal turbine blades can provide a promising solution to the erosion challenges faced by these materials in marine environments.

In conclusion, pursuing these research directions can lead to the development of more durable and dependable materials for tidal turbine blades, resulting in more efficient and sustainable energy generation from tidal sources. Furthermore, future testing protocols for tidal turbine materials, mechanistic evaluation, coatings versus uncoated structures, and new maps to be developed using techniques in the thesis can provide insights that can contribute to the development of erosion-resistant coatings for tidal turbine blades.

References

[1]   Iea-Reted, "Accelerating the Deployment of Offshore Wind, Tidal, and Wave Technologies," in *Offshore Renewable Energy* , 2011, p. 43.

[2]   Talal Husseini, "Riding the renewable wave: tidal energy advantages and disadvantages," *https://www.power-technology.com/features/tidal-energy-advantages-and-disadvantages/*, Oct. 26, 2018.

[3]   D. M. Grogan, S. B. Leen, C. R. Kennedy, and C. M. Ó Brádaigh, "Design of composite tidal turbine blades," *Renew Energy*, vol. 57, pp. 151–162, Sep. 2013, doi: 10.1016/J.RENENE.2013.01.021.

[4]   R. E. and M. M. N. McEwen, "Cost-Effective Tidal Turbine Blades, 4th International Conference on Ocean Energy," Dublin: (ICOE 2012), Oct. 2012.

[5]   Sloan Jeff, "Tidal turbine blade toughened for turbulent salt sea," *https://www.compositesworld.com/articles/tidal-turbine-blade-toughened-for-turbulent-salt-sea*, Nov. 30, 2012.

[6]   T. Flanagan, J. Maguire, C. Ó. Brádaigh, P. Mayorga, and A. Doyle, "Edinburgh Research Explorer Smart Affordable Composite Blades for Tidal Energy Smart Affordable Composite Blades for Tidal Energy," 2015.

[7]   CORDIS | European Commission, "Enabling sustainable electricity supply in Europe," *https://cordis.europa.eu/article/id/158547-enabling-sustainable-electricity-supply-in-europe*, Oct. 11, 2021.

[8]   J. N. Goundar and M. R. Ahmed, "Design of a horizontal axis tidal current turbine," *Appl Energy*, vol. 111, pp. 161–174, Nov. 2013, doi: 10.1016/J.APENERGY.2013.04.064.

[9]   G. Rasool, S. Sharifi, C. Johnstone, and M. M. Stack, "Mapping Synergy of Erosion Mechanisms of Tidal Turbine Composite Materials in Sea Water Conditions," *J Bio Tribocorros*, vol. 2, no. 2, Jun. 2016, doi: 10.1007/s40735-016-0040-5.

[10]   R. A. R. Ahamed, C. M. Johnstone, and M. M. Stack, "Impact Angle Effects on Erosion Maps of GFRP: Applications to Tidal Turbines," *J Bio Tribocorros*, vol. 2, no. 2, Jun. 2016, doi: 10.1007/s40735-016-0044-1.

References

[11] G. Rasool and M. M. Stack, "Some Views on the Mapping of Erosion of Coated Composites In Tidal Turbine Simulated Conditions," *Tribology Transactions*, vol. 62, no. 3, pp. 512–523, 2019, doi: 10.1080/10402004.2019.1581313.

[12] G. Rasool, C. Johnstone, and M. M. Stack, "Tribology of Tidal Turbine Blades: Impact angle effects on erosion of polymeric coatings in sea water conditions."

[13] Belzona, "https://www.belzona.com/en/products/2000/2141.aspx."

[14] M. Roy and J. P. Davim, *Thermal sprayed coatings and their tribological performances*.

[15] K. Y, "'Erosion of Metals by Solid Particles,'" *J Mater*, vol. 2, p. 682, 1967.

[16] N. Miyazaki, "Solid particle erosion of composite materials: A critical review," *J Compos Mater*, vol. 50, no. 23, pp. 3175–3217, Dec. 2015, doi: 10.1177/0021998315617818.

[17] D. Aquaro and E. Fontani, "Erosion of Ductile and Brittle Materials," *Meccanica*, vol. 36, no. 6, pp. 651–661, 2001, doi: 10.1023/A:1016396719711.

[18] A. Evstifeev, N. Kazarinov, Y. Petrov, L. Witek, and A. Bednarz, "Experimental and theoretical analysis of solid particle erosion of a steel compressor blade based on incubation time concept," *Eng Fail Anal*, vol. 87, pp. 15–21, May 2018, doi: 10.1016/J.ENGFAILANAL.2018.01.006.

[19] E. Bousser, L. Martinu, and J. E. Klemberg-Sapieha, "Solid particle erosion mechanisms of protective coatings for aerospace applications," *Surf Coat Technol*, vol. 257, pp. 165–181, Oct. 2014, doi: 10.1016/J.SURFCOAT.2014.08.037.

[20] S. Ahmad Alidokht, P. Vo, S. Yue, and R. R. Chromik, "Erosive wear behavior of Cold-Sprayed Ni-WC composite coating," *Wear*, vol. 376–377, pp. 566–577, Apr. 2017, doi: 10.1016/J.WEAR.2017.01.052.

[21] M. Parsi, K. Najmi, F. Najafifard, S. Hassani, B. S. McLaury, and S. A. Shirazi, "A comprehensive review of solid particle erosion modeling for oil and gas wells and pipelines applications," *J Nat Gas Sci Eng*, vol. 21, pp. 850–873, Nov. 2014, doi: 10.1016/J.JNGSE.2014.10.001.

References

[22] M. Naveed, H. Schlag, F. König, and S. Weiß, "Influence of the Erodent Shape on the Erosion Behavior of Ductile and Brittle Materials," *Tribol Lett*, vol. 65, no. 1, p. 18, 2016, doi: 10.1007/s11249-016-0800-x.

[23] S. Nsoesie, R. Liu, K. Y. Chen, and M. X. Yao, "Analytical modeling of solid-particle erosion of Stellite alloys in combination with experimental investigation," *Wear*, vol. 309, no. 1–2, pp. 226–232, Jan. 2014, doi: 10.1016/J.WEAR.2013.11.026.

[24] Md. A. Islam, Z. N. Farhat, and E. M. Ahmed, "Influence of Impact Angle and Velocity on Erosion of AISI 1018 Steel Under Jet Impingement," 2012.

[25] S. J. Bull, "Using work of indentation to predict erosion behavior in bulk materials and coatings," *J Phys D Appl Phys*, vol. 39, no. 8, p. 1626, Mar. 2006, doi: 10.1088/0022-3727/39/8/023.

[26] C. Wang, "Indentation and Fracture Behaviour of Electroless Ni-P-based Composite Coatings," 2017.

[27] E. M. Fayyad, A. M. Abdullah, M. K. Hassan, A. M. Mohamed, G. Jarjoura, and Z. Farhat, "Recent advances in electroless-plated Ni-P and its composites for erosion and corrosion applications: a review," *Emergent Mater*, vol. 1, no. 1, pp. 3–24, 2018, doi: 10.1007/s42247-018-0010-4.

[28] A. Sadeghzadeh-Attar, G. AyubiKia, and M. Ehteshamzadeh, "Improvement in tribological behavior of novel sol-enhanced electroless Ni-P-SiO2 nanocomposite coatings," *Surf Coat Technol*, vol. 307, pp. 837–848, Dec. 2016, doi: 10.1016/J.SURFCOAT.2016.10.026.

[29] H. Tsukamoto, "Design against fracture of functionally graded thermal barrier coatings using transformation toughening," *Materials Science and Engineering: A*, vol. 527, no. 13–14, pp. 3217–3226, May 2010, doi: 10.1016/J.MSEA.2010.01.087.

[30] J. Hou, Q. Li, J. Lv, and H. Zuo, "Crack deflection by the transformable particles dispersed in composites," *Acta Mech*, vol. 227, no. 3, pp. 743–756, 2016, doi: 10.1007/s00707-015-1440-1.

[31] R. A. Filippov, A. B. Freidin, I. V Hussainova, and E. N. Vilchevskaya, "Critical radius of zirconia inclusions in transformation toughening of ceramics," *Physical Mesomechanics*, vol. 18, no. 1, pp. 33–42, 2015, doi: 10.1134/S1029959915010051.

References

[32] S. G. Warrier, B. S. Majumdar, and D. B. Miracle, "Interface effects on crack deflection and bridging during fatigue crack growth of titanium matrix composites," *Acta Mater*, vol. 45, no. 12, pp. 4969–4980, Dec. 1997, doi: 10.1016/S1359-6454(97)00179-1.

[33] G. Sundararajan, "The nature of plastic deformation during single impact and its relevance to solid particle erosion," 1981.

[34] M. Papini and S. Dhar, "Experimental verification of a model of erosion due to the impact of rigid single angular particles on fully plastic targets," *Int J Mech Sci*, vol. 48, no. 5, pp. 469–482, May 2006, doi: 10.1016/J.IJMECSCI.2005.12.010.

[35] A. A. Cenna, N. W. Page, E. Kisi, and M. G. Jones, "Single particle impact tests using gas gun and analysis of high strain-rate impact events in ductile materials," *Wear*, vol. 271, no. 9–10, pp. 1497–1503, Jul. 2011, doi: 10.1016/J.WEAR.2010.11.023.

[36] S. Dhar, T. Krajac, D. Ciampini, and M. Papini, "Erosion mechanisms due to impact of single angular particles," *Wear*, vol. 258, no. 1–4, pp. 567–579, Jan. 2005, doi: 10.1016/J.WEAR.2004.09.016.

[37] N. Ramanujam and T. Nakamura, "Erosion mechanisms of thermally sprayed coatings with multiple phases," *Surf Coat Technol*, vol. 204, no. 1–2, pp. 42–53, Sep. 2009, doi: 10.1016/J.SURFCOAT.2009.06.024.

[38] H. Gu, "Behaviours of glass fibre/unsaturated polyester composites under seawater environment," *Mater Des*, vol. 30, no. 4, pp. 1337–1340, Apr. 2009, doi: 10.1016/J.MATDES.2008.06.020.

[39] C. Johnstone, M. Stack, S. Sharifi, C. Johnstone, and M. M. Stack, "Tribological challenges of scaling up tidal turbine blades." [Online]. Available: https://www.researchgate.net/publication/299369786

[40] D. Miller, J. F. Mandell, D. D. Samborsky, B. A. Hernandez-Sanchez, and D. Todd Griffith, "2012 AIAA SDM Wind Energy Session Performance of Composite Materials Subjected to Salt Water Environments."

[41] H. G, "'Behaviors of Glass Fiber/Unsaturated Polyester Composites Under Seawater Environment,'" *Material Design*, vol. 30, p. 1337, 2009.

References

[42] B. Wei, H. Cao, and S. Song, "Degradation of basalt fibre and glass fibre/epoxy resin composites in seawater," *Corros Sci*, vol. 53, no. 1, pp. 426–431, Jan. 2011, doi: 10.1016/J.CORSCI.2010.09.053.

[43] J. F. Manwell, J. G. McGowan, and A. L. Rogers, "Front Matter and Index," in *Wind Energy Explained*, John Wiley & Sons, Ltd, 2003, pp. i–vii. doi: 10.1002/0470846127.fmatter_indsub.

[44] N. Gaudern, "A practical study of the aerodynamic impact of wind turbine blade leading edge erosion," *J Phys Conf Ser*, vol. 524, no. 1, p. 12031, Jun. 2014, doi: 10.1088/1742-6596/524/1/012031.

[45] M. D. Reder, E. Gonzalez, and J. J. Melero, "Wind Turbine Failures - Tackling current Problems in Failure Data Analysis," *J Phys Conf Ser*, vol. 753, no. 7, p. 72027, Sep. 2016, doi: 10.1088/1742-6596/753/7/072027.

[46] A. Sareen, C. A. Sapre, and M. S. Selig, "Effects of leading edge erosion on wind turbine blade performance," *Wind Energy*, vol. 17, no. 10, pp. 1531–1542, 2014, doi: https://doi.org/10.1002/we.1649.

[47] P. Davies and Y. D. S. Rajapakse Editors, "Solid Mechanics and Its Applications Durability of Composites in a Marine Environment." [Online]. Available: http://www.springer.com/series/6557

[48] National Renewable Energy Laboratory (lead) and Verdant Power, "Tidal Power Turbine Demonstrates Thermoplastic Blades," *https://www.energy.gov/eere/water/articles/tidal-power-turbine-demonstrates-thermoplastic-blades*, Mar. 09, 2022.

[49] V. Boggarapu, R. Gujjala, and S. Ojha, "A critical review on erosion wear characteristics of polymer matrix composites," *Mater Res Express*, vol. 7, no. 2, p. 22002, Feb. 2020, doi: 10.1088/2053-1591/ab6e7b.

[50] A. K. Sinha, H. K. Narang, and S. Bhattacharya, "Mechanical properties of hybrid polymer composites: a review," *Journal of the Brazilian Society of Mechanical Sciences and Engineering*, vol. 42, no. 8, p. 431, 2020, doi: 10.1007/s40430-020-02517-w.

References

[51] R. Guobys, Rodríguez, and L. Chernin, "Cavitation erosion of glass fibre reinforced polymer composites with unidirectional layup," *Compos B Eng*, vol. 177, p. 107374, Nov. 2019, doi: 10.1016/J.COMPOSITESB.2019.107374.

[52] M. M. Stack, N. Corlett, and S. Zhou, "Construction of erosion-corrosion maps for erosion in aqueous slurries," *Materials Science and Technology*, vol. 12, pp. 662–672, 1996.

[53] M. M. Stack, B. D. Jana, and S. M. Abdelrahman, "Models and mechanisms of erosion–corrosion in metals," *Tribocorrosion of Passive Metals and Coatings*, pp. 153–187e, Jan. 2011, doi: 10.1533/9780857093738.1.153.

[54] D. J. Stephenson, J. R. Nicholls, and P. C. Hancock, "The erosion of gas turbine blade materials by solid sea salt," *Corros Sci*, vol. 25, pp. 1181–1192, 1985.

[55] L. Chernin and D. V. Val, "Probabilistic prediction of cavitation on rotor blades of tidal stream turbines," *Renew Energy*, vol. 113, pp. 688–696, Dec. 2017, doi: 10.1016/J.RENENE.2017.06.037.

[56] Z. Ahmad, "TYPES OF CORROSION," *Principles of Corrosion Engineering and Corrosion Control*, pp. 120–270, 2006, doi: 10.1016/B978-075065924-6/50005-2.

[57] Wikipedia, "Fly ash," *https://en.wikipedia.org/wiki/Fly_ash*, May 2018.

[58] C. Verma, M. A. Quraishi, and D. S. Chauhan, Eds., "Fundamentals of Corrosion and Corrosion Inhibition," in *Green Corrosion Inhibition*, The Royal Society of Chemistry, 2022, p. 0. doi: 10.1039/9781839167461-00001.

[59] K. Friedrich, "Routes for achieving multifunctionality in reinforced polymers and composite structures," *Multifunctionality of Polymer Composites: Challenges and New Solutions*, pp. 3–41, Jan. 2015, doi: 10.1016/B978-0-323-26434-1.00001-5.

[60] W. Yin, Z. Han, H. Feng, J. Zhang, H. Cao, and Y. Tian, "Gas–Solid Erosive Wear of Biomimetic Pattern Surface Inspired from Plant," *Tribology Transactions*, vol. 60, no. 1, pp. 159–165, 2017, doi: 10.1080/10402004.2016.1154234.

[61] G. R. Desale, B. K. Gandhi, and S. C. Jain, "Effect of erodent properties on erosion wear of ductile type materials," *Wear*, vol. 261, no. 7–8, pp. 914–921, Oct. 2006, doi: 10.1016/J.WEAR.2006.01.035.

References

[62] G. A, "Effect of Impact Angle on Erosive Abrasive Wear of Ductile and Brittle Materials," *World Academy of Science, Engineering and Technology International Journal of Mechanical and Mechatronics Engineering*, vol. 9, 2015.

[63] R. G. Wellman and C. Allen, "The effects of angle of impact and material properties on the erosion rates of ceramics," *Wear*, vol. 186–187, no. PART 1, pp. 117–122, Jul. 1995, doi: 10.1016/0043-1648(95)07130-X.

[64] B. Bhushan, "Nanotribology and nanomechanics," *Wear*, vol. 259, no. 7–12, pp. 1507–1531, Jul. 2005, doi: 10.1016/J.WEAR.2005.01.010.

[65] I. M. Hutchings, "A MODEL FOR THE EROSION OF METALS BY SPHERICAL PARTICLES AT NORMAL INCIDENCE - eScholarship," 1981.

[66] A. Shewmon and G. Sundararajan, "The Erosion of Metals," *Annual Review of Materials Science*, vol. 13, pp. 301–318, 1983.

[67] C. G. Telfer, M. M. Stack, and B. D. Jana, "Particle concentration and size effects on the erosion-corrosion of pure metals in aqueous slurries," *Tribol Int*, vol. 53, pp. 35–44, Sep. 2012, doi: 10.1016/J.TRIBOINT.2012.04.010.

[68] A. W. Ruff and L. K. Ives, "Measurement of solid particle velocity in erosive wear," *Wear*, vol. 35, no. 1, pp. 195–199, Nov. 1975, doi: 10.1016/0043-1648(75)90154-4.

[69] A. V. Levy and P. Chik, "The effects of erodent composition and shape on the erosion of steel," *Wear*, vol. 89, no. 2, pp. 151–162, Aug. 1983, doi: 10.1016/0043-1648(83)90240-5.

[70] N. Miyazaki, "Solid particle erosion of composite materials: A critical review," *J Compos Mater*, vol. 50, no. 23, pp. 3175–3217, 2016, doi: 10.1177/0021998315617818.

[71] National Geographic Society, "Erosion," *https://education.nationalgeographic.org/resource/erosion/*, Jun. 06, 2022.

[72] Encyclopedia Britannica, "erosion," *https://www.britannica.com/science/erosion-geology*, Dec. 16, 2022.

[73] material properties, "What is Erosion – Corrosion – Definition," *https://material-properties.org/what-is-erosion-corrosion-definition/*, Mar. 11, 2023.

References

[74] B. Taherkhani, A. P. Anaraki, J. Kadkhodapour, N. K. Farahani, and H. Tu, "Erosion Due to Solid Particle Impact on the Turbine Blade: Experiment and Simulation," *Journal of Failure Analysis and Prevention*, vol. 19, no. 6, pp. 1739–1744, 2019, doi: 10.1007/s11668-019-00775-y.

[75] A. A. Hamed, W. Tabakoff, R. B. Rivir, K. Das, and P. Arora, "Turbine Blade Surface Deterioration by Erosion," *J Turbomach*, vol. 127, no. 3, pp. 445–452, Mar. 2004, doi: 10.1115/1.1860376.

[76] J. Alqallaf, N. Ali, J. A. Teixeira, and A. Addali, "Solid Particle Erosion Behaviour and Protective Coatings for Gas Turbine Compressor Blades—A Review," *Processes*, vol. 8, no. 8, 2020, doi: 10.3390/pr8080984.

[77] M. M. Stack and D. Peña, "Solid particle erosion of Ni☐CrWC metal matrix composites at elevated temperatures: construction of erosion mechanism and process control maps," *Wear*, vol. 203–204, pp. 489–497, Mar. 1997, doi: 10.1016/S0043-1648(96)07387-5.

[78] C. E. Morris, D. M. O'Doherty, T. O'Doherty, and A. Mason-Jones, "Kinetic energy extraction of a tidal stream turbine and its sensitivity to structural stiffness attenuation," *Renew Energy*, vol. 88, pp. 30–39, Apr. 2016, doi: 10.1016/J.RENENE.2015.10.037.

[79] N. Miyazaki, "Solid particle erosion of composite materials: A critical review," *J Compos Mater*, vol. 50, no. 23, pp. 3175–3217, 2016.

[80] T. A. Ring, P. Feeney, D. Boldridge, J. Kasthurirangan, S. Li, and J. A. Dirksen, "Brittle and Ductile Fracture Mechanics Analysis of Surface Damage Caused During CMP."

[81] A. K. Cousens, "THE EROSION OF DUCTILE METALS BY SOLID PARTICLE IMPACT," 1984.

[82] A. R. Hemmati, M. Soltanieh, and S. M. Masoudpanah, "Effect of Flow Velocity and Impact Angle on Erosion–Corrosion Behavior of Chromium Carbide Coating," *J Tribol*, vol. 139, no. 3, Nov. 2016, doi: 10.1115/1.4034424.

[83] R. Rattan and J. Bijwe, "Influence of impingement angle on solid particle erosion of carbon fabric reinforced polyetherimide composite," *Wear*, vol. 262, no. 5–6, pp. 568–574, Feb. 2007, doi: 10.1016/J.WEAR.2006.07.001.

[84] J. Zahavi and G. F. Schmitt, "Solid particle erosion of reinforced composite materials," *Wear*, vol. 71, no. 2, pp. 179–190, Sep. 1981, doi: 10.1016/0043-1648(81)90337-9.

References

[85] Y. Fouad, M. A. H. El-meniawi, and A. Afifi, "Erosion behaviour of epoxy based unidirectionl (GFRP) composite materials," *alexandria engineering journal*, vol. 50, pp. 29–34, 2011.

[86] "II. SLURRY TANK AND MIXTURE DESIGN."

[87] S. Majumdar and A. Sarajedini, "A review of solid particle erosion of engineering materials," 1987.

[88] N. Miyazaki, "Solid particle erosion of composite materials: A critical review," *J Compos Mater*, vol. 50, no. 23, pp. 3175–3217, 2016, doi: 10.1177/0021998315617818.

[89] T. Sinmazcelik and N. Y. Sari, "Erodent size effect on the erosion of polyphenylene sulfide composite," *Polym Compos*, vol. 31, no. 6, pp. 985–994, 2010, doi: https://doi.org/10.1002/pc.20883.

[90] C. Subramanian, "Wear properties of aluminium-based alloys," *Surface Engineering of Light Alloys: Aluminium, Magnesium and Titanium Alloys*, pp. 40–57, 2010, doi: 10.1533/9781845699451.1.40.

[91] "Research into the Physical Mechanism of Erosion," in *Solid Particle Erosion: Occurrence, Prediction and Control*, London: Springer London, 2008, pp. 51–65. doi: 10.1007/978-1-84800-029-2_2.

[92] Haynes international, "Solid Particle Erosion," *https://haynesintl.com/alloys/corrosion-guide/erosion*, Mar. 2023.

[93] GE research, "Polymer & Composite Materials," *https://www.ge.com/research/technology-domains/materials/polymer-composite-materials*, 2022.

[94] R. Hsissou, R. Seghiri, Z. Benzekri, M. Hilali, M. Rafik, and A. Elharfi, "Polymer composite materials: A comprehensive review," *Compos Struct*, vol. 262, p. 113640, Apr. 2021, doi: 10.1016/J.COMPSTRUCT.2021.113640.

[95] G. Wang, D. Yu, A. D. Kelkar, and L. Zhang, "Electrospun nanofiber: Emerging reinforcing filler in polymer matrix composite materials," *Prog Polym Sci*, vol. 75, pp. 73–107, Dec. 2017, doi: 10.1016/j.progpolymsci.2017.08.002.

References

[96]   S. Sarkar, V. G. Sekharan, R. Mitra, and M. Roy, "The Solid Particle Erosion Behavior of Carbon/Carbon and Carbon/Phenolic Composite Used in Re-entry Vehicles," *Tribology Transactions*, vol. 52, no. 6, pp. 777–787, 2009, doi: 10.1080/10402000903097411.

[97]   Y. Fouad, M. El-Meniawi, and A. Afifi, "Erosion behaviour of epoxy based unidirectionl (GFRP) composite materials," *Alexandria Engineering Journal*, vol. 50, no. 1, pp. 29–34, Mar. 2011, doi: 10.1016/J.AEJ.2011.01.005.

[98]   N. M. Barkoula and J. Karger-Kocsis, "Effects of fibre content and relative fibre-orientation on the solid particle erosion of GF/PP composites," *Wear*, vol. 252, no. 1–2, pp. 80–87, Jan. 2002, doi: 10.1016/S0043-1648(01)00855-9.

[99]   S. Chauhan, A. Kumar, A. Patnaik, A. Satapathy, and I. Singh, "Mechanical and Wear Characterization of GF Reinforced Vinyl Ester Resin Composites with Different Co-Monomers," *Journal of Reinforced Plastics and Composites*, vol. 28, no. 21, pp. 2675–2684, 2009, doi: 10.1177/0731684408093823.

[100] N. Yang and H. Nayeb-Hashemi, "The Effect of Solid Particle Erosion on the Mechanical Properties and Fatigue Life of Fiber-reinforced Composites," *J Compos Mater*, vol. 41, no. 5, pp. 559–574, 2007, doi: 10.1177/0021998306065288.

[101] A. Patnaik, A. Satapathy, N. Chand, N. M. Barkoula, and S. Biswas, "Solid particle erosion wear characteristics of fiber and particulate filled polymer composites: A review," *Wear*, vol. 268, no. 1–2, pp. 249–263, Jan. 2010, doi: 10.1016/J.WEAR.2009.07.021.

[102] NIST, "What are Taguchi designs?," *https://www.itl.nist.gov/div898/handbook/pri/section5/pri56.htm*, Mar. 2023.

[103] T. Sinmazçelik and I. Taşkiran, "Erosive wear behaviour of polyphenylenesulphide (PPS) composites," *Mater Des*, vol. 28, no. 9, pp. 2471–2477, Jan. 2007, doi: 10.1016/J.MATDES.2006.08.007.

[104] B. S. and R. N. Ismail M, "Investigations on mechanical and erosive wear behaviour of cenosphere filled carbon-epoxy composites," *International Conference on Mechanical, Automotive and Materials Engineering (ICMAME'2012), Planetary scientific research proceedings*, 2012.

References

[105] A. G. Joshi, M. P. Kumar, and S. Basavarajappa, "Influence of Al2O3 Filler on Slurry Erosion Behavior of Glass/Epoxy Composites," *Procedia Materials Science*, vol. 5, pp. 863–872, Jan. 2014, doi: 10.1016/J.MSPRO.2014.07.372.

[106] M. P. K. and S. B. Ajith G. Joshi, "INVESTIGATION ON SLURRY EROSION OF Al2O3 INCORPORATED GLASS/EPOXY COMPOSITES," *International Journal of Surface Science and Engineering*, Dec. 2020.

[107] A. G. Joshi, M. P. Kumar, and S. Basavarajappa, "Influence of Al2O3 Filler on Slurry Erosion Behavior of Glass/Epoxy Composites," *Procedia Materials Science*, vol. 5, pp. 863–872, 2014.

[108] A. Gupta, A. Kumar, A. Patnaik, and S. Biswas, "Effect of Filler Content and Alkalization on Mechanical and Erosion Wear Behavior of CBPD Filled Bamboo Fiber Composites," *J Surf Eng Mater Adv Technol*, vol. 02, no. 03, pp. 149–157, 2012, doi: 10.4236/jsemat.2012.23024.

[109] S. Biswas and A. Satapathy, "Tribo-performance analysis of red mud filled glass-epoxy composites using Taguchi experimental design," *Mater Des*, vol. 30, no. 8, pp. 2841–2853, Sep. 2009, doi: 10.1016/J.MATDES.2009.01.018.

[110] S. Biswas and A. Satapathy, "A comparative study on erosion characteristics of red mud filled bamboo–epoxy and glass–epoxy composites," *Mater Des*, vol. 31, no. 4, pp. 1752–1767, Apr. 2010, doi: 10.1016/J.MATDES.2009.11.021.

[111] H. Jena and A. K. Satapathy, "Fabrication, Mechanical Characterization and Wear Response of Hybrid Composites Filled with Red Mud: an Alumina Plant Waste," 2011. [Online]. Available: https://www.researchgate.net/publication/272482758

[112] A. A. M and A. W. Y, "Particle Erosion of Epoxy Resin," 2016. [Online]. Available: www.jmest.org

[113] M. Bagci, "Determination of solid particle erosion with Taguchi optimization approach of hybrid composite systems," *Tribol Int*, vol. 94, pp. 336–345, Feb. 2016, doi: 10.1016/J.TRIBOINT.2015.09.032.

[114] M. Bagci and H. Imrek, "Application of Taguchi method on optimization of testing parameters for erosion of glass fiber reinforced epoxy composite materials," *Materials*

References

   & Design (1980-2015), vol. 46, pp. 706–712, Apr. 2013, doi: 10.1016/J.MATDES.2012.11.024.

[115] M. Bagci and H. Imrek, "Solid particle erosion behaviour of glass fibre reinforced boric acid filled epoxy resin composites," *Tribol Int*, vol. 44, no. 12, pp. 1704–1710, Nov. 2011, doi: 10.1016/J.TRIBOINT.2011.06.033.

[116] N. Chand, P. Sharma, and M. Fahim, "Correlation of mechanical and tribological properties of organosilane modified cenosphere filled high density polyethylene," *Materials Science and Engineering: A*, vol. 527, no. 21–22, pp. 5873–5878, Aug. 2010, doi: 10.1016/J.MSEA.2010.06.022.

[117] A. Patnaik, A. Satapathy, S. S. Mahapatra, and R. R. Dash, "Parametric Optimization Erosion Wear of Polyester-GF-Alumina Hybrid Composites using the Taguchi Method," *Journal of Reinforced Plastics and Composites*, vol. 27, no. 10, pp. 1039–1058, 2008, doi: 10.1177/0731684407086867.

[118] M. Sudheer, K. Hemanth, K. Raju, and T. Bhat, "Enhanced Mechanical and Wear Performance of Epoxy/glass Composites with PTW/Graphite Hybrid Fillers," *Procedia Materials Science*, vol. 6, pp. 975–987, Jan. 2014, doi: 10.1016/J.MSPRO.2014.07.168.

[119] V. K. Srivastava, "Effects of wheat starch on erosive wear of E-glass fibre reinforced epoxy resin composite materials," *Materials Science and Engineering: A*, vol. 435–436, pp. 282–287, Nov. 2006, doi: 10.1016/J.MSEA.2006.07.144.

[120] A. K. Rout and A. Satapathy, "Study on mechanical and tribo-performance of rice-husk filled glass–epoxy hybrid composites," *Mater Des*, vol. 41, pp. 131–141, Oct. 2012, doi: 10.1016/J.MATDES.2012.05.002.

[121] K. Sudarshan Rao, Y. S. Varadarajan, and N. Rajendra, "Erosive Wear Behaviour of Carbon Fiber-reinforced Epoxy Composite," *Mater Today Proc*, vol. 2, no. 4–5, pp. 2975–2983, Jan. 2015, doi: 10.1016/J.MATPR.2015.07.280.

[122] P. Panda, S. Mantry, S. Mohapatra, S. K. Singh, and A. Satapathy, "A study on erosive wear analysis of glass fiber–epoxy–AlN hybrid composites," *J Compos Mater*, vol. 48, no. 1, pp. 107–118, 2014, doi: 10.1177/0021998312469239.

References

[123] E. Hassan *et al.*, "Erosion Mapping of Through-Thickness Toughened Powder Epoxy Gradient Glass-Fiber-Reinforced Polymer (GFRP) Plates for Tidal Turbine Blades," *Lubricants*, vol. 9, no. 3, p. 22, Feb. 2021, doi: 10.3390/lubricants9030022.

[124] J. B. Zu, I. M. Hutchings, and G. T. Burstein, "Design of a slurry erosion test rig," *Wear*, vol. 140, no. 2, pp. 331–344, Nov. 1990, doi: 10.1016/0043-1648(90)90093-P.

[125] N. A. Riley, "Projection sphericity," *Journal of Sedimentary Research*, vol. 11, no. 2, pp. 94–95, Aug. 1941, doi: 10.1306/D426910C-2B26-11D7-8648000102C1865D.

[126] N. MacLeod, "Geometric morphometrics and geological shape-classification systems," *Earth Sci Rev*, vol. 59, no. 1–4, pp. 27–47, Nov. 2002, doi: 10.1016/S0012-8252(02)00068-5.

[127] G. P. Tilly, "A two stage mechanism of ductile erosion," *Wear*, vol. 23, no. 1, pp. 87–96, Jan. 1973, doi: 10.1016/0043-1648(73)90044-6.

[128] A. V. Levy and P. Chik, "The effects of erodent composition and shape on the erosion of steel," *Wear*, vol. 89, no. 2, pp. 151–162, Aug. 1983, doi: 10.1016/0043-1648(83)90240-5.

[129] H. Arabnejad, S. A. Shirazi, B. S. McLaury, H. J. Subramani, and L. D. Rhyne, "The effect of erodent particle hardness on the erosion of stainless steel," *Wear*, vol. 332–333, pp. 1098–1103, May 2015, doi: 10.1016/J.WEAR.2015.01.017.

[130] "HC 1624 The Future of Marine Renewables in the UK Eleventh Report of Session 2010-12," 2012. [Online]. Available: www.parliament.uk/ecc

[131] P. Alam, C. Robert, and C. M. Ó Brádaigh, "Tidal turbine blade composites - A review on the effects of hygrothermal aging on the properties of CFRP," *Compos B Eng*, vol. 149, pp. 248–259, 2018, doi: https://doi.org/10.1016/j.compositesb.2018.05.003.

[132] G. Rasool, A. C. Middleton, and M. M. Stack, "Mapping Raindrop Erosion of GFRP Composite Wind Turbine Blade Materials: Perspectives on Degradation Effects in Offshore and Acid Rain Environmental Conditions," *J Tribol*, vol. 142, no. 6, Feb. 2020, doi: 10.1115/1.4046014.

[133] K.-K. J, "'Effects of Fibre Content and Relative Fibre Orientation on the Solid Particle Erosion of GF/PP Composites,'" *Wear,* vol. 252, p. 80, 2002.

References

[134] G. Prashar, H. Vasudev, and L. Thakur, "Performance of different coating materials against slurry erosion failure in hydrodynamic turbines: A review," *Eng Fail Anal*, vol. 115, p. 104622, Sep. 2020, doi: 10.1016/J.ENGFAILANAL.2020.104622.

[135] N. S. K, "'Synergy of Cavitation and Slurry Erosion in the Slurry Pot Tester,'" *Wear,* vol. 290–291, p. 25, 2012.

[136] S. M. M, "'Mapping Synergy of Erosion Mechanisms Of Tidal Turbine Composite Materials in Seawater Conditions,'" *Bio-Tribo-Corrosion*, vol. 2, p. 13, 2016.

[137] C. H. M, "'A Model of Particle Velocities and Trajectories in a Slurry Pot Erosion Tester,'" *Wear,* vol. 160, p. 95, 1993.

[138] S. M. M, "'A Note on Threshold Velocity Criteria for Modelling the Solid Particle Erosion of WC/Co MMCs,'" *Wear*, vol. 270, p. 439, 2011.

[139] A. Suresh, A. P. Harsha, and M. K. Ghosh, "Solid particle erosion of unidirectional fibre reinforced thermoplastic composites," *Wear*, vol. 267, no. 9–10, pp. 1516–1524, Sep. 2009, doi: 10.1016/j.wear.2009.03.041.

[140] V. Javaheri, D. Porter, and V. T. Kuokkala, "Slurry erosion of steel – Review of tests, mechanisms and materials," *Wear*, vol. 408–409, pp. 248–273, Aug. 2018, doi: 10.1016/J.WEAR.2018.05.010.

[141] R. Schmitt, "Scanning Electron Microscope," in *CIRP Encyclopedia of Production Engineering*, G. Laperrière Luc and Reinhart, Ed., Berlin, Heidelberg: Springer Berlin Heidelberg, 2014, pp. 1085–1089. doi: 10.1007/978-3-642-20617-7_6595.

[142] B. J. , B. S. and J. D. C. Ford, "https://www.britannica.com/technology/scanning-electron-microscope," *scanning electron microscope*, Feb. 15, 2023.

[143] L. X. Cai, Y. Li, S. Sen Wang, Y. He, F. Li, and Z. K. Liu, "Investigation of the erosion damage mechanism and erosion prediction of boronized coatings at elevated temperatures," *Materials*, vol. 14, no. 1, pp. 1–18, Jan. 2021, doi: 10.3390/ma14010123.

[144] K. Martyniuk, B. F. Sørensen, P. Modregger, and E. M. Lauridsen, "3D in situ observations of glass fibre/matrix interfacial debonding," *Compos Part A Appl Sci Manuf*, vol. 55, pp. 63–73, Dec. 2013, doi: 10.1016/J.COMPOSITESA.2013.07.012.

References

[145] D. Mortell, D. Tanner, and C. Mccarthy, "An experimental investigation into multi-scale damage progression in laminated composites in bending," *Compos Struct*, vol. 149, Mar. 2016, doi: 10.1016/j.compstruct.2016.03.054.

[146] M. Naveed, H. Schlag, F. König, and S. Weiß, "Influence of the Erodent Shape on the Erosion Behavior of Ductile and Brittle Materials," *Tribol Lett*, vol. 65, no. 1, p. 18, 2016, doi: 10.1007/s11249-016-0800-x.

[147] T. Sinmazcelik and N. Sari, "Erodent Size Effect on the Erosion of Polyphenylene Sulfide Composite," *Polym Compos*, vol. 31, pp. 985–994, Mar. 2009, doi: 10.1002/pc.20883.

[148] S. C. P, "'Fabrication and Testing of Slurry Pot Erosion Tester,'" *Transactions of the Indian Institute of Metals*, vol. 64, p. 493, 2011.

[149] J. Li, Y. Yang, B. Jia, H. Huang, B. Li, and T. Wang, "GFRP erosion depth model under alkaline solution erosion," *IOP Conf Ser Earth Environ Sci*, vol. 783, no. 1, p. 12031, May 2021, doi: 10.1088/1755-1315/783/1/012031.

[150] J. Basumatary and R. J. K. Wood, "Different methods of measuring synergy between cavitation erosion and corrosion for nickel aluminium bronze in 3.5% NaCl solution."

[151] P. Alam, C. Robert, and C. M. Ó Brádaigh, "Tidal turbine blade composites - A review on the effects of hygrothermal aging on the properties of CFRP," *Compos B Eng*, vol. 149, pp. 248–259, 2018, doi: https://doi.org/10.1016/j.compositesb.2018.05.003.

[152] A. A. Hamed, W. Tabakoff, R. B. Rivir, K. Das, and P. Arora, "Turbine Blade Surface Deterioration by Erosion," *J Turbomach*, vol. 127, no. 3, pp. 445–452, Mar. 2004, doi: 10.1115/1.1860376.

[153] K. Pugh, G. Rasool, and M. M. Stack, "Some Thoughts on Mapping Tribological Issues of Wind Turbine Blades Due to Effects of Onshore and Offshore Raindrop Erosion," *J Bio Tribocorros*, vol. 4, pp. 1–8, 2018.

[154] S. Groucott, K. Pugh, I. Zekos, and M. M Stack, "A Study of Raindrop Impacts on a Wind Turbine Material: Velocity and Impact Angle Effects on Erosion MAPS at Various Exposure Times," *Lubricants*, vol. 9, no. 6, 2021, doi: 10.3390/lubricants9060060.

References

[155] A. R. Hemmati, M. Soltanieh, and S. M. Masoudpanah, "Effect of Flow Velocity and Impact Angle on Erosion–Corrosion Behavior of Chromium Carbide Coating," *J Tribol*, vol. 139, no. 3, Nov. 2016, doi: 10.1115/1.4034424.

[156] J. Köbler, M. Schneider, F. Ospald, H. Andrä, and R. Müller, "Fiber orientation interpolation for the multiscale analysis of short fiber reinforced composite parts," *Comput Mech*, vol. 61, no. 6, pp. 729–750, 2018, doi: 10.1007/s00466-017-1478-0.

[157] C. Robert, T. Pecur, J. M. Maguire, A. D. Lafferty, E. D. McCarthy, and C. M. Ó. Brádaigh, "A novel powder-epoxy towpregging line for wind and tidal turbine blades," *Composites Part B-engineering*, vol. 203, p. 108443, 2020.

[158] P. Davies and M. Arhant, "Fatigue behaviour of acrylic matrix composites: influence of seawater," *Applied Composite Materials*, vol. 26, no. 2, pp. 507–518, 2019.

[159] T. P. Sathishkumar, S. Satheeshkumar, and J. Naveen, "Glass fiber-reinforced polymer composites–a review," *Journal of reinforced plastics and composites*, vol. 33, no. 13, pp. 1258–1275, 2014.

[160] F. Rubino, A. Nisticò, F. Tucci, and P. Carlone, "Marine application of fiber reinforced composites: A review," *J Mar Sci Eng*, vol. 8, no. 1, p. 26, 2020.

[161] J. M. Maguire, K. Nayak, and C. M. Ó. Brádaigh, "Characterisation of epoxy powders for processing thick-section composite structures," *Mater Des*, vol. 139, pp. 112–121, 2018.

[162] B. Liu, L. Bao, and A. Xu, "Effect of fabric orientation and impact angle on the erosion behavior of high-performance thermoplastic composites reinforced with ductile fabric," *Wear*, vol. 352–353, pp. 24–30, Apr. 2016, doi: 10.1016/J.WEAR.2016.01.016.

[163] V. Boggarapu, R. Gujjala, and S. Ojha, "A critical review on erosion wear characteristics of polymer matrix composites," *Materials Research Express*, vol. 7, no. 2. Institute of Physics Publishing, 2020. doi: 10.1088/2053-1591/ab6e7b.

[164] P. Agarwal, A. Sharma, M. Choudhary, T. K. Patnaik, and A. Patnaik, "Numerical simulation of solid particle erosion for glass fiber reinforced epoxy composites," *Mater Today Proc*, vol. 38, pp. 285–288, Jan. 2021, doi: 10.1016/J.MATPR.2020.07.206.

[165] J. Sloan and M. Stack, "On the Construction of Raindrop Erosion Maps for Steel," 2020.

References

[166] GAA Tech, "https://www.gaatech.com/materials/fr4-g10-g9-gop3-sheet-laminates-epoxyglass-fibreglass/."

[167] S. Roshanmanesh, F. Hayati, and M. Papaelias, "Tidal turbines," *Non-Destructive Testing and Condition Monitoring Techniques for Renewable Energy Industrial Assets*, pp. 143–158, Jan. 2020, doi: 10.1016/B978-0-08-101094-5.00010-1.

[168] A. Muratoglu and M. I. Yuce, "Performance Analysis of Hydrokinetic Turbine Blade Sections," 2015.

[169] J. F. Manwell, J. G. McGowan, and A. L. Rogers, "Wind Energy Explained: Theory, Design and Application," 2010.

[170] A. Dashtkar *et al.*, "Rain erosion-resistant coatings for wind turbine blades: A review," *Polymers and Polymer Composites*, vol. 27, no. 8, pp. 443–475, May 2019, doi: 10.1177/0967391119848232.

[171] S. Wang, G. Liu, J. Mao, Q. He, and Z. Feng, "Effects of Coating Thickness, Test Temperature, and Coating Hardness on the Erosion Resistance of Steam Turbine Blades," *J Eng Gas Turbine Power*, vol. 132, no. 2, Nov. 2009, doi: 10.1115/1.3155796.

[172] S. Hassani, J. E. Klemberg-Sapieha, M. Bielawski, W. Beres, L. Martinu, and M. Balazinski, "Design of hard coating architecture for the optimization of erosion resistance," *Wear*, vol. 265, no. 5–6, pp. 879–887, Aug. 2008, doi: 10.1016/J.WEAR.2008.01.021.

[173] J. S. Chouhan *et al.*, "Preliminary investigation of slurry erosion behaviour of tantalum," *Wear*, vol. 516–517, p. 204605, Mar. 2023, doi: 10.1016/J.WEAR.2022.204605.

[174] S. H. Musavi, B. Davoodi, and M. Nankali, "Assessment of Tool Wear and Surface Integrity in Ductile Cutting Using a Developed Tool," *Arab J Sci Eng*, vol. 46, no. 8, pp. 7773–7787, 2021, doi: 10.1007/s13369-021-05560-4.

[175] M. Patel, D. Patel, S. Sekar, P. B. Tailor, and P. V. Ramana, "Study of Solid Particle Erosion Behaviour of SS 304 at Room Temperature," *Procedia Technology*, vol. 23, pp. 288–295, 2016, doi: 10.1016/j.protcy.2016.03.029.

[176] J. Shingledecker and M. Takeyama, *Joint EPRI–123HiMAT International Conference on Advances in High-Temperature Materials*. ASM International, 2019.

References

[177] G. Rasool and M. M. Stack, "Some views on the mapping of erosion of coated composites in tidal turbine simulated conditions." [Online]. Available: http://mc.manuscriptcentral.com/tandf/tribtrans,

[178] A. Klimek, J. Kluczyński, J. Łuszczek, A. Bartnicki, K. Grzelak, and M. Małek, "Wear Analysis of Additively Manufactured Slipper-Retainer in the Axial Piston Pump," *Materials*, vol. 15, no. 6, Mar. 2022, doi: 10.3390/ma15061995.

[179] L. Murugesh and R. O. Scattergood, "Effect of erodent properties on the erosion of alumina," *J Mater Sci*, vol. 26, pp. 5456–5466, 1991.

[180] N. Trigoulet *et al.*, "Surface topography effects on glow discharge depth profiling analysis," in *Surface and Interface Analysis*, Apr. 2010, pp. 328–333. doi: 10.1002/sia.3165.

[181] I. Christodoulou *et al.*, "Degradation mechanism of porous metal-organic frameworks by in situ atomic force microscopy," *Nanomaterials*, vol. 11, no. 3, pp. 1–17, Mar. 2021, doi: 10.3390/nano11030722.

[182] S. Panier, G. Franz, J. Bijwe, and L. Hui, "Finite Element Analysis of the damage occurring in the sliding contact between a metallic ball and a composite plate," in *Proceedings of asia international conference on tribology. Malaysia*, 2018, pp. 246–247.

[183] F. Wang, J. Liu, O. Mohummad, and Y. Wang, "Experimental Study on GFRP surface cracks detection using truncated-correlation photothermal coherence tomography," *Int J Thermophys*, vol. 39, pp. 1–10, 2018.

[184] P. A. Dearnley, *Introduction to surface engineering*. Cambridge University Press, 2017.

[185] A. Al-Kawaz, "Surface Engineering."

Appendices

Chapter 4

MATLAB code for erosion map Fig 16

```matlab
function createaxes(Parent1, xdata1, ydata1, zdata1)
%CREATEAXES(Parent1, xdata1, ydata1, zdata1)
%  PARENT1:  axes parent
%  XDATA1:  surface xdata
%  YDATA1:  surface ydata
%  ZDATA1:  surface zdata

%  Auto-generated by MATLAB on 04-Mar-2023 10:10:14

% Create axes
axes1 = axes('Parent',Parent1,...
    'Position',[223.04 288.222928059897 1204.7 827.09373860678],...
    'Units','pixels');
hold(axes1,'on');

% Create surf
surf(xdata1,ydata1,zdata1,'Parent',axes1,'FaceLighting','gouraud',...
    'LineStyle','--',...
    'FaceColor','interp');

% Create zlabel
zlabel('Z Axis');

% Create ylabel
ylabel('Mass Loss (g)','HorizontalAlignment','center');

% Create xlabel
xlabel('Impact Angle (Deg)','HorizontalAlignment','right');

% Create title
title('0 Fibre Orientation','HorizontalAlignment','center',...
    'FontWeight','bold');

% Uncomment the following line to preserve the X-limits of the axes
% xlim(axes1,[10 90]);
% Uncomment the following line to preserve the Y-limits of the axes
% ylim(axes1,[-0.00499999988824129 0.025000000372529]);
% Uncomment the following line to preserve the Z-limits of the axes
% zlim(axes1,[0 1.39999997615814]);
hold(axes1,'off');
% Set the remaining axes properties
set(axes1,'ALim',[0 2],'CLim',[0.1 1.3],'CameraUpVector',[0 0 0],...

'CameraViewAngle',7.0125559666728,'ClippingStyle','rectangle','ContextMenu'
,...
    'DataAspectRatio',[2666.66664348708 1
46.6666654662954],'Projection',...
    'perspective','XTick',[15 30 45 60 75 90],'YTick',...
    [0 0.005 0.01 0.015 0.02 0.025]);
```

Appendices

MATLAB code for erosion map Fig 17

```matlab
function createfigure(xdata1, ydata1, zdata1)
%CREATEFIGURE(xdata1, ydata1, zdata1)
%  XDATA1:  surface xdata
%  YDATA1:  surface ydata
%  ZDATA1:  surface zdata

%  Auto-generated by MATLAB on 11-Sep-2023 11:58:24

% Create figure
figure('OuterPosition',...
    [446.333333333333 287.666666666667 1333.33333333333 844.666666666667]);

% Create axes
axes1 = axes;
hold(axes1,'on');

% Create surf
surf(xdata1,ydata1,zdata1,'FaceColor','interp');

% Create zlabel
zlabel('Erosion Value');

% Create ylabel
ylabel('Erosion Area');

% Create xlabel
xlabel('Blade Angle');

% Create title
title('Erosion Map at 90 (Deg) Fibre Orientation');

view(axes1,[-0.724657549116884 90]);
grid(axes1,'on');
hold(axes1,'off');
% Set the remaining axes properties
set(axes1,'Colormap',...
    [0.18995 0.07176 0.23217;0.19483 0.08339 0.26149;0.19956 0.09498
0.29024;0.20415 0.10652 0.31844;0.2086 0.11802 0.34607;0.21291 0.12947
0.37314;0.21708 0.14087 0.39964;0.22111 0.15223 0.42558;0.225 0.16354
0.45096;0.22875 0.17481 0.47578;0.23236 0.18603 0.50004;0.23582 0.1972
0.52373;0.23915 0.20833 0.54686;0.24234 0.21941 0.56942;0.24539 0.23044
0.59142;0.2483 0.24143 0.61286;0.25107 0.25237 0.63374;0.25369 0.26327
0.65406;0.25618 0.27412 0.67381;0.25853 0.28492 0.693;0.26074 0.29568
0.71162;0.2628 0.30639 0.72968;0.26473 0.31706 0.74718;0.26652 0.32768
0.76412;0.26816 0.33825 0.7805;0.26967 0.34878 0.79631;0.27103 0.35926
0.81156;0.27226 0.3697 0.82624;0.27334 0.38008 0.84037;0.27429 0.39043
0.85393;0.27509 0.40072 0.86692;0.27576 0.41097 0.87936;0.27628 0.42118
0.89123;0.27667 0.43134 0.90254;0.27691 0.44145 0.91328;0.27701 0.45152
0.92347;0.27698 0.46153 0.93309;0.2768 0.47151 0.94214;0.27648 0.48144
0.95064;0.27603 0.49132 0.95857;0.27543 0.50115 0.96594;0.27469 0.51094
0.97275;0.27381 0.52069 0.97899;0.27273 0.5304 0.98461;0.27106 0.54015
0.9893;0.26878 0.54995 0.99303;0.26592 0.55979 0.99583;0.26252 0.56967
0.99773;0.25862 0.57958 0.99876;0.25425 0.5895 0.99896;0.24946 0.59943
0.99835;0.24427 0.60937 0.99697;0.23874 0.61931 0.99485;0.23288 0.62923
0.99202;0.22676 0.63913 0.98851;0.22039 0.64901 0.98436;0.21382 0.65886
0.97959;0.20708 0.66866 0.97423;0.20021 0.67842 0.96833;0.19326 0.68812
0.9619;0.18625 0.69775 0.95498;0.17923 0.70732 0.94761;0.17223 0.7168
0.93981;0.16529 0.7262 0.93161;0.15844 0.73551 0.92305;0.15173 0.74472
0.91416;0.14519 0.75381 0.90496;0.13886 0.76279 0.8955;0.13278 0.77165
0.8858;0.12698 0.78037 0.8759;0.12151 0.78896 0.86581;0.11639 0.7974
0.85559;0.11167 0.80569 0.84525;0.10738 0.81381 0.83484;0.10357 0.82177
0.82437;0.10026 0.82955 0.81389;0.0975 0.83714 0.80342;0.09532 0.84455
0.79299;0.09377 0.85175 0.78264;0.09287 0.85875 0.7724;0.09267 0.86554
0.7623;0.0932 0.87211 0.75237;0.09451 0.87844 0.74265;0.09662 0.88454
0.73316;0.09958 0.8904 0.72393;0.10342 0.896 0.715;0.10815 0.90142 0.70599;0.11374
0.90673 0.69651;0.12014 0.91193 0.6866;0.12733 0.91701 0.67627;0.13526 0.92197
0.66556;0.14391 0.9268 0.65448;0.15323 0.93151 0.64308;0.16319 0.93609
```

130

Appendices

```
0.63137;0.17377 0.94053 0.61938;0.18491 0.94484 0.60713;0.19659 0.94901
0.59466;0.20877 0.95304 0.58199;0.22142 0.95692 0.56914;0.23449 0.96065
0.55614;0.24797 0.96423 0.54303;0.2618 0.96765 0.52981;0.27597 0.97092
0.51653;0.29042 0.97403 0.50321;0.30513 0.97697 0.48987;0.32006 0.97974
0.47654;0.33517 0.98234 0.46325;0.35043 0.98477 0.45002;0.36581 0.98702
0.43688;0.38127 0.98909 0.42386;0.39678 0.99098 0.41098;0.41229 0.99268
0.39826;0.42778 0.99419 0.38575;0.44321 0.99551 0.37345;0.45854 0.99663
0.3614;0.47375 0.99755 0.34963;0.48879 0.99828 0.33816;0.50362 0.99879
0.32701;0.51822 0.9991 0.31622;0.53255 0.99919 0.30581;0.54658 0.99907
0.29581;0.56026 0.99873 0.28623;0.57357 0.99817 0.27712;0.58646 0.99739
0.26849;0.59891 0.99638 0.26038;0.61088 0.99514 0.2528;0.62233 0.99366
0.24579;0.63323 0.99195 0.23937;0.64362 0.98999 0.23356;0.65394 0.98775
0.22835;0.66428 0.98524 0.2237;0.67462 0.98246 0.2196;0.68494 0.97941
0.21602;0.69525 0.9761 0.21294;0.70553 0.97255 0.21032;0.71577 0.96875
0.20815;0.72596 0.9647 0.2064;0.7361 0.96043 0.20504;0.74617 0.95593
0.20406;0.75617 0.95121 0.20343;0.76608 0.94627 0.20311;0.77591 0.94113
0.2031;0.78563 0.93579 0.20336;0.79524 0.93025 0.20386;0.80473 0.92452
0.20459;0.8141 0.91861 0.20552;0.82333 0.91253 0.20663;0.83241 0.90627
0.20788;0.84133 0.89986 0.20926;0.8501 0.89328 0.21074;0.85868 0.88655
0.2123;0.86709 0.87968 0.21391;0.8753 0.87267 0.21555;0.88331 0.86553
0.21719;0.89112 0.85826 0.2188;0.8987 0.85087 0.22038;0.90605 0.84337
0.22188;0.91317 0.83576 0.22328;0.92004 0.82806 0.22456;0.92666 0.82025
0.2257;0.93301 0.81236 0.22667;0.93909 0.80439 0.22744;0.94489 0.79634
0.228;0.95039 0.78823 0.22831;0.9556 0.78005 0.22836;0.96049 0.77181
0.22811;0.96507 0.76352 0.22754;0.96931 0.75519 0.22663;0.97323 0.74682
0.22536;0.97679 0.73842 0.22369;0.98 0.73 0.22161;0.98289 0.7214 0.21918;0.98549
0.7125 0.2165;0.98781 0.7033 0.21358;0.98986 0.69382 0.21043;0.99163 0.68408
0.20706;0.99314 0.67408 0.20348;0.99438 0.66386 0.19971;0.99535 0.65341
0.19577;0.99607 0.64277 0.19165;0.99654 0.63193 0.18738;0.99675 0.62093
0.18297;0.99672 0.60977 0.17842;0.99644 0.59846 0.17376;0.99593 0.58703
0.16899;0.99517 0.57549 0.16412;0.99419 0.56386 0.15918;0.99297 0.55214
0.15417;0.99153 0.54036 0.1491;0.98987 0.52854 0.14398;0.98799 0.51667
0.13883;0.9859 0.50479 0.13367;0.9836 0.49291 0.12849;0.98108 0.48104
0.12332;0.97837 0.4692 0.11817;0.97545 0.4574 0.11305;0.97234 0.44565
0.10797;0.96904 0.43399 0.10294;0.96555 0.42241 0.09798;0.96187 0.41093
0.0931;0.95801 0.39958 0.08831;0.95398 0.38836 0.08362;0.94977 0.37729
0.07905;0.94538 0.36638 0.07461;0.94084 0.35566 0.07031;0.93612 0.34513
0.06616;0.93125 0.33482 0.06218;0.92623 0.32473 0.05837;0.92105 0.31489
0.05475;0.91572 0.3053 0.05134;0.91024 0.29599 0.04814;0.90463 0.28696
0.04516;0.89888 0.27824 0.04243;0.89298 0.26981 0.03993;0.88691 0.26152
0.03753;0.88066 0.25334 0.03521;0.87422 0.24526 0.03297;0.8676 0.2373
0.03082;0.86079 0.22945 0.02875;0.8538 0.2217 0.02677;0.84662 0.21407
0.02487;0.83926 0.20654 0.02305;0.83172 0.19912 0.02131;0.82399 0.19182
0.01966;0.81608 0.18462 0.01809;0.80799 0.17753 0.0166;0.79971 0.17055
0.0152;0.79125 0.16368 0.01387;0.7826 0.15693 0.01264;0.77377 0.15028
0.01148;0.76476 0.14374 0.01041;0.75556 0.13731 0.00942;0.74617 0.13098
0.00851;0.73661 0.12477 0.00769;0.72686 0.11867 0.00695;0.71692 0.11268
0.00629;0.7068 0.1068 0.00571;0.6965 0.10102 0.00522;0.68602 0.09536
0.00481;0.67535 0.0898 0.00449;0.66449 0.08436 0.00424;0.65345 0.07902
0.00408;0.64223 0.0738 0.00401;0.63082 0.06868 0.00401;0.61923 0.06367
0.0041;0.60746 0.05878 0.00427;0.5955 0.05399 0.00453;0.58336 0.04931
0.00486;0.57103 0.04474 0.00529;0.55852 0.04028 0.00579;0.54583 0.03593
0.00638;0.53295 0.03169 0.00705;0.51989 0.02756 0.0078;0.50664 0.02354
0.00863;0.49321 0.01963 0.00955;0.4796 0.01583 0.01055],...
    'XTick',[15 30 45 60 75 90]);
```

Appendices

Chapter 5

MATLAB code for Fig 26

```
clc
clear all
m=[0.0008 0 0.0004 0.0006 0.0005 0.0008;
   0.0004 0.0013 0.0013 0.0016 0.0014 0.0014;
   0.0006 0.002 0.002 0.002 0.0015 0.0022;
   0.0012 0.0014 0.0023 0.0015 0.0029 0.0016;
   -0.00069 0.00278 0.00875 0.02389 0.01594 0.02467];

[X,Y]= meshgrid(15:0.05:90,5.14:0.05:9.04);
X1=[15;30;45;60;75;90];
Y1=[5.14;6.25;7.08;7.74;9.04];
Z1= griddata(X1,Y1,m,X,Y,'cubic');
mesh(X,Y,Z1),hold on
plot3(X1,Y1,m,'.'),hold on
figure;
h=xlabel('Linear velocity');
h=ylabel('Impact Angle');
h=zlabel('Percentage mass change');
shading interp
colourmapeditor
```

MATLAB code for Fig 27

```
clc
clear all
m=[0.0008 0 0.0004 0.0006 0.0005 0.0008;
   0.0004 0.0013 0.0013 0.0016 0.0014 0.0014;
   0.0006 0.002 0.002 0.002 0.0015 0.0022;
   0.0012 0.0014 0.0023 0.0015 0.0029 0.0016;
   -0.00015 0.06492 0.00776 0.01298 0.01857 0.01914];

[X,Y]= meshgrid(15:0.05:90,5.14:0.05:9.04);
X1=[15;30;45;60;75;90];
Y1=[5.14;6.25;7.08;7.74;9.04];
Z1= griddata(X1,Y1,m,X,Y,'cubic');
mesh(X,Y,Z1),hold on
plot3(X1,Y1,m,'.'),hold on
figure;
h=xlabel('Linear velocity');
h=ylabel('Impact Angle');
h=zlabel('Percentage mass change');
shading interp
colourmapeditor
```

Appendices

Chapter six

Erosion maps version 2
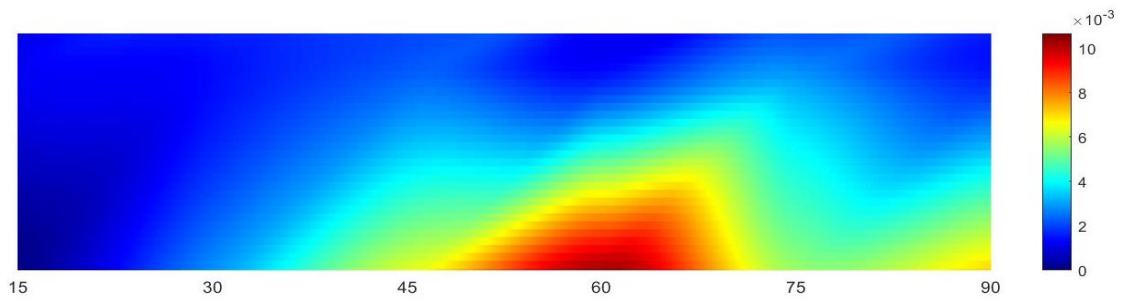
6.25 m/s
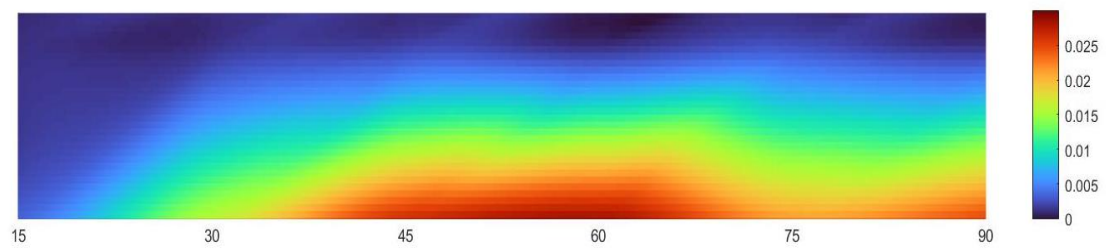
8.42 m/s
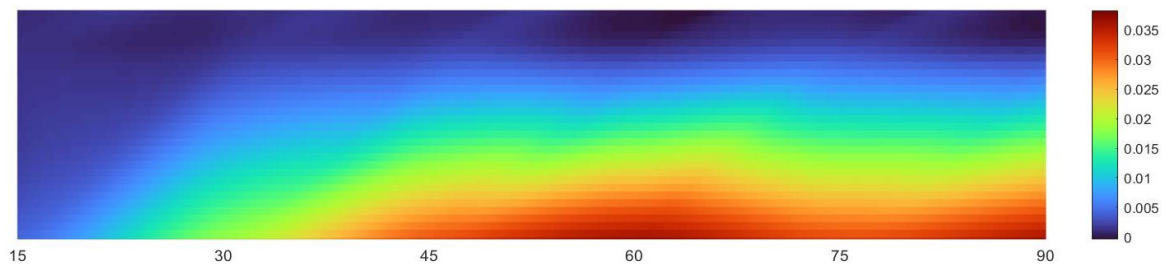
10.16 m/s

Appendices

MATLAB code for erosion map Fig34

```
function createfigure(xdata1, ydata1, zdata1)
%CREATEFIGURE(xdata1, ydata1, zdata1)
%  XDATA1:  surface xdata
%  YDATA1:  surface ydata
%  ZDATA1:  surface zdata

%  Auto-generated by MATLAB on 11-Sep-2023 12:16:01

% Create figure
figure('Colormap',...
    [0.18995 0.07176 0.23217;0.19483 0.08339 0.26149;0.19956 0.09498
0.29024;0.20415 0.10652 0.31844;0.2086 0.11802 0.34607;0.21291 0.12947
0.37314;0.21708 0.14087 0.39964;0.22111 0.15223 0.42558;0.225 0.16354
0.45096;0.22875 0.17481 0.47578;0.23236 0.18603 0.50004;0.23582 0.1972
0.52373;0.23915 0.20833 0.54686;0.24234 0.21941 0.56942;0.24539 0.23044
0.59142;0.2483 0.24143 0.61286;0.25107 0.25237 0.63374;0.25369 0.26327
0.65406;0.25618 0.27412 0.67381;0.25853 0.28492 0.693;0.26074 0.29568
0.71162;0.2628 0.30639 0.72968;0.26473 0.31706 0.74718;0.26652 0.32768
0.76412;0.26816 0.33825 0.7805;0.26967 0.34878 0.79631;0.27103 0.35926
0.81156;0.27226 0.3697 0.82624;0.27334 0.38008 0.84037;0.27429 0.39043
0.85393;0.27509 0.40072 0.86692;0.27576 0.41097 0.87936;0.27628 0.42118
0.89123;0.27667 0.43134 0.90254;0.27691 0.44145 0.91328;0.27701 0.45152
0.92347;0.27698 0.46153 0.93309;0.2768 0.47151 0.94214;0.27648 0.48144
0.95064;0.27603 0.49132 0.95857;0.27543 0.50115 0.96594;0.27469 0.51094
0.97275;0.27381 0.52069 0.97899;0.27273 0.5304 0.98461;0.27106 0.54015
0.9893;0.26878 0.54995 0.99303;0.26592 0.55979 0.99583;0.26252 0.56967
0.99773;0.25862 0.57958 0.99876;0.25425 0.5895 0.99896;0.24946 0.59943
0.99835;0.24427 0.60937 0.99697;0.23874 0.61931 0.99485;0.23288 0.62923
0.99202;0.22676 0.63913 0.98851;0.22039 0.64901 0.98436;0.21382 0.65886
0.97959;0.20708 0.66866 0.97423;0.20021 0.67842 0.96833;0.19326 0.68812
0.9619;0.18625 0.69775 0.95498;0.17923 0.70732 0.94761;0.17223 0.7168
0.93981;0.16529 0.7262 0.93161;0.15844 0.73551 0.92305;0.15173 0.74472
0.91416;0.14519 0.75381 0.90496;0.13886 0.76279 0.8955;0.13278 0.77165
0.8858;0.12698 0.78037 0.8759;0.12151 0.78896 0.86581;0.11639 0.7974
0.85559;0.11167 0.80569 0.84525;0.10738 0.81381 0.83484;0.10357 0.82177
0.82437;0.10026 0.82955 0.81389;0.0975 0.83714 0.80342;0.09532 0.84455
0.79299;0.09377 0.85175 0.78264;0.09287 0.85875 0.7724;0.09267 0.86554
0.7623;0.0932 0.87211 0.75237;0.09451 0.87844 0.74265;0.09662 0.88454
0.73316;0.09958 0.8904 0.72393;0.10342 0.896 0.715;0.10815 0.90142 0.70599;0.11374
0.90673 0.69651;0.12014 0.91193 0.6866;0.12733 0.91701 0.67627;0.13526 0.92197
0.66556;0.14391 0.9268 0.65448;0.15323 0.93151 0.64308;0.16319 0.93609
0.63137;0.17377 0.94053 0.61938;0.18491 0.94484 0.60713;0.19659 0.94901
0.59466;0.20877 0.95304 0.58199;0.22142 0.95692 0.56914;0.23449 0.96065
0.55614;0.24797 0.96423 0.54303;0.2618 0.96765 0.52981;0.27597 0.97092
0.51653;0.29042 0.97403 0.50321;0.30513 0.97697 0.48987;0.32006 0.97974
0.47654;0.33517 0.98234 0.46325;0.35043 0.98477 0.45002;0.36581 0.98702
0.43688;0.38127 0.98909 0.42386;0.39678 0.99098 0.41098;0.41229 0.99268
0.39826;0.42778 0.99419 0.38575;0.44321 0.99551 0.37345;0.45854 0.99663
0.3614;0.47375 0.99755 0.34963;0.48879 0.99828 0.33816;0.50362 0.99879
0.32701;0.51822 0.9991 0.31622;0.53255 0.99919 0.30581;0.54658 0.99907
0.29581;0.56026 0.99873 0.28623;0.57357 0.99817 0.27712;0.58646 0.99739
0.26849;0.59891 0.99638 0.26038;0.61088 0.99514 0.2528;0.62233 0.99366
0.24579;0.63323 0.99195 0.23937;0.64362 0.98999 0.23356;0.65394 0.98775
0.22835;0.66428 0.98524 0.2237;0.67462 0.98246 0.2196;0.68494 0.97941
0.21602;0.69525 0.9761 0.21294;0.70553 0.97255 0.21032;0.71577 0.96875
0.20815;0.72596 0.9647 0.2064;0.7361 0.96043 0.20504;0.74617 0.95593
0.20406;0.75617 0.95121 0.20343;0.76608 0.94627 0.20311;0.77591 0.94113
0.2031;0.78563 0.93579 0.20336;0.79524 0.93025 0.20386;0.80473 0.92452
0.20459;0.8141 0.91861 0.20552;0.82333 0.91253 0.20663;0.83241 0.90627
0.20788;0.84133 0.89986 0.20926;0.8501 0.89328 0.21074;0.85868 0.88655
0.2123;0.86709 0.87968 0.21391;0.8753 0.87267 0.21555;0.88331 0.86553
0.21719;0.89112 0.85826 0.2188;0.8987 0.85087 0.22038;0.90605 0.84337
0.22188;0.91317 0.83576 0.22328;0.92004 0.82806 0.22456;0.92666 0.82025
0.2257;0.93301 0.81236 0.22667;0.93909 0.80439 0.22744;0.94489 0.79634
0.228;0.95039 0.78823 0.22831;0.9556 0.78005 0.22836;0.96049 0.77181
```

134

```
0.22811;0.96507 0.76352 0.22754;0.96931 0.75519 0.22663;0.97323 0.74682
0.22536;0.97679 0.73842 0.22369;0.98 0.73 0.22161;0.98289 0.7214 0.21918;0.98549
0.7125 0.2165;0.98781 0.7033 0.21358;0.98986 0.69382 0.21043;0.99163 0.68408
0.20706;0.99314 0.67408 0.20348;0.99438 0.66386 0.19971;0.99535 0.65341
0.19577;0.99607 0.64277 0.19165;0.99654 0.63193 0.18738;0.99675 0.62093
0.18297;0.99672 0.60977 0.17842;0.99644 0.59846 0.17376;0.99593 0.58703
0.16899;0.99517 0.57549 0.16412;0.99419 0.56386 0.15918;0.99297 0.55214
0.15417;0.99153 0.54036 0.1491;0.98987 0.52854 0.14398;0.98799 0.51667
0.13883;0.9859 0.50479 0.13367;0.9836 0.49291 0.12849;0.98108 0.48104
0.12332;0.97837 0.4692 0.11817;0.97545 0.4574 0.11305;0.97234 0.44565
0.10797;0.96904 0.43399 0.10294;0.96555 0.42241 0.09798;0.96187 0.41093
0.0931;0.95801 0.39958 0.08831;0.95398 0.38836 0.08362;0.94977 0.37729
0.07905;0.94538 0.36638 0.07461;0.94084 0.35566 0.07031;0.93612 0.34513
0.06616;0.93125 0.33482 0.06218;0.92623 0.32473 0.05837;0.92105 0.31489
0.05475;0.91572 0.3053 0.05134;0.91024 0.29599 0.04814;0.90463 0.28696
0.04516;0.89888 0.27824 0.04243;0.89298 0.26981 0.03993;0.88691 0.26152
0.03753;0.88066 0.25334 0.03521;0.87422 0.24526 0.03297;0.8676 0.2373
0.03082;0.86079 0.22945 0.02875;0.8538 0.2217 0.02677;0.84662 0.21407
0.02487;0.83926 0.20654 0.02305;0.83172 0.19912 0.02131;0.82399 0.19182
0.01966;0.81608 0.18462 0.01809;0.80799 0.17753 0.0166;0.79971 0.17055
0.0152;0.79125 0.16368 0.01387;0.7826 0.15693 0.01264;0.77377 0.15028
0.01148;0.76476 0.14374 0.01041;0.75556 0.13731 0.00942;0.74617 0.13098
0.00851;0.73661 0.12477 0.00769;0.72686 0.11867 0.00695;0.71692 0.11268
0.00629;0.7068 0.1068 0.00571;0.6965 0.10102 0.00522;0.68602 0.09536
0.00481;0.67535 0.0898 0.00449;0.66449 0.08436 0.00424;0.65345 0.07902
0.00408;0.64223 0.0738 0.00401;0.63082 0.06868 0.00401;0.61923 0.06367
0.0041;0.60746 0.05878 0.00427;0.5955 0.05399 0.00453;0.58336 0.04931
0.00486;0.57103 0.04474 0.00529;0.55852 0.04028 0.00579;0.54583 0.03593
0.00638;0.53295 0.03169 0.00705;0.51989 0.02756 0.0078;0.50664 0.02354
0.00863;0.49321 0.01963 0.00955;0.4796 0.01583 0.01055],...
    'OuterPosition',[936.333333333333 298.333333333333 1347.33333333333
1004.66666666667]);

% Create axes
axes1 = axes;
hold(axes1,'on');

% Create surf
surf(xdata1,ydata1,zdata1,'FaceColor','interp','EdgeColor','flat');

% Create zlabel
zlabel('Z-axis');

% Create ylabel
ylabel('Mass Loss');

% Create xlabel
xlabel('Impact Angle');

% Create title
title('Coated GFRP');

% Uncomment the following line to preserve the X-limits of the axes
% xlim(axes1,[15 90]);
view(axes1,[-89.8999195965226 -90]);
hold(axes1,'off');
% Set the remaining axes properties
set(axes1,'CameraViewAngle',6.60861036031192,'Colormap',...
    [0.18995 0.07176 0.23217;0.19483 0.08339 0.26149;0.19956 0.09498
0.29024;0.20415 0.10652 0.31844;0.2086 0.11802 0.34607;0.21291 0.12947
0.37314;0.21708 0.14087 0.39964;0.22111 0.15223 0.42558;0.225 0.16354
0.45096;0.22875 0.17481 0.47578;0.23236 0.18603 0.50004;0.23582 0.1972
0.52373;0.23915 0.20833 0.54686;0.24234 0.21941 0.56942;0.24539 0.23044
0.59142;0.2483 0.24143 0.61286;0.25107 0.25237 0.63374;0.25369 0.26327
0.65406;0.25618 0.27412 0.67381;0.25853 0.28492 0.693;0.26074 0.29568
0.71162;0.2628 0.30639 0.72968;0.26473 0.31706 0.74718;0.26652 0.32768
0.76412;0.26816 0.33825 0.7805;0.26967 0.34878 0.79631;0.27103 0.35926
0.81156;0.27226 0.3697 0.82624;0.27334 0.38008 0.84037;0.27429 0.39043
```

Appendices

```
0.85393;0.27509 0.40072 0.86692;0.27576 0.41097 0.87936;0.27628 0.42118
0.89123;0.27667 0.43134 0.90254;0.27691 0.44145 0.91328;0.27701 0.45152
0.92347;0.27698 0.46153 0.93309;0.2768 0.47151 0.94214;0.27648 0.48144
0.95064;0.27603 0.49132 0.95857;0.27543 0.50115 0.96594;0.27469 0.51094
0.97275;0.27381 0.52069 0.97899;0.27273 0.5304 0.98461;0.27106 0.54015
0.9893;0.26878 0.54995 0.99303;0.26592 0.55979 0.99583;0.26252 0.56967
0.99773;0.25862 0.57958 0.99876;0.25425 0.5895 0.99896;0.24946 0.59943
0.99835;0.24427 0.60937 0.99697;0.23874 0.61931 0.99485;0.23288 0.62923
0.99202;0.22676 0.63913 0.98851;0.22039 0.64901 0.98436;0.21382 0.65886
0.97959;0.20708 0.66866 0.97423;0.20021 0.67842 0.96833;0.19326 0.68812
0.9619;0.18625 0.69775 0.95498;0.17923 0.70732 0.94761;0.17223 0.7168
0.93981;0.16529 0.7262 0.93161;0.15844 0.73551 0.92305;0.15173 0.74472
0.91416;0.14519 0.75381 0.90496;0.13886 0.76279 0.8955;0.13278 0.77165
0.8858;0.12698 0.78037 0.8759;0.12151 0.78896 0.86581;0.11639 0.7974
0.85559;0.11167 0.80569 0.84525;0.10738 0.81381 0.83484;0.10357 0.82177
0.82437;0.10026 0.82955 0.81389;0.0975 0.83714 0.80342;0.09532 0.84455
0.79299;0.09377 0.85175 0.78264;0.09287 0.85875 0.7724;0.09267 0.86554
0.7623;0.0932 0.87211 0.75237;0.09451 0.87844 0.74265;0.09662 0.88454
0.73316;0.09958 0.8904 0.72393;0.10342 0.896 0.715;0.10815 0.90142 0.70599;0.11374
0.90673 0.69651;0.12014 0.91193 0.6866;0.12733 0.91701 0.67627;0.13526 0.92197
0.66556;0.14391 0.9268 0.65448;0.15323 0.93151 0.64308;0.16319 0.93609
0.63137;0.17377 0.94053 0.61938;0.18491 0.94484 0.60713;0.19659 0.94901
0.59466;0.20877 0.95304 0.58199;0.22142 0.95692 0.56914;0.23449 0.96065
0.55614;0.24797 0.96423 0.54303;0.2618 0.96765 0.52981;0.27597 0.97092
0.51653;0.29042 0.97403 0.50321;0.30513 0.97697 0.48987;0.32006 0.97974
0.47654;0.33517 0.98234 0.46325;0.35043 0.98477 0.45002;0.36581 0.98702
0.43688;0.38127 0.98909 0.42386;0.39678 0.99098 0.41098;0.41229 0.99268
0.39826;0.42778 0.99419 0.38575;0.44321 0.99551 0.37345;0.45854 0.99663
0.3614;0.47375 0.99755 0.34963;0.48879 0.99828 0.33816;0.50362 0.99879
0.32701;0.51822 0.9991 0.31622;0.53255 0.99919 0.30581;0.54658 0.99907
0.29581;0.56026 0.99873 0.28623;0.57357 0.99817 0.27712;0.58646 0.99739
0.26849;0.59891 0.99638 0.26038;0.61088 0.99514 0.2528;0.62233 0.99366
0.24579;0.63323 0.99195 0.23937;0.64362 0.98999 0.23356;0.65394 0.98775
0.22835;0.66428 0.98524 0.2237;0.67462 0.98246 0.2196;0.68494 0.97941
0.21602;0.69525 0.9761 0.21294;0.70553 0.97255 0.21032;0.71577 0.96875
0.20815;0.72596 0.9647 0.2064;0.7361 0.96043 0.20504;0.74617 0.95593
0.20406;0.75617 0.95121 0.20343;0.76608 0.94627 0.20311;0.77591 0.94113
0.2031;0.78563 0.93579 0.20336;0.79524 0.93025 0.20386;0.80473 0.92452
0.20459;0.8141 0.91861 0.20552;0.82333 0.91253 0.20663;0.83241 0.90627
0.20788;0.84133 0.89986 0.20926;0.8501 0.89328 0.21074;0.85868 0.88655
0.2123;0.86709 0.87968 0.21391;0.8753 0.87267 0.21555;0.88331 0.86553
0.21719;0.89112 0.85826 0.2188;0.8987 0.85087 0.22038;0.90605 0.84337
0.22188;0.91317 0.83576 0.22328;0.92004 0.82806 0.22456;0.92666 0.82025
0.2257;0.93301 0.81236 0.22667;0.93909 0.80439 0.22744;0.94489 0.79634
0.228;0.95039 0.78823 0.22831;0.9556 0.78005 0.22836;0.96049 0.77181
0.22811;0.96507 0.76352 0.22754;0.96931 0.75519 0.22663;0.97323 0.74682
0.22536;0.97679 0.73842 0.22369;0.98 0.73 0.22161;0.98289 0.7214 0.21918;0.98549
0.7125 0.2165;0.98781 0.7033 0.21358;0.98986 0.69382 0.21043;0.99163 0.68408
0.20706;0.99314 0.67408 0.20348;0.99438 0.66386 0.19971;0.99535 0.65341
0.19577;0.99607 0.64277 0.19165;0.99654 0.63193 0.18738;0.99675 0.62093
0.18297;0.99672 0.60977 0.17842;0.99644 0.59846 0.17376;0.99593 0.58703
0.16899;0.99517 0.57549 0.16412;0.99419 0.56386 0.15918;0.99297 0.55214
0.15417;0.99153 0.54036 0.1491;0.98987 0.52854 0.14398;0.98799 0.51667
0.13883;0.9859 0.50479 0.13367;0.9836 0.49291 0.12849;0.98108 0.48104
0.12332;0.97837 0.4692 0.11817;0.97545 0.4574 0.11305;0.97234 0.44565
0.10797;0.96904 0.43399 0.10294;0.96555 0.42241 0.09798;0.96187 0.41093
0.0931;0.95801 0.39958 0.08831;0.95398 0.38836 0.08362;0.94977 0.37729
0.07905;0.94538 0.36638 0.07461;0.94084 0.35566 0.07031;0.93612 0.34513
0.06616;0.93125 0.33482 0.06218;0.92623 0.32473 0.05837;0.92105 0.31489
0.05475;0.91572 0.3053 0.05134;0.91024 0.29599 0.04814;0.90463 0.28696
0.04516;0.89888 0.27824 0.04243;0.89298 0.26981 0.03993;0.88691 0.26152
0.03753;0.88066 0.25334 0.03521;0.87422 0.24526 0.03297;0.8676 0.2373
0.03082;0.86079 0.22945 0.02875;0.8538 0.2217 0.02677;0.84662 0.21407
0.02487;0.83926 0.20654 0.02305;0.83172 0.19912 0.02131;0.82399 0.19182
0.01966;0.81608 0.18462 0.01809;0.80799 0.17753 0.0166;0.79971 0.17055
0.0152;0.79125 0.16368 0.01387;0.7826 0.15693 0.01264;0.77377 0.15028
0.01148;0.76476 0.14374 0.01041;0.75556 0.13731 0.00942;0.74617 0.13098
0.00851;0.73661 0.12477 0.00769;0.72686 0.11867 0.00695;0.71692 0.11268
```

```
0.00629;0.7068 0.1068 0.00571;0.6965 0.10102 0.00522;0.68602 0.09536
0.00481;0.67535 0.0898 0.00449;0.66449 0.08436 0.00424;0.65345 0.07902
0.00408;0.64223 0.0738 0.00401;0.63082 0.06868 0.00401;0.61923 0.06367
0.0041;0.60746 0.05878 0.00427;0.5955 0.05399 0.00453;0.58336 0.04931
0.00486;0.57103 0.04474 0.00529;0.55852 0.04028 0.00579;0.54583 0.03593
0.00638;0.53295 0.03169 0.00705;0.51989 0.02756 0.0078;0.50664 0.02354
0.00863;0.49321 0.01963 0.00955;0.4796 0.01583 0.01055],...
    'DataAspectRatio',[1872.65917602996 1 253.682896379526],'XTick',...
    [15 30 45 60 75 90]);
```